Bergische Universität Wuppertal

Fachbereich C – Mathematik und Naturwissenschaften

Makromolekulare Chemie

PhD – Thesis

Title:

The Design and Synthesis of Conjugated Polymers with Aggregation-Induced Emission and Their Application in Fluorescence Sensing

Wenyue Dong, born in Heilongjiang

Wuppertal, September 2015

Die Dissertation kann wie folgt zitiert werden:

urn:nbn:de:hbz:468-20150910-125459-4
[http://nbn-resolving.de/urn/resolver.pl?urn=urn%3Anbn%3Ade%3Ahbz%3A468-20150910-125459-4]

To my beloved parents

This work was carried out during the period from October 2012 to September 2015 in the Department of Chemistry, Macromolecular Chemistry group, Bergische Universität Wuppertal, under the supervision of Prof. Dr. Ullrich Scherf.

1. **Supervisor: Prof. Dr. Ullrich Scherf, Bergische Universität Wuppertal.**
2. **Reviewer: Prof. Dr. Yuguang Ma, South China University of Technology.**

Abstract

Conjugated, semiconducting polymers are widely used as active compounds of optoelectronic devices. Usually, they are applied as thin films or layers. However, most "conventional" luminogens show an aggregation-caused quenching (ACQ), which is detrimental for their application. In 2001, Tang *et al.* reported a novel aggregation-induced emission (AIE) phenomenon: Such luminogens weakly emit in dilute solution but intensely in the aggregated state. Restriction of intramolecular motions has been demonstrated to be the main mechanism for occurrence of the AIE effect by theoretical and experimental studies. Till now, plenty of AIE-active molecules have been synthesized, for the applications in organic light emitting devices (OLEDs), chemo/biosensors, cell imaging, and so on. However, most of them are low molecular weight compounds. Based on superior film forming and mechanical properties, also the design of high molecular weight, polymeric luminogens is promising, *e.g.* for the use in large-area or flexible devices.

In this thesis, we introduce a new class of AIE polymers with AIE- or crystallization-induced emission (CIE)-active tri-/tetraphenylethylene and 2,3,3-triphenylacrylonitrile (TPAN) side chains. This strategy guarantees the occurrence of AIE properties without greatly affecting the electronic properties of the polymers' backbones. The obtained AIE-active polymers were applied in the detection of nitroaromatic explosives with two main benefits: a) their high fluorescence quantum yields in the aggregated state; b) their twisted and loose structure, which accelerates the diffusion of analyte molecules, thus enhancing the quenching efficiency. This thesis is comprised of four parts.

1. Carbazole is a typical electron-rich building block, which is beneficial for the interaction with electron-deficient nitroaromatic explosives based on the fluorescence changes. Hence, a series of polycarbazoles (PCz3PEs, PCzTPEs) with AIE-active tri-/tetraphenylethylene side groups have been designed and synthesized. Among them, PCzTPEs showed distinct AIE effect and possess high fluorescence quantum yields in solid film. For the application in the detection of 1,3,5-trinitrobenzene (TNB) as prototypical nitroaromatic analyte, a sensitive

and amplified quenching effect was observed with a maximum quenching constant of 1.26×10^6 M^{-1} based on PCzTPE0.5 aggregates in 1/9 THF/water. Solid-state paper strips experiments based on PCzTPE and PCzTPE0.5 also showed sensitive PL quenching.

2. Similar to carbazole, triphenylamine (TPA) buiding blocks also exhibit electron-rich characteristics and can serve as electron-donor moiety. Polytriphenylamines (**P1** and **P2**) with tetraphenylethylene (TPE) side chains have been synthesized. **P1** and **P2** showed distinct AIE behavior and have been used as films for the detection of TNB vapour, with excellent fluorescence response. 89% PL quenching within 10 min and outstanding repeatability have been observed. One disadvantage of **P1** and **P2** is their poor solubility. To solve this problem, bis(*tert*-butyl)-TPE groups were introduced to the backbone of the copolymers. The obtained copolymers showed improved solubility in common organic solvents and reasonable AIE properties leading to high solid state fluorescence quantum yields.

3. Two polymers PCzTPAN and PTPATPAN have been developed with electron-rich carbazole- or TPA-based backbones and 2,3,3-triphenylacrylonitrile (TPAN) side chains. As a congener of TPE, TPAN is crystallization-induced emission (CIE)-active. Our polymers containing TPAN side groups showed distinct AIE properties. Moreover, the introduction of the electron-deficient TPAN units led to the occurrence of intramolecular charge transfer (ICT) effects. For TNB detection, both polymers showed sensitive PL responses with a maximum PL quenching constant of 5.5×10^5 M^{-1}. Furthermore, PTPATPAN was used as dopant for detecting the glass transition temperature of polymers, with polystyrene as the example. The method is a straightforward, simple and sensitive way for the detection of the glass transition temperature, especially of thin films.

4. In the last part, we designed conjugated polymers with electron-rich phenothiazine (PTz)- and thiophene-based backbones and TPE or TPAN as side chains. The obtained PTz polymers showed the expected AIE phenomenon. The polythiophenes, however, displayed ACQ effects, also in the presence of the AIE-active side chains, thus demonstrating a competition between intermolecular π-stacking and restriction of intramolecular motion. The photophysical properties of the polymers were studied in detail.

Table of Contents

Chapter 1

1. Introduction

Organic, π-conjugated and luminescent materials are of many fundamental and technological implications and represent a rapidly developing field. They have attracted huge academic and industrial interest[1-7]. Due to their attractive optoelectronic characteristics, they are today used as active material in real or prospective applications, such as organic field effect transistors[8-10] (OFETs), organic light emitting devices (OLEDs)[11-13], organic photovoltaics[14-16] (OPVs), chemo/biosensors[17-21], bio-imaging[22-25], organic solid lasers[26-28], and many others.

1.1 Aggregation-Caused Quenching (ACQ)

For their practical application in optoelectronic devices, the organic, luminescent materials are commonly used as solid-state materials, *e.g.* as thin films in the fabrication of OLEDs and OPV devices. Therefore, it is obviously of high importance that the chromophores can strongly emit in their aggregated state. However, most "conventional" organic luminophores exhibit high photoluminescence (PL) efficiency in (dilute) solution but are weakly or even non-emissive in concentrated solution or in the solid state. The effect is known as aggregation-caused quenching (ACQ)[29-31]. In the aggregated state, strong intermolecular interactions including electron transfer, Förster resonance energy transfer and excimer/exciplex occur and cause PL quenching of the materials.

Traditional, fluorescent molecules, which are usually flat, often disk-like aromatic molecules, often experience strong intermolecular interactions in concentrated solutions or in solid-state aggregates, such as pyrene, perylene or fluorescein. They are typical ACQ luminophores and the existence of this ACQ phenomenon is often detrimental for practical applications. To solve this problem, several chemical, physical or engineering approaches[32-37] have been developed. For example, the synthesis of compounds with spiro-kinks or bulky substituents covalently attached to the luminophores[39,40] or an adjustment of the aggregation type[41-43] (*e.g. J*-aggregation). However, it is an often difficult approach with limited success, because one has to fight against an intrinsic and very natural process – the energetically favored

formation of chromophore aggregates in the solid state. So, it would make life much easier if aggregation could be beneficial, not detrimental, to the occurrence of fluorescence.

1.2 Aggregation-Induced Emission (AIE)

In 2001, Tang *et al.* first described a novel phenomenon, called aggregation-induced emission[44,45] (AIE) which is opposite to the ACQ effect: The propeller-shaped molecule hexaphenylsilole (HPS) emits strongly in its solid state with a PL quantum yield (PLQY) of 78% but is nearly non-emissive in solution (PLQY of 0.22%). This unusual phenomenon was further investigated in different solvent/non-solvent mixtures (acetonitrile/water): The emission intensity increased for high water fractions. Since HPS is very soluble in acetonitrile but insoluble in water, it aggregates for high water contents. The formation of aggregates was verified by absorption spectroscopy and particle size analysis[46,47] (see Figure 1.1). In the absorption spectra, the solutions of high water fraction show absorption level-off tails into the long wavelength region, which is well known for the Mie effect of nanoaggregates. The particle size analysis revealed the existence of particles with average sizes of 190 nm or 130 nm in solvent mixtures with 80% or 90% water, respectively, confirming that the HPS molecules are indeed aggregated into nanoaggregates. In contrast, absorption spectra and particle size analysis did not show any characteristics of nanoaggregate formation for low water contents, thus demonstrating that HPS is AIE-active. Occurrence of AIE effects has opened a new platform for the development of solid-state luminescence applications.

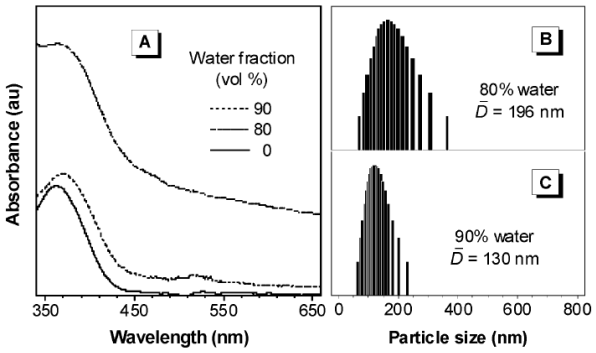

Figure 1.1. (A) Absorption spectra of HPS in acetonitrile-water mixtures. Size distributions of nanoparticles of HPS in acetonitrile-water mixtures containing (B) 80% and (C) 90% water, image taken from Ref. [47] with permission.

1.3 The Mechanism of AIE

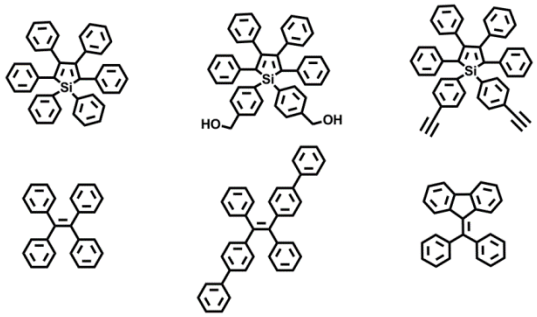

Figure 1.2. Examples of AIE luminophores reported in the literature.

The AIE phenomenon was first observed in the silole family, another class of AIE-active compounds is tetraphenylethylene (TPE) derivatives. Some structures are depicted in Figure 1.2. Next, understanding of the AIE mechanism was very important, in addition to the design of new families of more efficient and functionalized AIE molecules. As we know, any kind of motion, no matter microscopic or macroscopic, consumes energy. As for molecules, main types of motion are rotations and vibrations. In dilute solution, the modes of intramolecular motion (rotation and vibration) are thermally activated due to the high freedom of space, but can be restricted in the aggregated state (Figure 1.3). These activated motions can serve as relaxation channels for the excited state decay. However, if motions are blocked in the aggregated state, non-radiative deactivation paths may be closed thus leading to an increased radiative decay. So, the restriction of intramolecular motions (RIM)[48] in the aggregated state is the main source of AIE effects, as concluded from both experimental and theoretical studies.

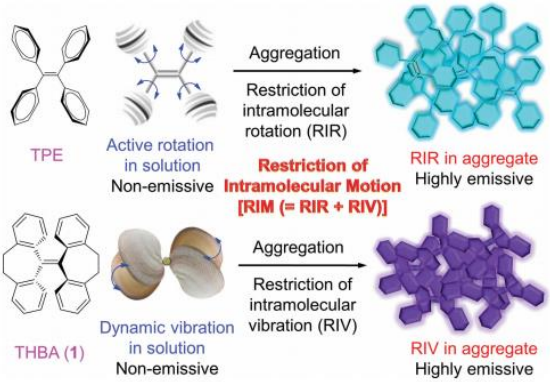

Figure 1.3. AIE-active propeller-shaped luminogen TPE showing restriction of intramolecular rotation (RIR), and mussel shell-like luminogen 10,10′,11,11′-tetrahydro-5,5′-bidibenzo[a,d][7]annulenylidene (THBA) showing restriction of intramolecular vibrations (RIV), image taken from Ref. [48] with permission.

1.3.1 Restriction of Intramolecular Rotation (RIR)

In HPS, as an example, the six peripheral phenyl rings work as propeller, which can rotate freely against the silole core in dilute solution, but the rotation is restricted in aggregates due to the physical constraints, leading to the AIE behavior. This mechanism has been proved in a series of tests by Tang's Group[46,49].

1.3.1.1 Viscosity Effect[46]

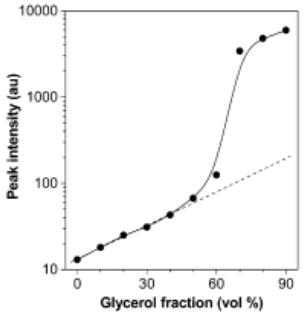

Figure 1.4. PL peak intensity of HPS *vs.* composition of glycerol/methanol mixtures, image taken from Ref. [46] with permission.

In viscous media, the intramolecular rotations are supposed to be slowed down thus enhancing PL emission. Glycerol and methanol were chosen for such viscosity experiment, since glycerol is a very viscous liquid (934 cP) with a viscosity ~1720 times higher than that of methanol (0.544 cP) at room temperature. Mixing of these two solvents is used to generate solutions of different viscosity. Figure 1.4 shows PL intensities *vs.* glycerol fraction of glycerol/methanol mixtures. As expected, the PL emission increases with higher viscosity due to the RIR process.

1.3.1.2 Temperature Effect[46]

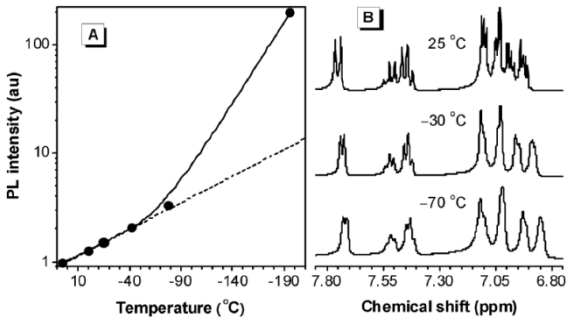

Figure 1.5. (A) Effect of temperature on PL intensity of HPS in THF. (B) ^{1}H NMR spectra of HPS in dichloromethane-d_2 at different temperatures, image taken from Ref. [47] with permission.

Experiments with a variation of the temperature have been also carried out, since cooling can also restrict intramolecular rotations to some extent. THF was chosen as the solvent because of its high solvating power, low melting point (-108 °C) and its low viscosity (0.456 cP at 25 °C) with a small temperature coefficient (~0.008 cP/K) thus ensuring that the PL enhancement is not caused by increasing/decreasing viscosity. In such an experiment, the PL of HPS strongly increases with decreasing temperature (Figure 1.5A). The occurring RIR process was also verified by dynamic NMR experiments (Figure 1.5B). Active conformational exchange (intramolecular rotation) leads to sharp NMR peaks, and they are broadened by cooling, thus indicating that intramolecular rotation is restricted at low temperatures.

1.3.1.3 Pressure Effect[49]

Increasing the pressure to a HPS film can bring the molecules much closer, thus further enhancing the RIR process. Figure 1.6 shows pressure tests with AIE-active HPS and AlQ_3 as a typical ACQ compound. For the HPS film, the PL increases with increasing pressure up to 104 atm but slightly decreases with further pressurization, probably caused by excimer formation due to increased intermolecular interaction. However, the PL intensity at 450 atm is still higher than that of the original film. On the other hand, the emission intensity of a AlQ_3 film decreases in the whole pressure region. The pressure experiments further confirm the RIR mechanism for AIE luminogens.

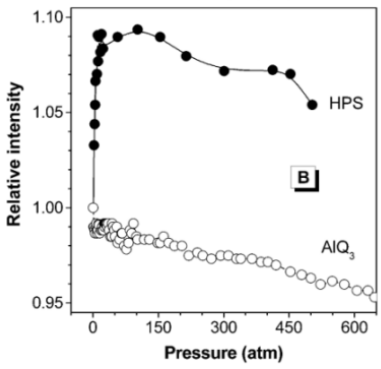

Figure 1.6. Pressure effect on the PL intensity of HPS and AlQ_3 films, image taken from Ref. [49] with permission.

1.3.1.4 Other Effects

Aldred *et al.*[50] reported investigations with two *ortho*-methyl substituted TPE compounds, DMTPE and TMTPE, the structures are shown in Figure 1.7. Among these TPE derivatives,

TMTPE showed a high PLQY (64.3%) in THF solution and low AIE-activity, very different from the behavior of TPE and DMTPE (Figure 1.7). This is caused by an enhanced steric hindrance between germinal phenyl rings in TMTPE, thus restricting intramolecular motions.

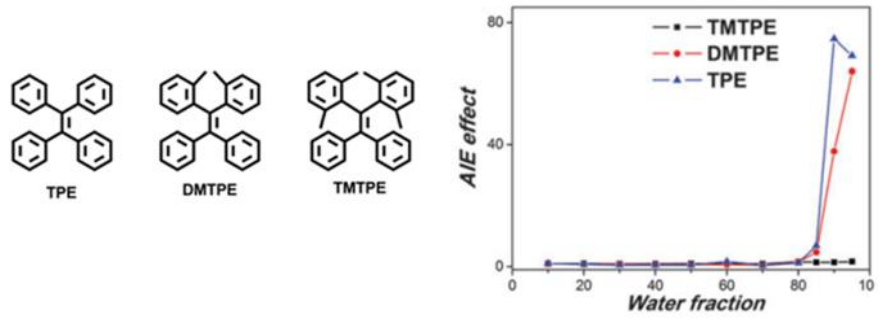

Figure 1.7. Chemical structures and AIE effects of TPE, DMTPE and TMTPE, image taken from Ref. [50] with permission.

Zhao *et al.*[51] synthesized a series of folded and linear TPE derivatives. The folded TPE derivatives (such as (Z)-*o*-BBPTPE, Figure 1.8) show higher PL emission efficiency if compared to linear counterparts, due to the partial suppression of intramolecular rotation of the phenyl rotors. This finding also indicates that RIR is responsible for the observed AIE phenonmenon.

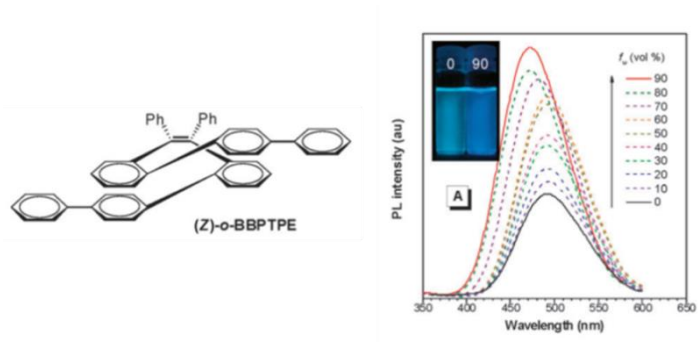

Figure 1.8. Chemical structure and PL spectra of (Z)-*o*-BBPTPE in THF/water mixtures with different water content, image taken from Ref. [51] with permission.

1.3.2 Restriction of Intramolecular Vibration (RIV)

Other AIE-active molecules, *e.g.* THBDBA in Figure 1.9, do not bear rotatory elements. So, the RIR mechanism cannot explain the occurrence of the AIE phenomenon. Tang *et al.* proposed a novel mechanism by using a computational QM/MM (quantum mechanics and molecular mechanics) model, which involves the restriction of intramolecular vibrations[52] (RIV). In the crystal structure of THBDBA, couples of phenyl rings are locked by ethyl

bridges thus adopting a “boat” conformation. By activation THBDBA can switch into a “chair” conformation as well as into “mixed” conformations between chair and boat form. Conformational motions (low frequency vibrational motions) in solution facilitate non-radiative decay of the excited-state. A larger reorganization energy was obtained from the QM/MM mode calculations for single molecules if compared to clusters, which means, that more excited state energy is consumed by these vibrational motions for a single molecule. Between a single molecule and a molecule as part of a cluster the authors obtained an energy difference of 1663.6 cm^{-1} (significant normal mode frequencies with reorganization energy above 200 cm^{-1}) corresponding to 30% of the total excited state energy. Therefore, a combination of restriction of vibrational channels and a reduction of the total reorganization energy in the cluster state likely causes the AIE phenomenon of THBDBA. Due to the modeling, the majority of the motions are in-plane/out-of-plane bending vibrations of phenyl ring carbon atoms. These vibrations consume much of the excited state energy in solution. The intense emission of aggregates originates from the RIV effect. Overall, RIR and RIV processes together (as RIM) well explain the occurrence of AIE phenomenons.

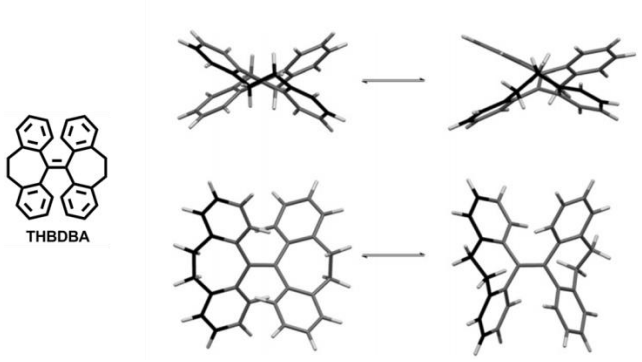

Figure 1.9. Chemical structure of THBDBA and calculated conformations (Left: “chair”; right: “boat”. Top: view along the axis of an ethane bridge; bottom: top view on ethane bridges), image taken from Ref. [52] with permission.

1.4 Applications of AIE Materials

Due to the high fluorescence quantum yield of AIE materials in the aggregated state, such as nanoaggregates in dispersion or thin films, they are promising candidates for optoelectronic applications since technological applications of luminescent materials are mainly realized in the aggregated state. Many scientists have devoted their research towards the development of efficient AIE emitters and their application in devices. Till now, AIE materials have found a wide variety of prospective high-tech applications in OLEDs[53-64], chemical sensors[65-75],

bioimaging[76-82] and others[83-89]. In the following sections, some progresses in these areas will be briefly discussed.

1.4.1 OLEDs

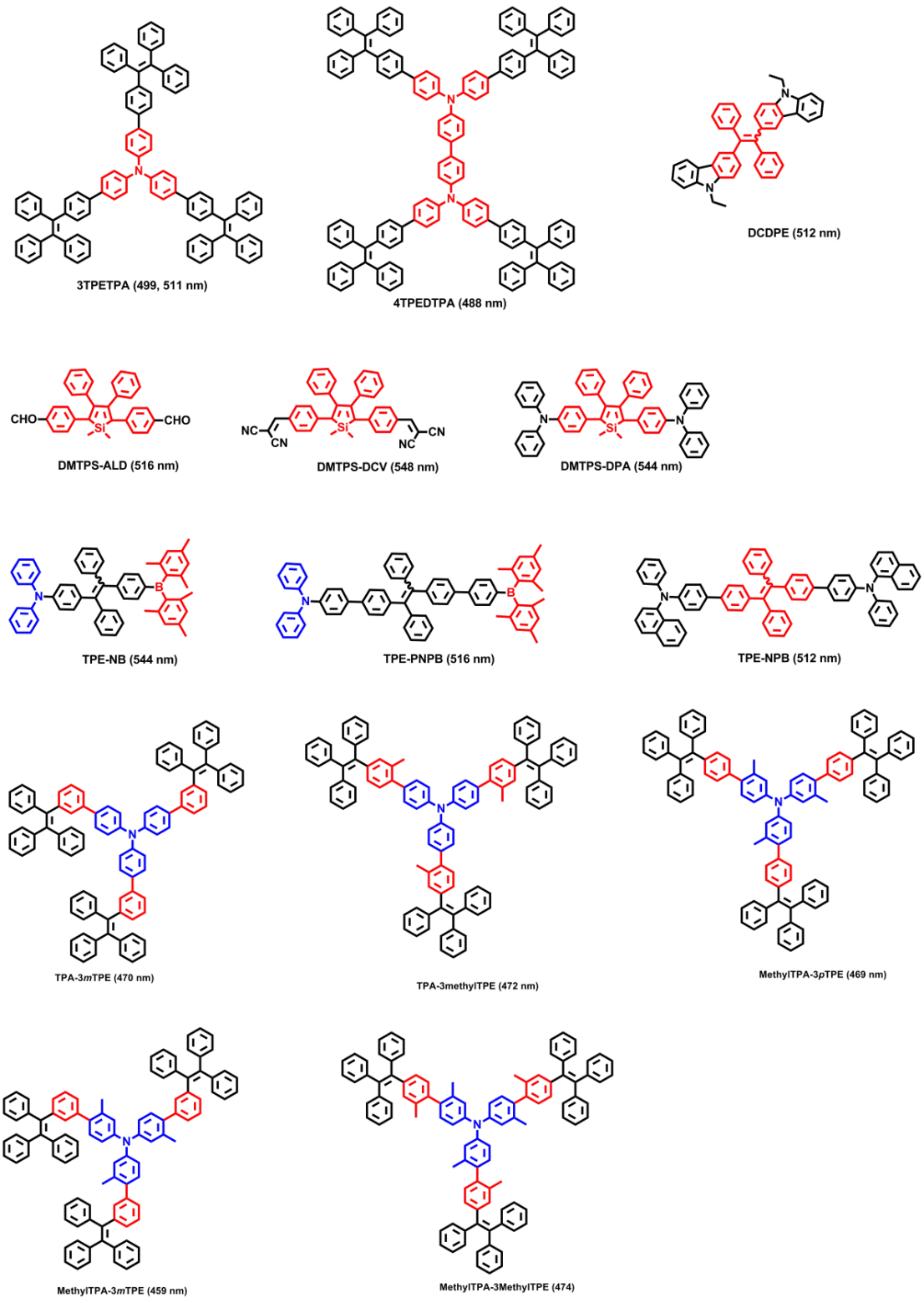

Figure 1.10. Examples of AIE luminogens used in OLED with blue or green light emission.

OLEDs have attracted great interests among researchers, due to their potential in display and lighting applications. “Conventional” luminogens show a severe ACQ effect which often causes a poor performance in devices. Since the AIE phenomenon was discovered, many OLEDs have been fabricated based on AIE luminogens.

Figure 1.10 shows some examples of AIE luminogens which were used in OLEDs through smart design and facile synthesis. In 3TPETPA and 4TPEDTPA[53], multiple TPE substituents were attached to TPA and DTPA cores, leading to PLQYs in films of up to 100%. Thanks to AIE effect and the hole-transport ability of TPA and DTPA, devices based on these two molecules without any hole transport layer (HTL) showed an even better performance than ones with a HTL, with a low turn-on voltage (V_{on}) of 4.5 V, a maximum luminance (L_{max}) of 6935 cd cm^{-2} and a current efficiency (CE_{max}) of 4.0 cd A^{-1} for 3TPETPA, and V_{on} of 4.1 V, L_{max} of 10723 cd m^{-2} and CE_{max} of 8.0 cd A^{-1} for 4TPEDTPA, respectively. A carbazole-containing tetrasubstituted ethene (DCDPE)[54] and a TPE-modified NPB (TPE-NPB)[55] were also synthesized for use in OLEDs. OLED devices using these molecules without HTL emitted bluish-green light with V_{on} of 4.5 V, L_{max} of 5060 cd m^{-2} and CE_{max} of 5.7 cd A^{-1} for DCDPE, and V_{on} of 3.9 V, L_{max} of 12607 cd m^{-2} and CE_{max} of 13.1 cd A^{-1} for TPE-NPB, respectively, values which are again better than the ones by using additional HTLs due to the hole transport capabilities of the carbazole and NPB unites. Three dimethyltetraphenylsiloles (DMTPSs)[56] symmetrically substituted with aldehyde (ALD), dicyanovinyl (DCV) and diphenylamine (DPA) moieties were also reported. Due to their acceptor (A) or donor (D) substituents, DMTPS-ALD exhibits almost no response to the solvent polarity, DMTPS-DCV and DMTPS-DPA, however, exhibit significant intramolecular charge transfer (ICT) effects. The best device performance for multilayer devices fabricated with DMTPS-type materials as emitter was reported for DMTPS-DPA, which showed V_{on}, L_{max}, CE_{max} and maximum power efficiency (PE_{max}) of 3.1 V, 13405 cd m^{-1}, 8.28 cd A^{-1}, and 7.88 lm W^{-1}, respectively. Other D-A molecules (TPE-NB and TPE-PNPB)[57] were also synthesized and showed high PLQY up to 94%. Hereby, especially TPE-PNPB displayed promising EL properties. Generally, strong D-A interactions, *e.g.* in TPE-NB, decrease PL and EL efficiencies. An excellent OLED device performance without HTL was obtained for TPE-PNPB: V_{on} of 3.2 V, L_{max} of 13678 cd m^{-2} and CE_{max} of 16.2 cd A^{-1}. Five hole transport-dominated blue AIE luminogens (TPA-TPEs)[58] were reported by Li *et al.* by changing the linkage mode and intramolecular torsion angles. Among them, MethylTPA-3*p*TPE demonstrated the best EL performance with CE_{max} of 8.03 cd A^{-1}

and PE_{max} of 7.04 lm W^{-1}. This design provides a promising approach to construct deep blue AIE emitters.

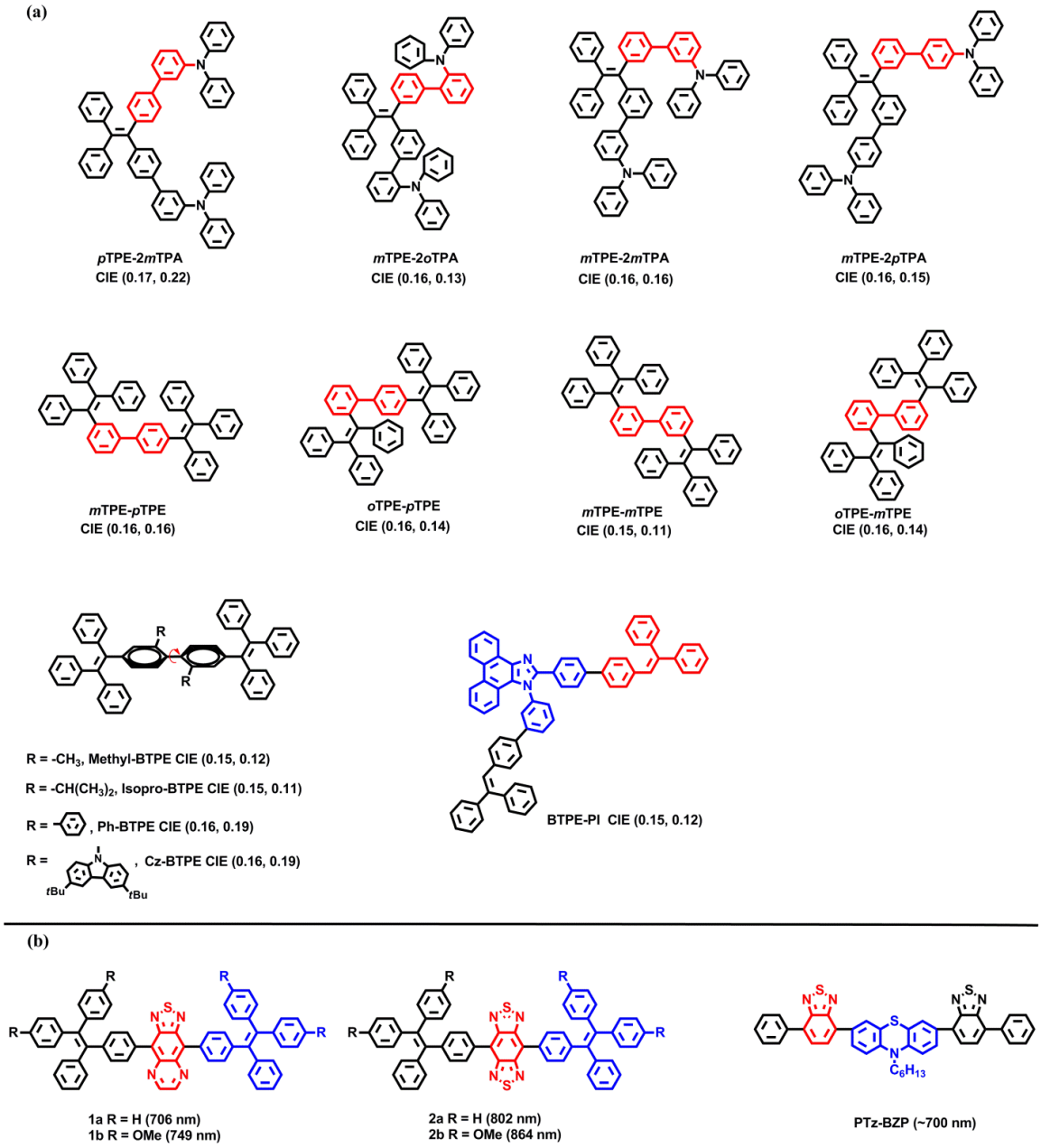

Figure 1.11. Examples of AIE luminogens used in efficient OLED devices with (a) deep blue and (b) NIR light emission.

The availability of deep blue emitters is a crucial need for realizing full color displays and white lighting. Since the intrinsic wide bandgap of blue emitters makes it difficult to inject charges and due to the occurrence of ACQ effects many researchers have tried to generate deep blue AIE emitters whose π-conjugation length is adjusted by different linking positions, by substituents of different size or by using AIE cores connected to deep blue emitting

building blocks, as depicted in Figure 1.11a. Four TPE-2TPA derivatives[59] with different linking positions were synthesized and utilized for OLEDs by Li *et al*. Their π-conjugation length has been reduced *via meta*-linkages between the building blocks thus exhibiting blue to almost deep-blue emission color. Another example of varing linkage mode was reported for BTPE derivatives[60]. They showed deep-blue emission peaking at 435 to 459 nm with CE_{max} of up to 2.8 cd A^{-1}. The behavior is completely different from a BTPE derivative linked in *para*-position (488 nm). Modification of *para*-linked BTPE with tunable dihedral angle within the biphenyl core was also reported[61]. The introduction of methyl, isopropyl, phenyl and carbazyl substituents in *ortho*-position of the biphenyl core allows for tuning of the central aryl-aryl dihedral angle and results in blue to deep blue light emission. The deep blue emitting AIE luminogen BTPE-PI[62] consisting with two AIE-active triphenylethene substituents at a deep blue emitting building block phenanthro[9,10-d]imidazole shows improved charge transport properties. An OLED device with BTPE-PI as active material exhibited performance parameters L_{max}, CE_{max} and PE_{max} of 20300 cd m^{-1}, 5.9 cd A^{-1} and 5.3 lm W^{-1}, respectively, one of the best parameter set for deep blue AIE emitters so far. In addition, also efficient white OLEDs have been made with the AIE-active BTPE-PI as deep blue emitter and bis[2-(2'-benzothienyl)pyridinato-N,C3'](acetylacetonato)-iridium(III) $Ir(btp)_2(acac)$ and tris[2-phenylpyridinato-C2,N]-iridium(III) $Ir(ppy)_3$ as dopants with 4,4'-bis(9*H*-carbazol-9-yl)biphenyl (CBP) as host, with CIE color coordinates of (0.33, 0.33).

Extension of the spectral range of OLEDs from visible to far-red and near-infrared (NIR) has become a new and challenging research target, especially for potential applications in chemosensors, night-vision devices and high-information-security displays. Examples of AIE materials used for NIR OLEDs are shown in Figure 1.11b. A family of D-A-D type NIR luminogens (1a, 1b, 2a and 2b)[63] was synthesized consisting of AIE-active TPE moieties attached to [1,2,5]thiadiazole[3,4-g]quinoxaline or benzo[1,2-c;4,5-c']bis[1,2,5]thiadiazole acceptor cores. The introduction of TPE units into a low bandgap chromophore allows for the realization of the AIE effects in the NIR region from 600-1100 nm. Non-doped OLED devices gave NIR emissions above 700 nm in moderate efficiency with a maximum external quantum efficiency (EQE_{max}) of up to 0.89%. Another NIR-emitting A-D-A compound PTZ-BZP[64] with a twisted bowl-shaped phenothiazine unit was reported, that showed AIE behaviour and an EQE_{max} of the undoped NIR OLED of 1.54%. Moreover, a high radiative electron/photon ratio of 48% was observed, more as the usual 25% in "conventional" fluorescent OLED devices.

1.4.2 Chemical Sensors

AIE molecules have been applied in various chemical sensors towards external inputs as the pH value, temperature and presence of analytes like ions, water or nitroaromatic compounds, due to a fast, amplified response with high sensitivity. Figure 1.12 depicts examples of AIE luminogens used as (chemo)sensors.

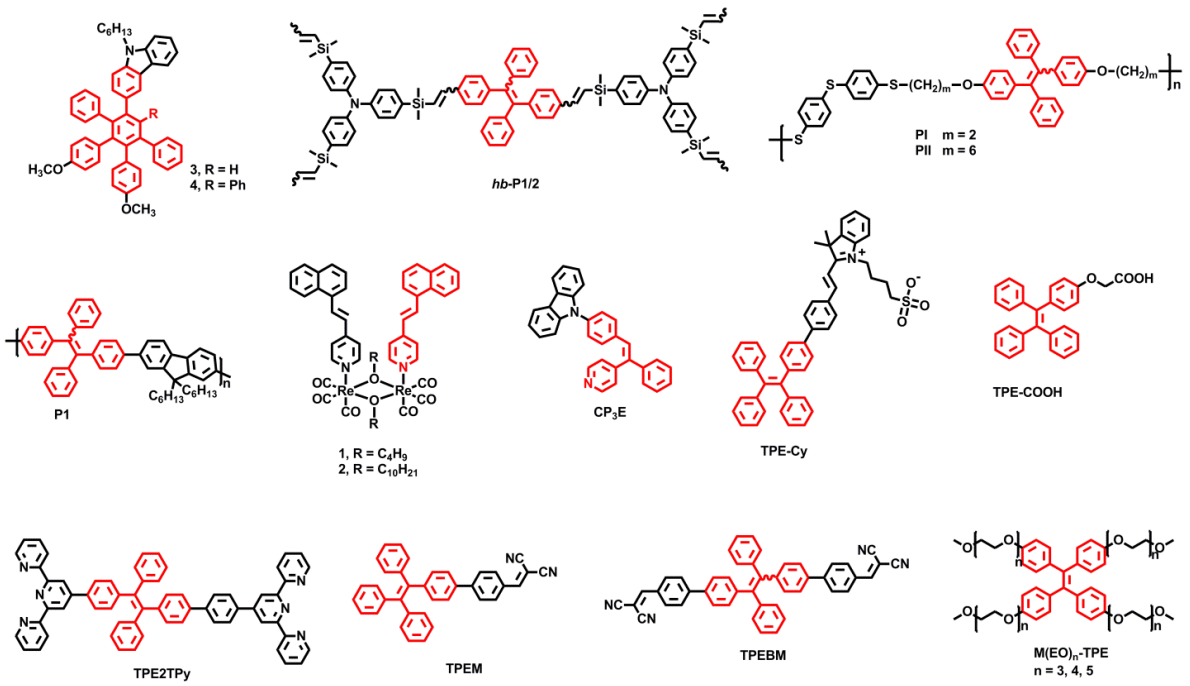

Figure 1.12. Examples of AIE luminogens used as chemosensor materials.

Explosive detection is of great importance and received much research interest driven by homeland security and anti-terrorism implications. AIE-active aryl-substituted carbazole derivatives[65] **3** and **4** (Figure 1.12) have been tested as explosive sensor for the selective detection of 2,4,6-trinitrotoluene (TNT) vapors or TNT in condensed phase *e.g.* as aqueous dispersion. Hereby, the electron-rich carbazole units improve the interaction with electron-poor nitroaromatic analytes. A high sensitivity towards TNT on the picogram level was detected. Stern-Volmer plots of **3** and **4** aggregates in aqueous dispersion (8/2 water/THF) give quenching constants (K_{sv}) of 13.3×10^5 M^{-1} and 10.0×10^5 M^{-1}, respectively, which are among the highest values from literature. *Hb*-P1/2[66] is a hyperbranched polymer and nanoaggregates of *Hb*-P1/2 in aqueous dispersion (9/1 water/THF) were used to detect picric acid (PA) as another nitroaromatic analyte. The quenching efficiency is nonlinearly enhanced with increasing quencher concentration, in line with a superamplification effect, that means the Stern-Volmer plots are upward bended thus

indicating more efficient PL quenching with increasing nitroaromatic explosive concentration. A similar behaviour was observed for other polymers, PI and PII[67], which were synthesized *via* thiol-bromo click polymerization, as well as polymer P1[68]. Two metal-containing binuclear rhenium (I) complexes (**1** and **2**)[69] with AIE behaviour were also reported. Nanoaggregates of **2** in 1/9 DCM/CH_3CN were used to detect PA and showed superamplified PL quenching with a K_{sv} of 1.0×10^5 M^{-1} for low PA concentration. The reason of the observed superamplification effects maybe that the three-dimensional interaction of the sensor molecules within the nanoaggregates allows for an efficient exciton diffusion, thus increasing the quenching radius in the condensed state.

The pH value is a very important parameter for all kinds of life, because small changes can cause distinct responses. So, a series of AIE luminogens has been developed for pH sensing. For example, a pyridinyl-containing molecule CP_3E[70] was used as pH sensor both in solution and in the solid state, as well as chemosensor for acidic and basic organic vapors through reversible protonation and deprotonation of the pyridinyl moiety. The intracellular pH (pH_i) is an important factor under "normal" and pathological conditions. A biocompatible and cell-permeable pH_i sensor was prepared based on the AIE-active TPE-Cy[71] containing zwitterionic and hydrophilic cyanine units. TPE-Cy shows different emission colors from red to blue when going from an extracellular pH 10 to an intracellular physiological pH range of pH_i 4.7 – 8.0. So, the emission color can serve as a reliable indicator for the local proton concentration. Metal ion detection with AIE probes was also demonstrated. Terpyridine-functionalized TPE (TPE2TPy)[72] was utilized as a "turn-off" PL sensor for metal ions due to the strong and directed metal-coordination capacity of terpyridine. Among different ions, especially Zn(II) and Fe(II) gave significant responses: A ~50 nm bathochromic shift was observed after addition of Zn(II), which allows discrimination against other metal ions. In contrast, addition of Fe(II) causes an obvious color change from colorless to magenta for a fast identification of Fe(II) in aqueous solution, also by the naked eye. In another publication, the detection of Al(III) ion in living cells based on an AIE luminogen called TPE-COOH[73] was reported. TPE-COOH functions as "turn-on" sensor due to the interaction between carboxyl group of TPE-COOH and Al(III) under activation of the fluorescence of the molecule with a high sensitivity detection limit of 21.6 nM. The effect is coupled with a high selectivity towards other metal ions. Furthermore, an imaging detection and real-time monitoring of Al(III) in living Hela cells was realized thanks to the PL acceleration through the AIE effect. TPE derivatives (TPEM and TPEBM)[74] containing terminal dicyanovinyl

moieties showing distinct AIE and ICT effects were also reported. Due to strong solvatochromic effects TPEM and TPEBM are also sensitive water indicators, both qualitatively and harf-quantitatively, with low detection limits of 63 ppm and 109 ppm for water in THF, respectively. Moreover, the presence of dicyanovinyl groups also allows for a nucleophilic interaction with cyanide. Under assistance of cetyltrimethylammonium bromide as surfactant a sensitive and selective sensing for cyanide in water with a low detection limit of 0.2 µM and a short detection time of 100 s was possible. The last example for AIE-active molecules as chemical sensors concerns the TPE derivatives ($M(EO)_n$-TPE)[75] which were utilized as temperature sensor based on the temperature-dependent hydration of the hydrophilic peripheral oligo(ethylene glycol) chains of $M(EO)_n$-TPE. Upon heating an aqueous solution over a certain cloud point the solution became turbid due to aggregation. Simultaneously, the PL of the solutions abruptly increase driven by the aggregation of individual $M(EO)_n$-TPE molecules. These thermoresponsive properties favour $M(EO)_n$-TPE as potential optical temperature sensors.

1.4.3 Bioimaging

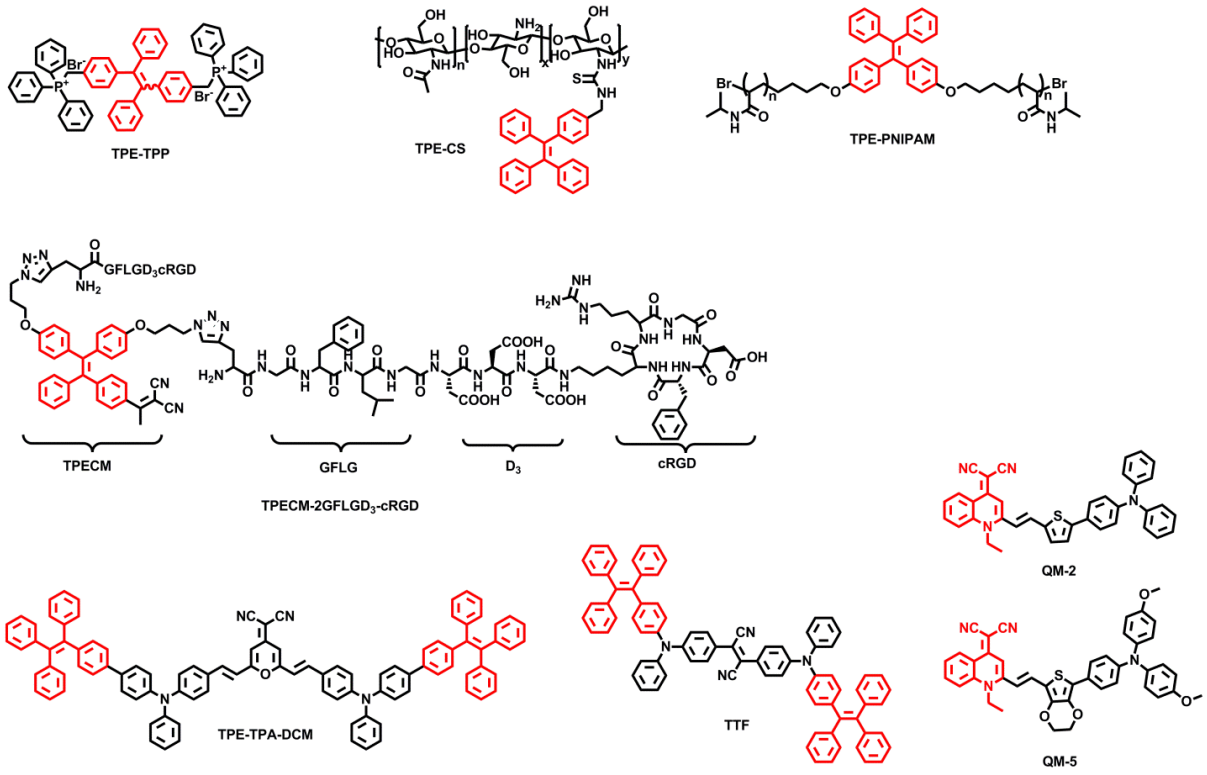

Figure 1.13. Chemical structures of AIE luminogens used for cell imaging applications.

Bioimaging is a very promising and challenging research area in bio-pharmaceutical science. Compared with other bioimaging techniques, fluorescence imaging (PL imaging) shows certain advantages such as high sensitivity, simple operation and potentially low costs. Inorganic quantum dots (QDs) and organic nanoparticles have been widely studied for bioimaging. Nevertheless, QDs often show a potential cytotoxicity (*e.g.* Se-based or Cd-based systems). Organic nanoparticles often suffer from the ACQ effect. Therefore, organic, AIE-based nanoparticles may be a reasonable alternative thanks to their good biocompatibility, sufficient photostability, and promising AIE properties. Some examples of AIE luminogens used for cell imaging applications are depicted in Figure 1.13.

An AIE fluorescent probe (TPE-TPP)[76] consisting two triphenylphosphonium (TPP) substituents coupled to an AIE-active TPE core was designed for mitochondrial imaging. The TPP groups bring in the mitochondrial-targeting ability due to their lipophilicity and electrophoretic force. TPE-TPP also exhibits excellent photostability (the condensed state of the nanoaggregates reduces photobleaching and photooxidation) and tolerance to microenvironmental changes. Together with the distinct AIE effect TPE-TPP represents a promising probe for cell tracking and imaging. TPE-CS[77] bioconjugates also show typical AIE behavior and pH sensitivity (caused by its poor solubility at high pH), as a potentially promising fluorescence turn-on (light-up) probe for intracellular imaging. Long retention times of TPE-CS particles within cells allow for a tracing of stained cells up to 15 passages. Temperature-sensitive nanoparticles composed of two PNIPAM chains attached to a TPE core (TPE-PNIPAM)[78] show a good biocompatibility and no cytotoxicity. The size of the particles can be tuned by changing the temperature due to the occurrence of a lower critical solution temperature (LCST). These nanoparticles were readily internalized by HeLa cells and used for long-term cellular tracing. The AIE luminogen TPECM-2GFLGD$_3$-cRGD[79] was used for the cell-specific turn-on (light-up) imaging. Hereby, the response signal for MDA-MB-231 cells was much stronger than that for MCF7 and 293T cells. Moreover, it can be also used as semiquanlitative AIE probe inside cells since the PL response in the cells after incubation is concentration-dependent. In living systems, far-red and near-infrared (FR/NIR) emission (>650 nm) can overcome interference problems coupled to the optical absorption, light scattering and autofluorescence of biological media. The AIE luminogen TPE-TPA-DCM loaded onto BSA NPs[80] (668 nm) were used for *in vitro* and *in vivo* FR/NIR bioimaging with low cytotoxicity for MCF-7 breast-cancer cells and murine hepatoma-22(H_{22})-tumor-bearing mice models, respectively. Compared to bare

TPE-TPA-DCM NPs, TPE-TPA-DCM-loaded BSA NPs showed an enhanced cancer cell uptake and a clear differentiation of tumor cells against other tissues due to the enhanced permeability and retention effects. Red-emissive TTF-doped-silica NPs[81] were studied for multimodal, non-linear optical microscopic imaging of tumor cells and *in vivo* imaging of mouse brains, with strong photobleaching and photoblinking resistance and excellent biocompatibility. First shape-specific tumor targeting experiments using bare AIE-active NIR NPs were reported based on quinolone-malononitrile (QM) derivatives[82]. QM-5 nanoaggregates with spherical shape exhibited much higher tumor-targeting capacity than rod-like QM-2 nanoaggregates, a behavior, that was ascribed to a so-called "passive" tumor-targeting by enhanced permeability and retention.

In summary, AIE-active organic materials have been studied for many optical and electronic applications based on their distinctive AIE activity (they are highly emissive in the aggregated/solid state). They show remarkable advantages in the aforementioned application fields. Although a lot of work has been already done till now, there are still more possibilities to be explored. Through further molecules design and testing, a deeper understanding of the underlying effects will be extracted. Furthermore, also novel applications in medicine, life science, optoelectronic devices may be explored in the near future.

1.5 References

1. S. Bonacchi, D. Genovese, R. Juris, M. Montalti, L. Prodi, E. Rampazzo and N. Zaccheroni, *Angew. Chem., Int. Ed.*, 2011, **50**, 4056-4066.
2. S. N. Baker and G. A. Baker, *Angew. Chem., Int. Ed.*, 2010, **49**, 6726-6744.
3. Z. Zhao, J. W. Y. Lam and B. Z. Tang, *Soft Matter*, 2013, **9**, 4564-4579.
4. K. M. C. Wong and V. W. W. Yam, *Acc. Chem. Res.*, 2011, **44**, 424-434.
5. L. Maggini and D. Bonifazi, *Chem. Soc. Rev.*, 2012, **41**, 211-241.
6. G. Accorsi, A. Listorti, K. Yoosaf and N. Armaroli, *Chem. Soc. Rev.*, 2009, **38**, 1690-1700.
7. Y. J. Cui, Y. F. Yue, G. D. Qian and B. L. Chen, *Chem. Rev.*, 2012, **112**, 1126-1162.
8. B. Souharce, C. J. Kudla, M. Forster, J. Steiger, R. Anselmann, H. Thiem and U. Scherf, *Macromol. Rapid Commun.*, 2009, **30**, 1258-1262.
9. S. Gamerith, A. Klug, H. Scheiber, U. Scherf, E. Moderegger and E. J. W. List, *Adv. Funct. Mater.*, 2007, **17**, 3111-3118.
10. J. Yong Choi, W. Kang, B. Kang, W. Cha, S. K. Son, Y. Yoon, H. Kim, Y. Kang, M. J. Ko, H. J. Son, K. Cho, J. H. Cho and B. Kim, *ACS Appl. Mater. Interfaces*, 2015, **7**, 6002-6012.
11. H. Yersin, Highly Efficient OLEDs with Phosphorescent Materials, *Wiley-VCH, Weinheim*, 2008.
12. K. Müllen and U. Scherf, Organic Light-Emitting Devices. Synthesis Properties and Applications, *Wiley-VCH, Weinheim*, 2006.
13. W. Y. Wong and C. L. Ho, *J. Mater. Chem.*, 2009, **19**, 4457-4482.
14. R. C. Mulherin, S. Jung, S. Huettner, K. Johnson, P. Kohn, M. Sommer, S. Allard, U. Scherf and N. C. Greenham, *Nano Lett.*, 2011, **11**, 4846-4851.
15. K. A. Mazzio and C. K. Luscombe, *Chem. Soc. Rev.*, 2015, **44**, 78-90.
16. H. Youn, H. J. Park and L. J. Guo, *Small*, 2015, **11**, 2228-2246.
17. A. Burns, H. Ow and U. Wiesner, *Chem. Soc. Rev.*, 2006, **35**, 1028-1042.
18. J. S. Wu, W. M. Liu, J. C. Ge, H. Y. Zhang and P. F. Wang, *Chem. Soc. Rev.*, 2011, **40**, 3483-3495.
19. Y. Salinas, R. MartinezManez, M. D. Marcos, F. Sancenon, A. M. Costero, M. Parra and S. Gil, *Chem. Soc. Rev.*, 2012, **41**, 1261-1296.
20. M. Schaferling, *Angew. Chem., Int. Ed.*, 2012, **51**, 3532-3554.
21. E. L. Que, D. W. Domaille and C. J. Chang, *Chem. Rev.*, 2008, **108**, 1517-1549.

22. Y. M. Yang, Q. Zhao, W. Feng and F. Y. Li, *Chem. Rev.*, 2013, **113**, 192-270.
23. H. Mattoussi, G. Palui and H. B. Na, *Adv. Drug Deliv. Rev.*, 2012, **64**, 138-166.
24. K. Kikuchi, *Chem. Soc. Rev.*, 2010, **39**, 2048-2053.
25. Y. Nia and J. Wu, *Org. Biomol. Chem.*, 2014, **12**, 3774-3791.
26. N. Tessler, G. J. Denton and R. H. Friend, *Nature*, 1996, **382**, 695-697.
27. M. D. McGehee and A. J. Heeger, *Adv. Mater.*, 2000, **12**, 1655-1668.
28. U Scherf, S Riechel, U Lemmer and R.F Mahrt, *Curr. Opin. Solid State Mater. Sci.*, 2001, **5**, 143-154.
29. M. Belletête, J. Bouchard, M. Leclerc and G. Durocher, *Macromolecules*, 2005, **38**, 880-887.
30. R. Jakubiak, C. J. Collison, W. C. Wan and L. Rothberg, *J. Phys. Chem. A*, 1999, **103**, 2394-2398.
31. M. Grell, D. D. C. Bradley, X. Long, T. Chamberlain, M. Inbasekaran, E. P. Woo and M. Soliman, *Acta Polym.*, 1998, **49**, 439-444.
32. J. Wang, Y. Zhao, C. Dou, H. Sun, P. Xu, K. Ye, J. Zhang, S. Jiang, F. Li and Y. Wang, *J. Phys. Chem. B*, 2007, **111**, 5082-5089.
33. S.-F. Lim, R. H. Friend, I. D. Rees, J. Li, Y. Ma, K. Robinson, A. B. Holms, E. Hennebicq, D. Beljonne and F. Cacialli, *Adv. Funct. Mater.*, 2005, **15**, 981-988.
34. C.-W. Wu, C.-M. Tsai and H.-C. Lin, *Macromolecules*, 2006, **39**, 4298-4305.
35. A. Kraft, A. C. Grimsdale and A. B. Holmes, *Angew. Chem., Int. Ed.*, 1998, **37**, 402-428.
36. L. Chen, S. Xu, D. McBranch and D. Whitten, *J. Am. Chem. Soc.*, 2000, **122**, 9302-9303.
37. S. Setayesh, A. C. Grimsdale, T. Weil, V. Enkelmann, K. Müllen, F. Meghdadi, E. J. W. List and G. Leising, *J. Am. Chem. Soc.*, 2001, **123**, 946-953.
38. F. He, Y. Tang, S. Wang, Y. Li and D. Zhu, *J. Am. Chem. Soc.*, 2005, **127**, 12343-12346.
39. S. Setayesh, A. C. Grimsdale, T. Weil, V. Enkelmann, K. Müllen, F. Meghdadi, E. J. W. List and G. Leising, *J. Am. Chem. Soc.*, 2001, **123**, 946-953.
40. S. Hecht and J. M. J. Frechet, *Angew. Chem., Int. Ed.*, 2001, **40**, 74-91.
41. Z. Xie, B. Yang, F. Li, G. Cheng, L. Liu, G. Yang, H. Xu, L. Ye, M. Hanif, S. Liu, D. Ma and Y. Ma, *J. Am. Chem. Soc.*, 2005, **127**, 14152-14153.
42. B. K. An, S. K. Kwon, S. D. Jung, S. Y. Park, *J. Am. Chem. Soc.*, 2002, **124**, 14410-14415.
43. N. Sanyal and P. M. Lahti, *Cryst. Growth Des.*, 2006, **6**, 1253-1255.
44. J. Luo, Z. Xie, J. W. Y. Lam, L. Cheng, H. Chen, C. Qiu, H. S. Kwok, X. Zhan, Y. Liu, D. Zhu and B. Z. Tang, *Chem. Commun.*, 2001, 1740-1741.

45. B. Z. Tang, X. Zhan, G. Yu, P. P. S. Lee, Y. Liu and D. Zhu, *J. Mater. Chem.*, 2001, **11**, 2974-2978.
46. J. Chen, C. C. W. Law, J. W. Y. Lam, Y. Dong, S. M. F. Lo, I. D. Williams, D. Zhu and B. Z. Tang, *Chem. Mater.*, 2003, **15**, 1535-1546.
47. Y. Hong, J. W. Y. Lam and B. Z. Tang, *Chem. Commun.*, 2009, 4332-4353.
48. J. Mei , Y. Hong , J. W. Y. Lam , A. Qin , Y. Tang and B. Z. Tang, *Adv. Mater.*, 2014, **26**, 5429-5479.
49. X. Fan, J. Sun, F. Wang, Z. Chu, P. Wang, Y. Dong, R. Hu, B. Z. Tang and D. Zou, *Chem. Commun.*, 2008, 2989-2991.
50. G.-F. Zhang, Z.-Q. Chen, M. P. Aldred, Z. Hu, T. Chen, Z. Huang, X. Meng and M.-Q. Zhu, *Chem. Commun.*, 2014, **50**, 12058-12060.
51. Z. Zhao, B. He, H. Nie, B. Chen, P. Lu, A. Qin and B. Z. Tang, *Chem. Commun.*, 2014, **50**, 1131-1133.
52. N. L. C. Leung, N. Xie, W. Yuan, Y. Liu, Q. Wu, Q. Peng, Q. Miao, J. W. Y. Lam and B. Z. Tang, *Chem. Eur. J.*, 2014, **20**, 15349-15353.
53. W. Z. Yuan, P. Lu, S. Chen, J. W. Y. Lam, Z. Wang, Y. Liu, H. S. Kwok, Y. Ma and B. Z. Tang, *Adv. Mater.*, 2010, **22**, 2159-2163.
54. Y. Liu, X. Ye, G. Liu, Y. Lv, X. Zhang, S. Chen, J. W. Y. Lam, H. S. Kwok, X. Tao and B. Z. Tang, *J. Mater. Chem. C*, 2014, **2**, 1004-1009.
55. W. Qin, J. Liu, S. Chen, J. W. Y. Lam, M. Arseneault, Z. Yang, Q. Zhao, H. S. Kwok and B. Z. Tang, *J. Mater. Chem. C*, 2014, **2**, 3756-3761.
56. J. Mei, J. Wang, J. Z. Sun, H. Zhao, W. Yuan, C. Deng, S. Chen, H. H. Y. Sung, P. Lu, A. Qin, H. S. Kwok, Y. Ma, I. D. Williams and B. Z. Tang, *Chem. Sci.*, 2012, **3**, 549-558.
57. L. Chen, Y. Jiang, H. Nie, R. Hu, H. S. Kwok, F. Huang, A. Qin, Z. Zhao and B. Z. Tang, *ACS Appl. Mater. Interfaces*, 2014, **6**, 17215-17225.
58. J. Huang, N. Sun, J. Yang, R. Tang, Q. Li, D. Ma and Z. Li, *Adv. Funct. Mater.*, 2014, **24**, 7645-7654.
59. J. Huang, Y. Jiang, J. Yang, R. Tang, N. Xie, Q. Li, H. S. Kwok, B. Z. Tang and Z. Li, *J. Mater. Chem. C*, 2014, **2**, 2028-2036.
60. J. Huang, N. Sun, Y. Dong, R. Tang, P. Lu, P. Cai, Q. Li, D. Ma, J. Qin and Z. Li, *Adv. Funct. Mater.*, 2013, **23**, 2329-2337.
61. J. Huang, N. Sun, P. Chen, R. Tang, Q. Li, D. Ma and Z. Li, *Chem. Commun.*, 2014, **50**, 2136-2138.

62. W. Qin, Z. Yang, Y. Jiang, J. W. Y. Lam, G. Liang, H. S. Kwok and B. Z. Tang, *Chem. Mater.*, 2015, **27**, 3892-3901.
63. X. Du, J. Qi, Z. Zhang, D. Ma and Z. Y. Wang, *Chem. Mater.*, 2012, **24**, 2178-2185.
64. L. Yao, S. Zhang, R. Wang, W. Li, F. Shen, B. Yang and Y. Ma, *Angew. Chem., Int. Ed.*, 2014, **53**, 2119-2123.
65. M. Kumar, V. Vij and V. Bhalla, *Langmuir*, 2012, **28**, 12417-12421.
66. P. Lu, J. W. Y. Lam, J. Liu, C. K. W. Jim, W. Yuan, N. Xie, Y. Zhong, Q. Hu, K. S. Wong, K. K. L. Cheuk and B. Z. Tang, *Macromol. Rapid Commun.*, 2010, **31**, 834-839.
67. Y. Zhang, G. Chen, Y. Lin, L. Zhao, W. Z. Yuan, P. Lu, C. K. W. Jim, Y. Zhang and B. Z. Tang, *Polym. Chem.*, 2015, **6**, 97-105.
68. W. Wu, S. Ye, R. Tang, L. Huang, Q. Li, G. Yu, Y. Liu, J. Qin and Z. Li, *Polymer*, 2012, **53**, 3163-3171.
69. V. Sathish, A. Ramdass, Z.-Z. Lu, M. Velayudham, P. Thanasekaran, K.-L. Lu and S. Rajagopal, *J. Phys. Chem. B*, 2013, **117**, 14358-14366.
70. Z. Yang, W. Qin, J. W. Y. Lam, S. Chen, H. H. Y. Sung, I. D. Williams and B. Z. Tang, *Chem. Sci.*, 2013, **4**, 3725-373.
71. S. Chen, Y. Hong, Y. Liu, J. Liu, C. W. T. Leung, M. Li, R. T. K. Kwok, E. Zhao, J. W. Y. Lam, Y. Yu and B. Z. Tang, *J. Am. Chem. Soc.*, 2013, **135**, 4926-4929.
72. Y. Hong, S. Chen, C. W. T. Leung, J. W. Y. Lam, J. Liu, N.-W. Tseng, R. T. K. Kwok, Y. Yu, Z. Wang and B. Z. Tang, *ACS Appl. Mater. Interfaces*, 2011, **3**, 3411-3418.
73. S. Gui, Y. Huang, F. Hu, Y. Jin, G. Zhang, L. Yan, D. Zhang and R. Zhao, *Anal. Chem.*, 2015, **87**, 1470-1474.
74. Y. Zhang, D. Li, Y. Li and J. Yu, *Chem. Sci.*, 2014, **5**, 2710-2716.
75. X. Yin, F. Meng and L. Wang, *J. Mater. Chem. C*, 2013, **1**, 6767-6773.
76. C. W. T. Leung, Y. Hong, S. Chen, E. Zhao, J. W. Y. Lam and B. Z. Tang, *J. Am. Chem. Soc.*, 2013, **135**, 62-65.
77. Z. Wang, S. Chen, J. W. Y. Lam, W. Qin, R. T. K. Kwok, N. Xie, Q. Hu and B. Z. Tang, *J. Am. Chem. Soc.*, 2013, **135**, 8238-8245.
78. Z. Wang, T.-Y. Yong, J. Wan, Z.-H. Li, H. Zhao, Y. Zhao, L. Gan, X.-L. Yang, H.-B. Xu and C. Zhang, *ACS Appl. Mater. Interfaces*, 2015, **7**, 3420-3425.
79. Y. Yuan, C.-J. Zhang, M. Gao, R. Zhang, B. Z. Tang and B. Liu, *Angew. Chem., Int. Ed.*, 2015, **54**, 1780-1786.
80. W. Qin, D. Ding, J. Liu, W. Z. Yuan, Y. Hu, B. Liu and B. Z. Tang, *Adv. Funct. Mater.*, 2012, **22**, 771-779.

81. J. Qian, Z. Zhu, A. Qin, W. Qin, L. Chu, F. Cai, H. Zhang, Q. Wu, R. Hu, B. Z. Tang and S. He, *Adv. Mater.*, 2015, **27**, 2332-2339.
82. A. Shao, Y. Xie, S. Zhu, Z. Guo, S. Zhu, J. Guo, P. Shi, T. D. James, H. Tian and W.-H. Zhu, *Angew. Chem., Int. Ed.*, 2015, **54**, 7275-7280.
83. X. Li, K. Ma, S. Zhu, S. Yao, Z. Liu, B. Xu, B. Yang and W. Tian, *Anal. Chem.*, 2014, **86**, 298-303.
84. J. Tong, Y. Wang, J. Mei, J. Wang, A. Qin, J. Z. Sun and B. Z. Tang, *Chem. Eur. J.*, 2014, **20**, 4661-4670.
85. X. Zhu, R. Liu, Y. Li, H. Huang, Q. Wang, D. Wang, X. Zhu, S. Liu and H. Zhu, *Chem. Commun.*, 2014, **50**, 12951-12954.
86. R. Yoshii, A. Hirose, K. Tanaka and Y. Chujo, *J. Am. Chem. Soc.*, 2014, **136**, 18131-18139.
87. X. Wang, J. Hu, G. Zhang and S. Liu, *J. Am. Chem. Soc.*, 2014, **136**, 9890-9893.
88. Q. Lin, Q.-P. Yang, B. Sun, Y.-P. Fu, X. Zhu, T.-B. Wei and Y.-M. Zhang, *Soft Matter*, 2014, **10**, 8427-8432.
89. Q. Lin, T.-T. Lu, X. Zhu, B. Sun, Q.-P. Yang, T.-B. Wei and Y.-M. Zhang, *Chem. Commun.*, 2015, **51**, 1635-1638.

Chapter 2

2. Polycarbazoles with AIE-active Triphenylethylene and Tetraphenylethylene Side Groups[1]

Novel conjugated polymers based on 3,6-carbazole repeat units were synthesized by nickel-catalyzed Yamamoto coupling under microwave heating. The resulting poly(3,6-carbazole)s contain tetraphenylethylene (TPE) units in their side chains. The resultant polymers show aggregation induced emission (AIE) behavior. Hereby, the photoluminescence (PL) intensity of PCzTPE0.5 in 90% water/THF is 35 times higher than that in pure THF, connected to the introduction of TPE side chains. The ability of polymer PCzTPE0.5 for explosive sensing was also studied. A maximum Stern-Volmer quenching constant of $1.26\times10^6\ M^{-1}$ was observed for PL quenching of PCzTPE0.5 aggregates by trinitrobenzene (TNB). A solid state paper strip test based on PCzTPE0.5 and PCzTPE also demonstrates effective PL quenching towards both TNB vapor and solution.

2.1 Introduction

As outlined in the introduction, numerous AIE materials have been designed and tested for optoelectronic applications. However, most of them developed so far are low molecular weight molecules. Therefore, it is challenging to extend the synthetic approaches to AIE polymers. Polymers should be suitable for fabricating large-area, thin films, also with simple processes such as spin coating, film casting, doctor blading, or inkjet printing.

Tri- and tetraphenylethylene luminogens are widely used AIE chromophores[2-4], showing distinct AIE effects. They are accessible in simple synthetic schemes. Symmetrical tetraphenylethylene (TPE) derivatives can be synthesized through McMurry-type couplings (*e.g.* with $TiCl_3$ or $TiCl_4$ in THF)[5]. Asymmetrically substituted ones are obtained by treating benzophenone derivatives with diphenylmethyl lithium derivatives followed by acid-catalyzed dehydration[6]. Synthesis of TPE derivitives is much easier than that of silole-based AIE luminogens. As mentioned, TPE is an excellent and prototypical AIE chromophore[7]: The fluorescence quantum yield in THF solution is only 0.24%, but it

increases in the solid state (film) to 49.2%, with a large AIE coefficient α_{AIE} of 205. Several π-conjugated TPE derivatives have been reported in the literature, most of them with distinct AIE effects. They have been used for applications in OLEDs, chemosensors, as bioprobes, *etc.*

In this chapter, we prepared novel conjugated carbazole-based polymers with AIE-active tri/tetraphenylethylene side chains (as shown in Chart 2.1). For comparision, *n*-octyl-substituted polycarbazole (PCz) was investigated, which shows typical ACQ properties. The 3,6-carbazole repeat units[8-10] were chosen for constructing the polycarbazole backbone since their electron-donor character which should be beneficial for the interaction with electron-poor trinitroaromatics. The incorporation of tri/tetraphenylethylene unit into the side chains could adjust their AIE activity, without strongly affecting the electronic properties of the polycarbazole backbone. Based on this design principle we expect a high sensitivity for the detection of nitroaromatic compounds. Among them, PCzTPE and PCzTPE0.5 are the first AIE polyaromatics with the AIE-active groups in the side chain.

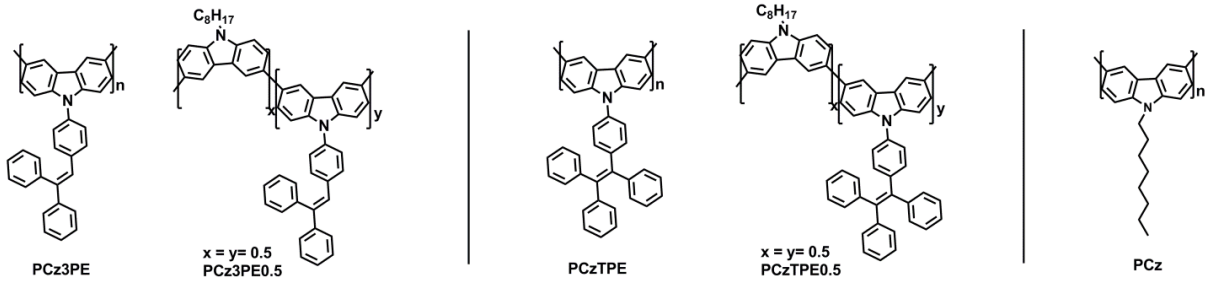

Chart 2.1. Chemical structures of polycarbazoles.

2.2 Results and Discussion

2.2.1 Synthesis and Characterization

The synthetic routes to the monomers and polymers are depicted in Scheme 2.1. Treatment of diethyl (4-iodobenzyl)phosphonate with *t*-BuOK followed by adding benzophenone afforded 2-(4-iodophenyl)-1,1-diphenylethylene *via* a Witting-Horner olefination. The *N*-carbazolyl-triphenylethylene derivative **1** was obtained by Ullmann coupling between 2-(4-iodophenyl)-1,1-diphenylethylene and 3,6-dibromocarbazole. Monofluoro-TPE was synthesized by treating 4-fluorobenzophenone with diphenylmethyl lithium followed by acid-catalyzed dehydration[6]. The *N*-carbazolyl-TPE derivative **2** was obtained by catalyst-free *N*-arylation in a direct nucleophilic substitution of monofluoro-TPE as nonactivated fluorobenzene with

3,6-dibromocarbazole[11]. 3,6-Dibromo-9-octylcarbazole **3** was synthesized according to a reported procedure[12]. Homopolymer PCz, PCz3PE and PCzTPE and random copolymer PCz3PE0.5 and PCzTPE0.5 were synthesized from monomers **1** or **2** and **3** by Yamamoto-type coupling using bis(1,5-cyclooctadiene)nickel(0) ($Ni(COD)_2$) as coupling reagent in a mixture of THF, 1,5-cyclooctadiene (COD) and 2,2'-bipyridine (BPy) under microwave (MW) heating[13]. Following these protocol we could obtain the target conjugated polymers in short reaction times. The structure elucidation of the monomers was performed by NMR spectroscopy, mass spectrometry and elemental analysis. The chemical structure of the obtained polymers was confirmed by NMR spectroscopy, GPC, thermal analysis and optical spectroscopy.

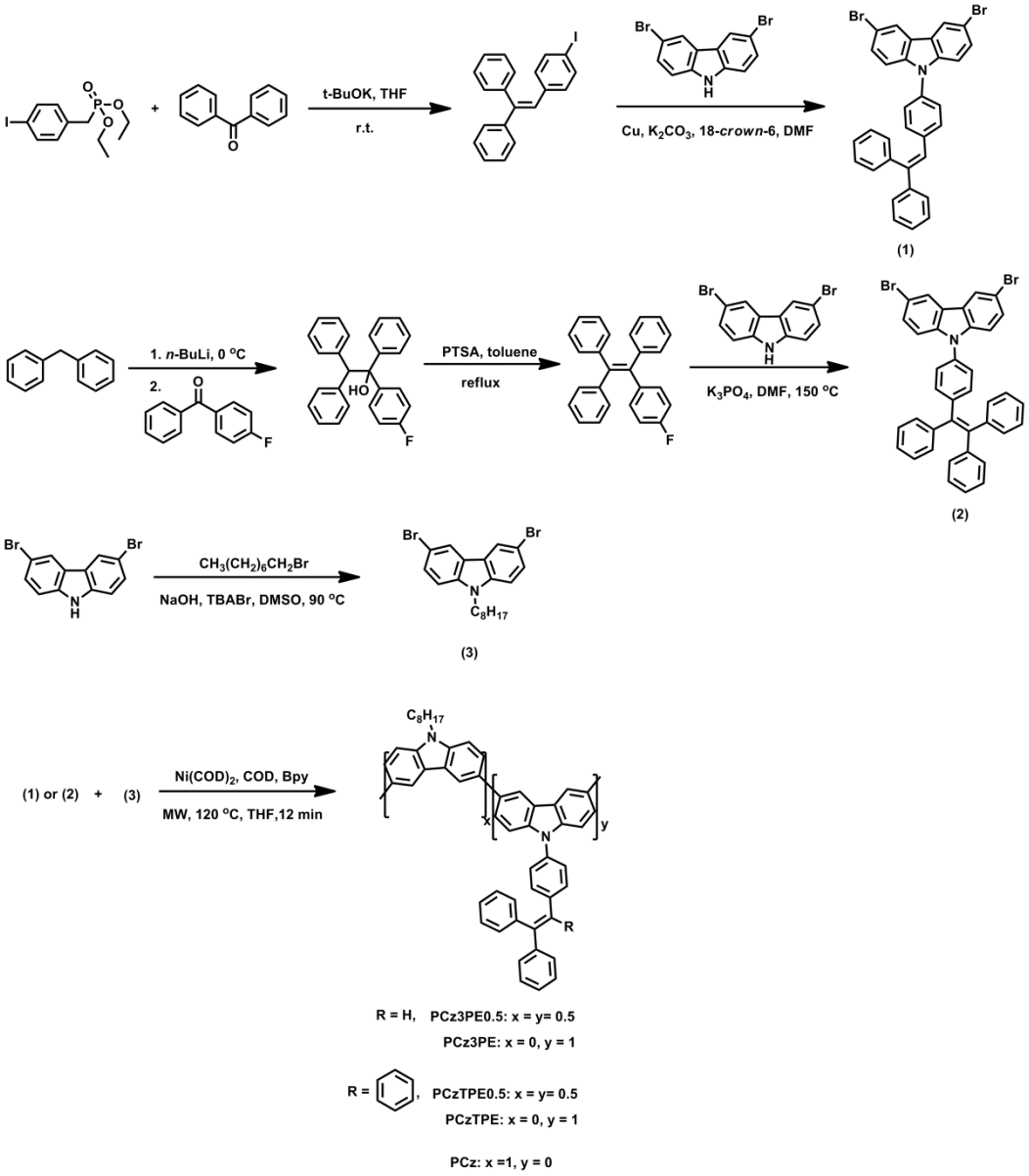

Scheme 2.1. Synthetic procedures for monomer and polymer synthesis.

2.2.2 Photophysical Properties

In the following paragraphs, we will discuss the photophysical properties of our novel polymers in two parts; since the polymers with triphenylethylene side groups and tetraphenylethylene groups show rather different behavior in nanoaggregate dispersions.

2.2.2.1 Triphenylethylene-substituted Polymers PCz3PE0.5 and PCz3PE

Table 2.1. Optical data of of PCz3PE and PCz3PE0.5.

	λ_{UV}/nm in THF	λ_{PL}/nm in THF	λ_{UV}/nm in film	λ_{PL}/nm in film	η_{PL} (%) in THF	η_{PL} (%) in film
PCz3PE0.5	319, 347 (sh)	476	320, 346 (sh)	467	38	14
PCz3PE	310, 353	475	315, 355	469	38	10

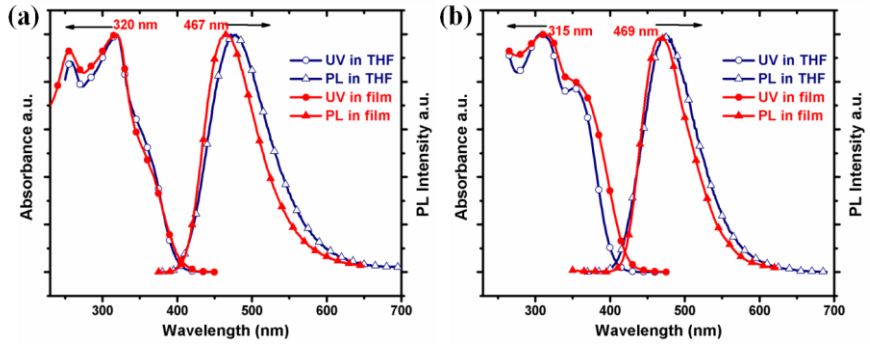

Figure 2.1. Absorption and PL spectra (excitation wavelength: 320 nm) of (a) PCz3PE0.5 and (b) PCz3PE in dilute THF solution (10^{-5} M) and as spin-coated films, measured at room temperature.

Figure 2.1 shows the absorption and PL spectra of PCz3PE0.5 and PCz3PE in THF solution and in the solid state (films). The absorption spectra of PCz3PE0.5 and PCz3PE are quite similar, their solid state absorption maxima appear at 320 and 315 nm, respectively. Both polymers show blue fluorescence with the PL maxima peaking around 470 nm. Note worthy the PL maxima of PCz3PE0.5 and PCz3PE in solution both show a minor red shift of 9 and 6 nm, respectively, compared to those of the films. Table 2.1 summarizes the optical data of PCz3PE0.5 and PCz3PE. The photoluminescence quantum yields (PLQYs) of PCz3PE and PCz3PE0.5 in dilute THF solution have been determined as 38% for both polymers, by using quinine sulfate as standard. The PLQYs of the films are 14% and 10% for PCz3PE0.5 and PCz3PE, respectively. As conclusion, the triphenylethylene-substituted polycarbazoles

PCz3PE0.5 and PCz3PE do not exhibit any AIE properties. Contrary, they show typical aggregation-caused quenching (ACQ) behavior.

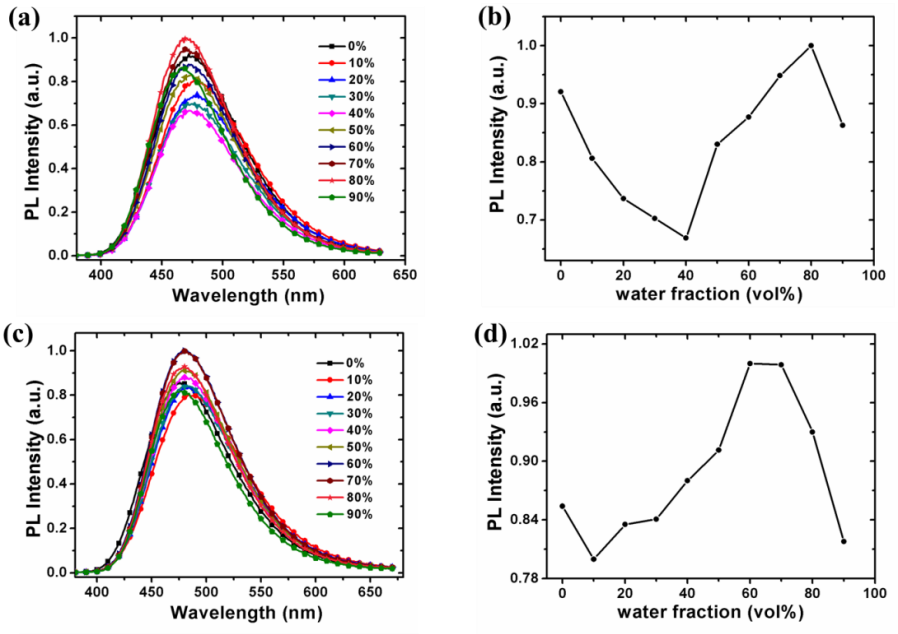

Figure 2.2. PL spectra of (a) PCz3PE0.5 and (c) PCz3PE in THF/water mixtures with different water content; PL intensity with increasing water fraction for (b) PCz3PE0.5 and (d) PCz3PE, respectively (polymer concentration: 10^{-5} M; excitation wavelength: 320 nm).

To further investigate the possible occurrence of AIE properties, we also recorded a series of PL spectra in THF/water solvent mixtures (see Figure 2.2). Hereby, THF is a good and water a non-solvent for both polymers. Therefore, the polymers are supposed to aggregate for a certain water fraction of the solvent mixtures. For PCz3PE0.5, the PL intensity first decreases with increasing water content up to 40%. After that, the PL intensity increases up to 80% water with an overall PL increase of ca. 1.5 times. For PCz3PE, the PL intensity first decreases up to 10% water, followed by a PL increase for 10% – 60% water, with a PL increase of ca. 1.3. These results again demonstrate that PCz3PE and PCz3PE0.5 do not show distinct AIE effects. That means, triphenylethylene-substitution of polycarbazoles does not result in good AIE luminogens.

2.2.2.2 Tetraphenylethylene-substituted Polymers PCzTPE and PCzTPE0.5

Table 2.2. Optical and electrochemical data of PCzTPE and PCzTPE0.5.

	λ_{UV}/nm in THF	λ_{PL}/nm in THF	λ_{UV}/nm in film	λ_{PL}/nm in film	η_{PL}(%) in THF	η_{PL}(%) in film	HOMO (eV)	LUMO (eV)
PCzTPE	307	314	495	495	1.1	20	-5.1	-2.0
PCzTPE0.5	305	310	490	493	0.8	21	-5.1	-1.9

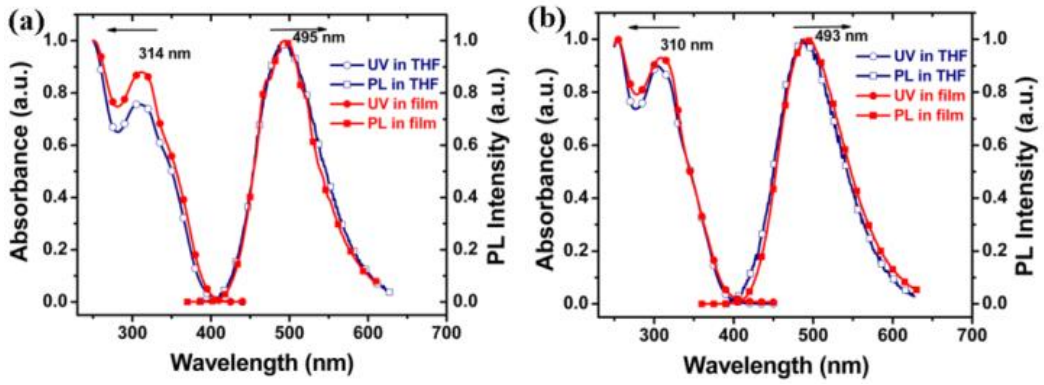

Figure 2.3. Absorption and PL spectra (excitation wavelength: 320 nm) of (a) PCzTPE and (b) PCzTPE0.5 in dilute THF solution (10^{-5} M) and as spin-coated films measured at room temperature.

According to the last paragraph, polycarbazoles with triphenylethylene substituents did not show obvious AIE phenomenons. Next, the triphenylethylene substituents were replaced by tetraphenylethlene (TPE) ones resulting in the polymers PCzTPE and PCzTPE0.5. With the exchange of a hydrogen by a phenyl ring (leading to the TPE structure) a more twisted conformation should result, what will be beneficial for the occurrence of AIE effects. Figure 2.3 shows the absorption and PL spectra of PCzTPE and PCzTPE0.5 in dilute THF solution and solid state films. The absorption spectra of PCzTPE and PCzTPE0.5 are very similar, with solid state peak maxima at 314 and 310 nm, respectively. In the PL spectra both polymers exhibit bluish-green emission peaking around 495 nm, both in solution and as thin films. This behavior is attributed to the incorporation of the TPE units – they effectively suppress π-π stacking in the condensed phase due to the presence of the propeller-shaped TPE side chain. The PLQYs of PCzTPE and PCzTPE0.5 in dilute THF solution, estimated by using quinine sulfate as standard, have been determined as 1.1% and 0.8%, respectively. The PLQYs distinctly increase to 20% and 21%, respectively, in solid state films, 18- and 26-fold higher if compared to THF solutions (see Table 2.2). Evidently, the transition into the

condensed state dramatically enhances the PL of the polymers. The AIE properties will be discussed in detail within the following paragraph.

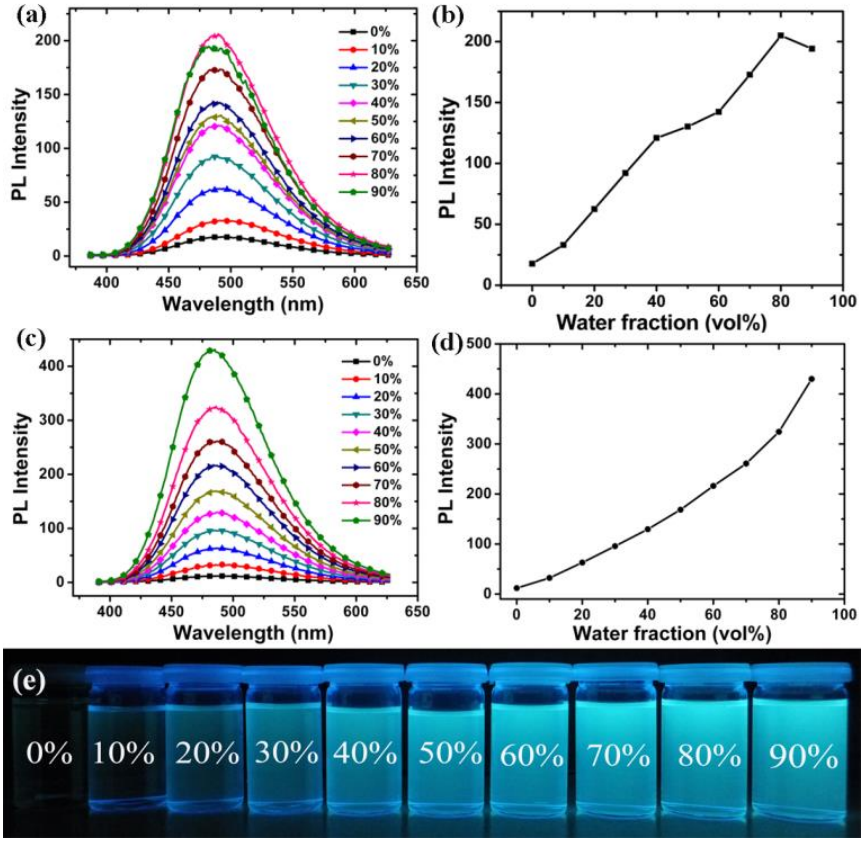

Figure 2.4. PL spectra of (a) PCzTPE and (c) PCzTPE0.5 in THF/water mixtures with different water content; increase of PL intensity with increasing water fraction for (b) PCzTPE and (d) PCzTPE0.5, respectively (polymer concentration: 10^{-5} M; excitation wavelength: 320 nm); (e) fluorescence images of PCzTPE0.5 in THF/water mixtures with different water content.

To further investigate the AIE effect with PCzTPE and PCzTPE0.5 a series of PL spectra in THF/water mixtures with increasing water fraction were recorded. Figure 2.4a/c show PL spectra of the polymers in such water/THF mixtures. The PL intensity increases progressively with increasing water fraction for both polymers. Hereby, polymer PCzTPE0.5 showed a more pronounced AIE effect if compared to the PCzTPE copolymer. For PCzTPE the PL intensity is 11 times higher for a water content of 80% if compared to pure THF (Figure 2.4b), and for PCzTPE0.5 35 times higher for a water content of 90% (Figure 2.4d). As water is a non-solvent for PCzTPE and PCzTPE0.5, both polymers are assumed to form solid-state aggregates in the THF/water mixtures with high water content, thus exhibiting aggregation-induced PL enhancement: they are AIE-active. The fluorescence images in

Figure 2.4e clearly show AIE effect with water addition. Caused by the high rotational freedom of the TPE side-chain moieties in solution, a high internal conversion rate results in weak emission. Within the aggregated (solid) state, however, the rotation of phenyl rings of the TPE units is strongly restricted, thus blocking non-radiative deactivation channels and leading to the AIE effect. A poly(*N*-octyl-3,6-carbazole) without TPE side groups that was generated as reference did not show any AIE activity (Figure 2.5).

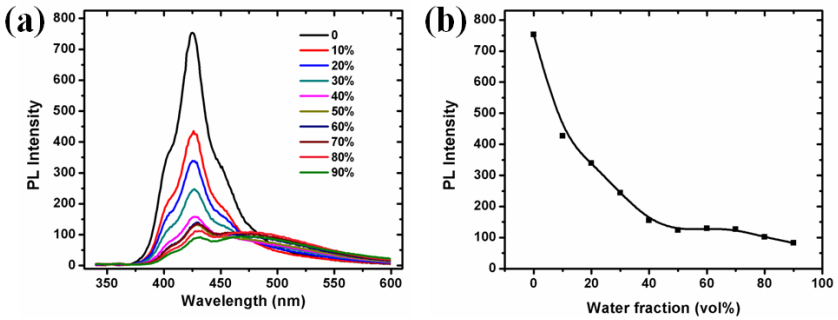

Figure 2.5. (a) PL spectra of PCz in THF/water mixtures with different water content; (b) PL intensity with increasing water fraction for PCz (polymer concentration: 10^{-5} M; excitation wavelength: 320 nm).

2.2.3 Thermal Properties

The thermal properties of PCzTPE0.5 and PCzTPE were investigated by TGA and DSC. Both polymers exhibit high thermal stability with 5% weight loss occurring at 490 and 430 °C, respectively. In DSC analysis we could not record glass transitions (T_g) up to 300 °C. High thermal stability is important for practical application in solid state sensors.

2.2.4 Explosive Detection

The detection of explosives, such as nitroaromatic compounds or peroxides becomes increasingly important in modern society, due to the concerns on global security and environmental protection[14-16]. Many methods have been developed for explosive detection, such as gas chromatography[17], mass spectrometry[18], surface enhanced Raman spectroscopy[19], ion mobility spectrometry[20], electrochemical sensing[21,22], PL spectroscopy[23,24], and others. Among them, PL sensors based on conjugated polymers[25] have been widely tested because of their simplicity and high sensitivity. Trinitroaromatic compounds containing three electron-withdrawing nitro groups are potent electron acceptors. The working principle of PL sensors for nitroaromatic compounds is based on a

photo-induced electron transfer from donor (conjugated polymer) to acceptor (nitroaromatic compound) thus resulting in PL quenching. Recently, AIE luminogens have been used in PL sensors for the detection of nitroaromatics[26-28], and there are two main benefits by using AIE luminogens for PL sensors: one is their high solid state fluorescence quantum yields; the other is their twisted, loosely packed structure, that accelerates diffusion of analyte molecules, thus enhancing the quenching efficiency.

2.2.4.1 Explosive Detection based on Aggregated PCzTPE0.5 Solutions

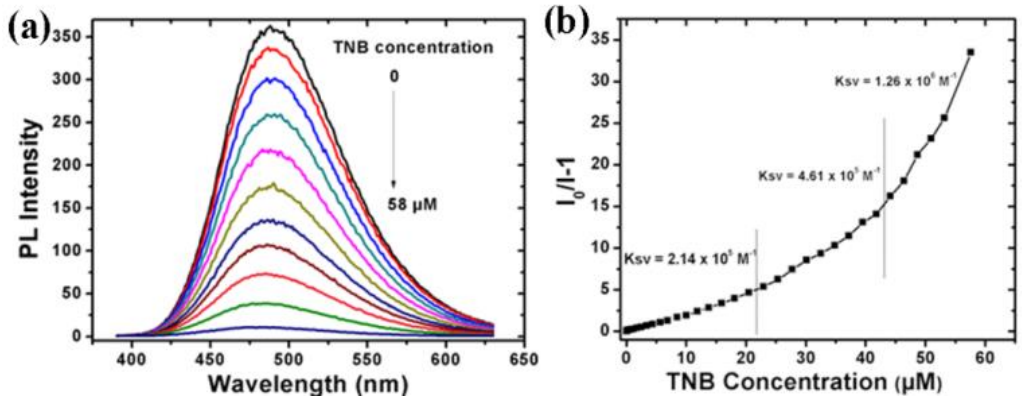

Figure 2.6. (a) PL spectra of PCzTPE0.5 in THF/water 1:9 containing different amounts of TNB (Polymer concentration: 10^{-5} M; λ_{ex}: 320 nm). (b) Stern-Volmer plots of PL intensity $I_0/I-1$ of PCzTPE0.5 *vs.* TNB concentration (I = PL intensity, I_0 = PL intensity at TNB concentration of 0 M).

PCzTPE and PCzTPE0.5 should show good electron-donor ability due to their electron-rich polycarbazole backbones. Moreover, their twisted 3D-structure should create effective pathways for interchain exciton diffusion leading to amplified PL quenching properties. Based on the above presented results we started our investigations with aggregated PCzTPE0.5 in THF/water 1:9 (polymer concentration: 10 µM). 1,3,5-trinitrobenzene (TNB) was chosen as prototypical nitroaromatic analyte. As shown in Figure 2.6a, the PL intensity of PCzTPE0.5 in THF/water 1:9 decreases progressively during addition of TNB, without changing the PL peak position, suggesting that different emissive species have not formed. The onset of PL quenching is found for addition of 50 nM TNB, low enough for the detection of submillimolar TNB concentrations. For a TNB concentration of 58 µM, the PL of the dispersed polymer nanoaggregates is fully quenched. The quenching response was analyzed by fitting the data with the Stern-Volmer equation, as depicted in Figure 2.6b. For TNB concentration below 21 µM, the Stern-Volmer plot is linear with a quenching constant of

2.14×10^5 M^{-1}. For higher analyte concentration, the curve bends upward, thus demonstrating an amplified quenching[29]. The quenching constant reaches ca. 1.26×10^6 M^{-1} between TNB concentration of 43 µM and 58 µM. This amplified quenching is attributed to the twisted 3D topology of the polymer chains in the nanoaggregates, leading to the formation of an increased number of quenching sites that can interact with TNB molecules and/or to an improved exciton diffusion to quenching sites[30].

2.2.4.2 Fluorescence Quenching Mechanism during Interaction with Nitroaromatic Compounds

Figure 2.7a shows that there is no spectral overlap between the absorption spectrum of TNB and the PL spectrum of PCzTPE0.5 (as prerequisite for Förster-type energy transfer) thus indicating that the main quenching mechanism for TNB addition should be an excited state charge transfer between the excited state of the host and the ground state of the TNB quencher, as depicted in Figure 2.8. The occurrence of charge transfer was further confirmed by cyclic voltammetry (Figure 2.7b). The HOMO (highest occupied molecular orbital) level of PCzTPE0.5 was estimated to ca. -5.1 eV, and the LUMO (lowest unoccupied molecular orbital) level of TNB to ca. -3.1 eV. Considering an optical bandgap (E_g) of 3.2 eV for PCzTPE0.5 from the onset of its UV/vis absorption band, the LUMO level of PCzTPE0.5 is calculated to be ca. -1.9 eV (Table 2.2). Therefore, the LUMO energy (-1.9 eV) of PCzTPE0.5 allows for an excited state electron transfer to the lower-lying LUMO level of TNB with a LUMO/LUMO offset of ca. 1.2 eV.

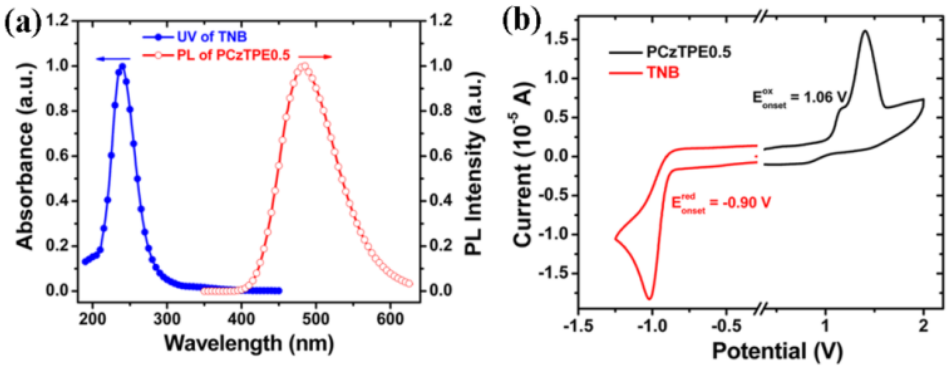

Figure 2.7. (a) Normalized absorption spectrum of TNB and PL spectrum of PCzTPE0.5 nanoaggregates in THF/water 1:9. (b) Cyclic voltammetry plots of PCzTPE0.5 in dichloromethane (oxidative scan) and TNB in acetonitrile (reductive scan), for the experimental conditions please see Experimental part.

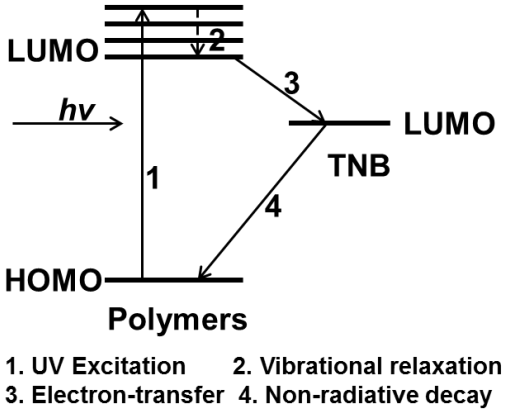

Figure 2.8. Schematic representation of the excited state electron-transfer process that causes PL quenching.

2.2.4.3 Explosive Detection based on PCzTPE and PCzTPE0.5 Paper Strips

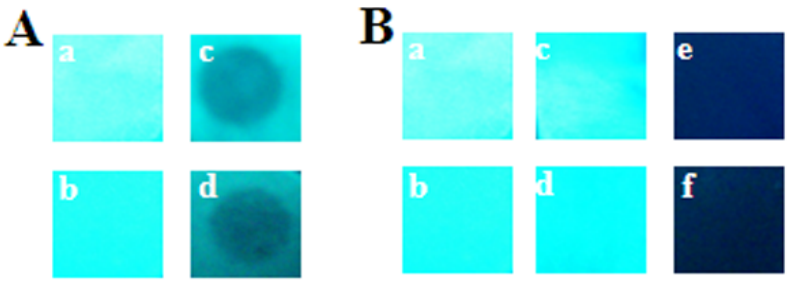

Figure 2.9. Paper strip tests. (A) Vapor-mode detection of TNB: test strips before (a,b) and after (c,d) placing the strips on top of a glass vial containing solid TNB for 5 min; for PCzTPE (a,c) or PCzTPE0.5 (b,d), respectively. (B) Solution-mode detection of TNB: test strips before (a,b) and after dipping the strips into pure THF (c,d) and into a 10^{-4} M TNB solution in THF (e,f); for PCzTPE (a,c,e) or PCzTPE0.5 (b,d,f), respectively.

For practical explosive detection, the availability of solid state sensor devices is of primary importance. Towards this goal, we prepared test strips by dip-coating Whatman filter paper into solutions of PCzTPE and PCzTPE0.5 in THF (10^{-4} M) followed by drying the strips in an air stream. First, for vapor-mode tests, we placed the fluorescent paper strips on top of a glass vial containing solid TNB for 5 min at room temperature. In this way, a circular area of the strip was exposed to TNB vapor. Within the exposed area the PL of the polymers was obviously distinctly quenched (Figure 2.9A). Second, for solution tests, the test strips containing both polymers were dipped into pure THF (as reference) and a solution of TNB in THF (10^{-4} M). As shown in Figure 2.9B, the fluorescences of the strips were quenched

completely after contact with the TNB solution for both polymers. The reference strips dipped into pure THF do not show significant PL quenching thus demonstrating that the majority of the polymers remain adsorbed at the test strips. These first promising results demonstrate the potential of our new polycarbazole-type polymers PCzTPE0.5 and PCzTPE for the fabrication of solid state sensors for nitroaromatic explosives with sufficient sensitivity.

2.3 Conclusions

In summary, two kinds of *N*-substituted poly(3,6-carbazole)s with triphenylethylene and tetraphenylethylene (TPE) side chains have been successfully synthesized. However, the polymers with triphenylethylene side chains PCz3PE and PCz3PE0.5 did not show distinct AIE effects. The polymers with TPE side chains PCzTPE and PCzTPE0.5 combine the electron-rich character of the polycarbazole backbone and the AIE behavior of the TPE containing side chains and both polymers PCzTPE and PCzTPE0.5 show distinct AIE properties. For sensing of nitroaromatic explosives PL quenching experiments were carried out. Aggregated PCzTPE0.5 shows amplified PL quenching during 1,3,5-trinitrobenzene (TNB) addition in THF/water mixtures (1:9, v/v) with a maximum Stern-Volmer quenching constant of 1.26×10^{6} M^{-1}, which is among the best results from the literatures. Solid-state paper strips with deposits of both polymers show obvious TNB-induced PL quenching, both towards TNB vapor or TNB solution thus demonstrating promising practical application potential in solid state sensors for nitroaromatic explosives.

2.4 Experimental

2.4.1 Materials

All reagents were obtained from commercial suppliers and were used without further purification. All reactions were carried out under argon atmosphere by standard and Schlenk techniques. The solvents were used as commercial p.a. quality.

2-(4-iodophenyl)-1,1-diphenylethylene

Diethyl (4-iodobenzyl)phosphonate (10 mL, 43.2 mmol) and *t*-BuOK (5.29 g, 47.1 mmol) was dissolved in dry THF (85 mL) under an argon atmosphere and stirred for 10 min. Benzophenone (7.16 g, 39.3 mmol) in dry THF (60 mL) was added into the above solution and stirred under room temperature overnight. The reaction was quenched by water and

extracted with dichloromethane. The organic phases were collected and dried over anhydrous $MgSO_4$. After filtration, the solvent was removed under vacuum. The product was purified by silica gel chromatography (eluent: dichloromethane/hexane = 1/1) to give the desired product as white powder in 89% yield (13.4 g). ^{1}H NMR (400 MHz, $C_2D_2Cl_4$) δ (ppm) 7.50 (d, J = 8.5 Hz, 2H), 7.46 - 7.29 (m, 8H), 7.28 - 7.19 (m, 2H), 6.92 (s, 1H), 6.79 (d, J = 8.4 Hz, 2H). ^{13}C NMR (100 MHz, $C_2D_2Cl_4$) δ (ppm) 143.78, 143.13, 140.02, 137.38, 137.15, 131.60, 130.42, 129.14, 128.62, 128.11, 128.01, 127.86, 127.10, 92.61.

3,6-dibromo-9-(4-(2,2-diphenylvinyl)phenyl)-9*H*-carbazole (**1**)

A mixture of 3,6-dibromo-9*H*-carbazole (3.54 g, 10.9 mmol), 2-(4-iodophenyl)-1,1-diphenylethylene (5 g, 13.1 mmol), copper powder (0.70 g, 11.0 mmol), K_2CO_3 (2.26 g, 16.4 mmol) and 18-*crown*-6 (0.29 g, 1.10 mmol) in dry DMF (110 mL) was stirred at 170 °C for 24 h under an argon atmosphere. The reaction was cooled down to room temperature, and diluted with dichloromethane. The copper powder was removed by filtration. The solution was washed with water and extracted with dichloromethane. The organic phase was dried over anhydrous $MgSO_4$ and concentrated under vacuum, the product was purified by silica gel chromatography (eluent: dichloromethane/hexane = 1/2) to give pure product as white powder in 51% yield (3.2 g). ^{1}H NMR (400 MHz, $C_2D_2Cl_4$) δ (ppm) 8.19 (d, J = 1.8 Hz, 2H), 7.51 (dd, J = 8.7, 1.9 Hz, 2H), 7.46 - 7.33 (m, 8H), 7.33 - 7.21 (m, 8H), 7.07 (s, 1H). ^{13}C NMR (100 MHz, $C_2D_2Cl_4$) δ (ppm) 144.01, 143.18, 140.11, 139.88, 137.40, 134.97, 131.36, 130.51, 129.68, 129.20, 128.68, 128.19, 128.13, 127.92, 127.10, 126.34, 124.11, 123.44, 113.33, 112.01. MS (Maldi-Tof): m/z calcd 579.32; found 579.00. Elemental Anal. Calcd for **1**: C, 66.34%; H, 3.65%; N, 2.42%. Found: C, 65.28%; H, 3.59%; N, 2.41%.

1-(4-fluorophenyl)-1,2,2-triphenylethylene

To a solution of diphenylmethane (8.08 g, 48 mmol) in dry THF (80 mL) 2.8 M solution of *n*-butyllithium (*n*-BuLi) in hexane (48 mmol) were added at 0 °C under an argon atmosphere. The resulting orange-red solution was stirred for 1 h at that temperature. To this solution 4-fluorobenzophenone (8.00 g, 40 mmol) was added, and the reaction mixture was allowed to warm up to room temperature overnight. The reaction was quenched with the addition of an aqueous solution of ammonium chloride. The organic layer was extracted with chloroform, and the combined organic layers were washed with a saturated brine solution and dried over anhydrous $MgSO_4$. The solvent was evaporated, and the resulting crude alcohol (containing excess diphenylmethane) was subjected to acid-catalyzed dehydration as follows.

The crude alcohol was dissolved in about 250 mL of toluene containing *p*-toluenesulphonic acid (PTSA) (2.0 g, 10.5 mmol) in a 500 mL flask, and the mixture was refluxed overnight. The toluene layer was washed with 10% aqueous $NaHCO_3$ solution and dried over $MgSO_4$ and evaporated to afford the crude tetraphenylethylene derivative. The crude product was purified by recrystallization from the mixture of dichloromethane and methanol to give the target compound as a white solid in 71% yield (10.0 g). ^{1}H NMR (400 MHz, $C_2D_2Cl_4$) δ (ppm) 7.15 - 7.07 (m, 9H), 7.06 - 6.95 (m, 8H), 6.80 (t, J = 8.8 Hz, 2H). ^{13}C NMR (100 MHz, $C_2D_2Cl_4$) δ (ppm) 160.24, 143.73. 143.69, 143.62, 141.41, 140.01, 139.97, 139.94, 133.23, 133.15, 131.51, 128.06, 128.00, 127.95, 126.76, 126.69, 114.94, 114.73.

1-[4-(3,6-dibromocarbazole-9-yl)phenyl]-1,2,2-triphenylethylene (**2**)

A solution of compound 1-(4-fluorophenyl)-1,2,2-triphenylethylene (3.00 g, 8.56 mmol), 3,6-dibromocarbazole (3.06 g, 9.42 mmol) and K_3PO_4 (9.08 g, 42.8 mmol) in DMF (120 mL) was stirred at 150 °C for 24 h under argon atmosphere. The reaction mixture was quenched with water and extracted with chloroform. The organic phases were collected, dried over $MgSO_4$, and concentrated in vacuum. The product was purified by silica gel chromatography (eluent: hexane/dichloromethane = 4/1) to give the desired compound as a white solid in 25% yield (1.4 g). ^{1}H NMR (400 MHz, $C_2D_2Cl_4$) δ (ppm) 8.19 (d, J = 1.9 Hz, 2H), 7.53 (dd, J = 8.7, 1.9 Hz, 2H), 7.26 (d, J = 8.6 Hz, 2H), 7.24 - 7.12 (m, 15H), 7.12 - 7.06 (m, 4H). ^{13}C NMR (100 MHz, $C_2D_2Cl_4$) δ (ppm) 143.94, 143.66, 143.42, 143.20, 142.42, 140.13, 139.99, 134.69, 133.20, 131.66, 131.60, 131.52, 129.69, 128.19, 128.05. 128.03, 127.04. 126.99, 126.10, 124.06, 123.44, 113.26, 111.94. MS (APLI): m/z calcd 655.03; found 655.03. Elemental Anal. Calcd for **2**: C, 69.64%; H, 3.84%; N, 2.14%. Found: C, 69.17%; H, 3.84%; N, 2.16%.

3,6-dibromo-9-octylcarbazole (**3**)

3,6-Dibromocarbazole (5.0 g, 1.55 mmol) and tetrabutylammonium bromide (TBABr) (500 mg, 1.55 mmol) were dissolved in DMSO (100 mL) under argon. Aqueous NaOH solution (1 g/mL, 8 mL) was added to the mixture, and the mixture stirred at 60 °C for 5 min. Then, 1-bromooctane (4 mL, 0.023 mol) and DMSO (10 mL) were added and the reaction mixture was heated to 90 °C overnight. The reaction mixture was quenched with water and extracted with chloroform. The organic phases were collected, dried over $MgSO_4$ and concentrated in vacuum. The product was purified by silica gel chromatography (eluent: hexane/dichloromethane = 3/1) to give the desired compound as a white solid in 81% yield

(5.4 g). ^{1}H NMR (400 MHz, $C_2D_2Cl_4$) δ (ppm) 8.15 (s, 2H), 7.58 (dd, J = 8.7, 1.9 Hz, 2H), 7.30 (d, J = 8.7 Hz, 2H), 4.23 (t, J = 7.0 Hz, 2H), 1.88 - 1.74 (m, 2H), 1.38 - 1.15 (m, 10H), 0.87 (t, J = 6.8 Hz, 3H). ^{13}C NMR (100 MHz, $C_2D_2Cl_4$) δ (ppm) 139.57, 129.37, 123.58, 123.49, 112.16, 110.88, 43.69, 32.03, 29.58, 29.40, 29.15, 27.49, 22.91, 14.48. MS (APLI): m/z calcd 437.02; found 437.06. Elemental Anal. Calcd for **3**: C, 54.94%; H, 5.30%; N, 3.20%. Found: C, 54.91%; H, 5.58%; N, 3.20%.

Polymer PCz3PE

A solution of compound **1** (493 mg, 0.851 mmol), $Ni(COD)_2$ (655 mg, 2.383 mmol), BPy (346 mg, 2.213 mmol) and COD (239 mg, 2.213 mmol) in THF (7 mL) was reacted under microwave heating at 120 °C for 12 min. The reaction mixture was quenched with water and extracted with chloroform. The collected organic phases were washed with aqueous 2 M HCl solution, aqueous $NaHCO_3$ solution, saturated, aqueous EDTA solution, and brine, and finally dried over $MgSO_4$. Afterwards, the solvents were removed under vacuum. The resulting solid was dissolved in a small amount of chloroform and precipitated into methanol (500 mL) to afford the target polymer as a light-green solid. Subsequent Soxhlet extractions were carried out with methanol, acetone, ethyl acetate and chloroform, respectively. After re-precipitation of the chloroform-soluble fraction into methanol, the light-green polymer was obtained with 77% yield (295 mg). ^{1}H NMR (400 MHz, $C_2D_2Cl_4$) δ (ppm) 8.68 - 8.36 (m, 2H), 7.92 - 7.69 (m, 2H), 7.69 - 7.18 (m, 18H), 7.16 - 7.05 (m, 1H). ^{13}C NMR (100 MHz, $C_2D_2Cl_4$) δ (ppm) 143.66, 143.37, 141.58, 140.53, 140.33, 136.67, 136.31, 134.62, 131.14, 130.54, 129.07, 128.58, 127.96, 127.86, 127.40, 126.22, 124.50, 119.07, 117.91, 110.65. M_n 8100, M_w 14000, M_w/M_n 1.73(GPC, PS calibration).

Polymer PCz3PE0.5

A solution of compound **1** (265 mg, 0.457 mmol), compound **3** (200 mg, 0.457 mmol), $Ni(COD)_2$ (629 mg, 2.287 mmol), BPy (357 mg, 2.287 mmol) and COD (247 mg, 2.287 mmol) in THF (7 mL) was reacted under microwave heating at 120 °C for 12 min. The workup procedure was similar to that described for the preparation of PCz3PE. The light-green polymer was obtained with 38% yield (120 mg). ^{1}H NMR (600 MHz, $C_2D_2Cl_4$) δ (ppm) 8.41 (d, *J* = 94.4 Hz, 7H), 7.82 (d, *J* = 37.5 Hz, 8H), 7.60 - 7.11 (m, 38H), 7.04 (s, 2H), 5.09 - 3.43 (m, 2H), 1.95 (d, *J* = 94.1 Hz, 4H), 1.49 - 0.99 (m, 23H), 0.84 (dd, *J* = 30.4, 6.4 Hz, 7H). M_n 10100, M_w 32300, M_w/M_n 3.19 (GPC, PS calibration).

Polymer PCzTPE

A solution of compound **2** (400 mg, 0.610 mmol), $Ni(COD)_2$ (436 mg, 1.587 mmol), BPy (110 mg, 0.701 mmol) and COD (172 mg, 1.587 mmol) in THF (7 mL) was reacted under microwave heating at 120 °C for 12 min. The workup procedure was similar to that described for the preparation of PCz3PE. The light-green polymer was obtained with 70% yield (211 mg). ^{1}H NMR (600 MHz, $C_2D_2Cl_4$, 60 °C) δ (ppm) 8.60 - 8.41 (m, 2H), 7.86 - 7.62 (m, 2H), 7.48 - 6.87 (m, 21H). ^{13}C NMR (150 MHz, $C_2D_2Cl_4$, 60 °C) δ (ppm) 143.76, 143.59, 143.43, 143.15, 142.26, 140.72, 140.51, 136.04, 134.62, 132.91, 131.55, 131.53, 131.47, 128.09, 128.01, 127.94, 126.93, 126.86, 126.78, 126.09, 124.46, 119.10, 110.54. M_n 6800, M_w 14300, M_w/M_n 2.10 (GPC, PS calibration).

Polymer PCzTPE0.5

A solution of compound **2** (300 mg, 0.457 mmol), compound **3** (200 mg, 0.457 mmol), $Ni(COD)_2$ (629 mg, 2.287 mmol), BPy (357 mg, 2.287 mmol) and COD (247 mg, 2.287 mmol) in THF (7 mL) was reacted under microwave heating at 120 °C for 12 min. The workup procedure was similar to that described for the preparation of PCz3PE. The light-green polymer was obtained with 54% yield (192 mg). ^{1}H NMR (600 MHz, $C_2D_2Cl_4$, 60 °C) δ (ppm) 8.49 (s, 4H), 8.01 - 7.66 (m, 4H), 7.58 - 6.94 (m, 23H), 4.26 (s, 2H), 1.88 (s, 2H), 1.29 (dd, J = 78.1, 27.6 Hz, 10H), 0.92 - 0.73 (m, 3H). M_n 9200, M_w 23400, M_w/M_n 2.54 (GPC, PS calibration).

Polymer PCz

A solution of compound **3** (400 mg, 0.915 mmol), $Ni(COD)_2$ (654 mg, 2.379 mmol), BPy (372 mg, 2.379 mmol) and COD (257 mg, 2.379 mmol) in THF (6 mL) was reacted under microwave heating at 120 °C for 12 min. The workup procedure was similar to that described for the preparation of PCz3PE. The grey polymer was obtained with 32% yield (90 mg). ^{1}H NMR (600 MHz, $C_2D_2Cl_4$, 60 °C) δ (ppm) 8.52 (s, J = 28.4 Hz, 2H), 7.90 (d, J = 8.5 Hz, 2H), 7.50 (d, J = 8.6 Hz, 2H), 4.31 (bs, 2H), 2.06 - 1.80 (m, 2H), 1.57 - 1.13 (m, 10H), 0.89 (t, J = 6.9 Hz, 3H). M_n 10100, M_w 34500, M_w/M_n 3.42 (GPC, PS calibration).

Preparation of nanoaggregates

First stock polymer solutions in THF with a concentration of 10^{-4} M were prepared. After adding proper volume of THF, water was added under vigorous stirring to furnish a 10^{-5} M

nanoaggregates solution. The solution was further used for measurements immediately after obtained.

2.4.2 Instrumentation

NMR spectra were recorded on a Bruker AVANCE 400 or AVANCE III 600. ^{1}H and ^{13}C NMR spectra were measured with tetramethylsilane (TMS) as internal standard. Gel permeation chromatography (GPC) measurements were carried out on a PSS/Agilent SECurity GPC System equipped with polystyrene gel columns using chloroform as eluent. APLI (Atmospheric Pressure Laser Ionization) measurements were carried out on Bruker Daltronik Bremen with micrOTOF. Maldi-Tof mass spectra were recorded on a Bruker Reflex TOF. UV-visible absorption spectra were recorded on a Jasco V-670 spectrometer, and PL spectra on a Varian CARY Eclipse F2500 or HORIBA Scientific FluroMax-4. Elemental analyses were performed on a Vario EL II (CHNS) instrument. Thermal gravimetric analysis (TGA) was undertaken on a TGA/DSC1 STAR System (Mettler Toledo) at a heating rate of 10 °C/min and an argon flow rate of 50 mL/min. Differential scanning calorimetry (DSC) was performed on a DSC1 STAR System (Mettler Toledo) at a heating rate of 10 °C/min under argon. The PL quantum efficiencies of polymer films were measured with an integrating sphere. Cyclic voltammetry (CV) measurements of the polymer films were performed on a standard three-electrode electrochemical cell attached to a VersaSTAT 4 electrochemical workstation in dichloromethane for polymers and acetonitrile for trinitrobenzene (TNB) with 0.1 M tetrabutylammonium perchlorate as supporting electrolyte at a scan rate of 0.1 V/s for polymers and 0.2 V/s for TNB. The potentials were measured against an $Ag/AgNO_3$ reference electrode (0.1 M $AgNO_3$ in acetonitrile, 0.6 V *vs*. NHE). The onset potentials were determined from the intersection of two tangents drawn at the rising current and background current of the cyclic voltammogram.

2.5 References

1. W. Dong, T. Fei, A. Palma-Cando and U. Scherf, *Polym. Chem.*, 2014, **5**, 4048-4053.
2. B. Xu, Z. Chi, Z. Yang, J. Chen, S. Deng, H. Li, X. Li, Y. Zhang, N. Xu and J. Xu, *J. Mater. Chem.*, 2010, **20**, 4135-4141.
3. H. Li, Z. Chi, B. Xu, X. Zhang, Z. Yang, X. Li, S. Liu, Y. Zhang and J. Xu, *J. Mater. Chem.*, 2010, **20**, 6103-6110.
4. W. Wu, S. Ye, L. Huang, L. Xiao, Y. Fu, Q. Huang, G. Yu, Y. Liu, J. Qin, Q. Li and Z. Li, *J. Mater. Chem.*, 2012, **22**, 6374-6382.
5. J. E. McMurry, *Chem. Rev.*, 1989, **89**, 1513-1524.
6. M. Banerjee, S. J. Emond, S. V. Lindeman and R. Rathore, *J. Org. Chem.*, 2007, **72**, 8054-8061.
7. W. Z. Yuan, Y. Gong, S. Chen, X. Y. Shen, J. W. Y. Lam, P. Lu, Y. Lu, Z. Wang, R. Hu, N. Xie, H. S. Kwok, Y. Zhang, J. Z. Sun and B. Z. Tang, *Chem. Mater.*, 2012, **24**, 1518-1528.
8. S. Grigalevicius, L. Ma, G. Qian, Z. Xie, M. Forster and U. Scherf, *Macromol. Chem. Phys.*, 2007, **208**, 349-355.
9. S. A. Patil, U. Scherf and A. Kadashchuk, *Adv. Funct. Mater.*, 2003, **13**, 609-614.
10. B. Souharce, C. J. Kudla, M. Forster, J. Steiger, R. Anselmann, H. Thiem and U. Scherf, *Macromol. Rapid Commun.*, 2009, **30**, 1258-1262.
11. F. Diness and D. P. Fairlie, *Angew. Chem., Int. Ed.*, 2012, **51**, 8012-8016.
12. D. Hu, G. Cheng, P. Lu, H. Liu, F. Shen, F. Li, Y. Lv, W. Dong and Y. Ma, *Macromol. Rapid Commun.*, 2011, **32**, 1467-1471.
13. F. Galbrecht, T. W. Bünnagel, U. Scherf and T. Farrell, *Macromol. Rapid Commun.*, 2007, **28**, 387-394.
14. J. W. Grate, *Chem. Rev.*, 2008, **108**, 726-745.
15. J.-S. Yang and T. M. Swager, *J. Am. Chem. Soc.*, 1998, **120**, 5321-5322.
16. S. W. Zhang and T. M. Swager, *J. Am. Chem. Soc.*, 2003, **125**, 3420-3421.
17. M. E. Walsh, *Talanta*, 2001, **54**, 427-438.
18. J. C. Mathurin, T. Faye, A. Brunot and J. C. Tabet, *Anal. Chem.*, 2000, **72**, 5055-5062.
19. J. M. Sylvia, J. A. Janni, J. D. Klein and K. M. Spencer, *Anal. Chem.*, 2000, **72**, 5834-5840.
20. E. Wallis, T. M. Griffin, N. Popkie Jr., M. A. Eagan, R. F. McAtee, D. Vrazel and J. McKinly, *Proc. SPIE Int. Soc. Opt. Eng.*, 2005, **5795**, 54-64.

21. M. Krausa and K. Schorb, *J. Electroanal. Chem.*, 1999, **461**, 10-13.
22. A. Palma-Cando and U. Scherf, *ACS Appl. Mater. Interfaces*, 2015, **7**, 11127−11133.
23. H. Nie, Y. Zhao, M. Zhang, Y. Ma, M. Baumgarten and K. Müllen, *Chem. Commun.*, 2011, **47**, 1234-1236.
24. C. McDonagh, C. S. Burke and B. D. MacCraith, *Chem. Rev.*, 2008, **108**, 400-422.
25. S. W. Thomas, G. D. Joly and T. M. Swager, *Chem. Rev.*, 2007, **107**, 1339-1386.
26. H. Li, H. Wu, E. Zhao, J. Li, J. Z. Sun, A. Qin and B. Z. Tang, *Macromolecules*, 2013, **46**, 3907-3914.
27. W. Wu, S. Ye, L. Huang, L. Xiao, Y. Fu, Q. Huang, G. Yu, Y. Liu, J. Qin, Q. Li and Z. Li, *J. Mater. Chem.*, 2012, **22**, 6374-6382.
28. P. Lu, J. W. Y. Lam, J. Liu, C. K. W. Jim, W. Yuan, N. Xie, Y. Zhong, Q. Hu, K. S. Wong, K. K. L. Cheuk and B. Z. Tang, *Macromol. Rapid Commun.*, 2010, **31**, 834-839.
29. C. Y. K. Chan, Z. Zhao, J. W. Y. Lam, J. Liu, S. Chen, P. Lu, F. Mahtab, X. Chen, H. H. Y. Sung, H. S. Kwok, Y. Ma, I. D. Williams, K. S. Wong and B. Z. Tang, *Adv. Funct. Mater.*, 2012, **22**, 378-389.
30. J. Li, J. Liu, J. W. Y. Lam and B. Z. Tang, *RSC Adv.*, 2013, **3**, 8193-8196.

Chapter 3

3. Polytriphenylamines with AIE-active Tetraphenylethylene Side Groups[1]

*Two polytriphenylamines (PTPAs) (**P1** and **P2**) with AIE-active tetraphenylethylene side groups have been designed and successfully synthesized. Both polymers only faintly emit in dilute solution but show strong emission in aggregated state, meaning that they are AIE-active. The detection of 1,3,5-trinitrobenzene (TNB) vapors has been investigated by photoluminescence (PL) quenching in polymer films. High solid state quantum yields and donor-acceptor interactions of the electron-rich PTPA chains with the TNB analyte, hereby, induce a high sensing sensitivity, both for **P1** and **P2** films towards TNB vapor. Contacting thin **P1** and **P2** films with saturated TNB vapor, the PL intensity was quenched by 85% for **P1** and 89% for **P2** within 600 s, respectively. The sensing process is reversible, >90% of the PL is recovered, also after repeated cycling.*

3.1 Introduction

In Chaper 2, tri- and tetraphenylethylene side groups have been introduced into polycarbazoles. The obtained polycarbazoles (PCzs) showed a quite different behavior: Triphenylethylene-substituted PCzs are not AIE-active, corresponding tetraphenylethylene (TPE)-substituted PCzs showed the occurrence of significant AIE effects, with a maximum AIE coefficient α_{AIE} of up to 26. Therefore, within this chapter, we concentrated on TPE side chains as substituents of polytriphenylamines.

Similar to PCzs, polytriphenylamines (PTPAs) also exhibit pronounced electron-donor character which should be beneficial for the interaction with electron-poor nitroaromatic compounds. However, there are only a few reports on PTPAs for PL-based explosive detection[2,3]. In this study, we prepared two novel PTPAs (**P1** and **P2**, Chart 3.1) with TPE side groups and investigated their ability for the sensing of nitroaromatic analytes. The incorporation of TPE side groups induces AIE activity, instead of ACQ properties generally observed for PTPAs, under conservation of the electronic properties of the PTPA backbone. Moreover, the twisted, loosely packed structure should generate efficient diffusion pathways

for the explosive molecules. Based on this design principle we could expect a high sensitivity for detection of nitroaromatic compounds in the solid state.

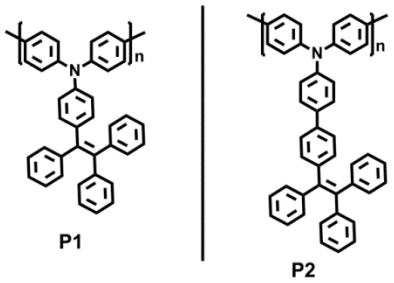

Chart 3.1. The chemical structures of polymer **P1** and **P2**.

3.2 Results and Discussion

3.2.1 Synthesis and Characterization

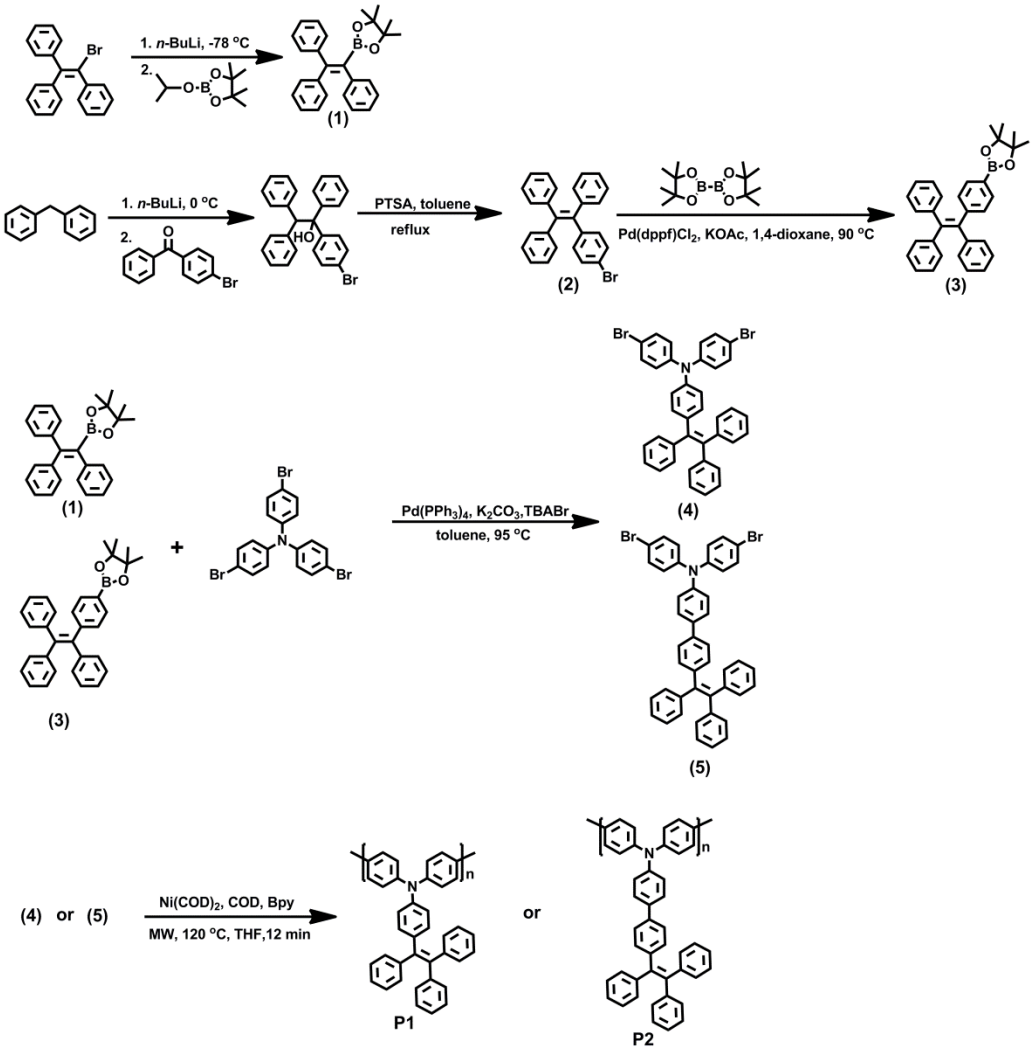

Scheme 3.1. Synthesis scheme for monomers **4** and **5** as well as the corresponding polymers **P1** and **P2**, respectively.

The synthetic route for monomers **4**/**5** and the corresponding polymers **P1**/**P2** is depicted in Scheme 3.1. Treatment of 1-bromo-1,2,2-triphenylethylene with an excess of *n*-butyllithium (*n*-BuLi) followed by addition of 2-*iso*propoxy-4,4,5,5-tetramethyl-1,3,2-dioxaborolane afforded the boronic ester **1**. Monobromo-TPE **2** was obtained by treating 4-bromobenzophenone with diphenylmethyl lithium followed by acid-catalyzed dehydration. The TPE boronic ester **3** was synthesized by Suzuki-Miyaura-type coupling of monobromo-TPE **2** and bis(pinacolato)diboron. The TPE-substituted dibromotriphenylamine monomers **4** and **5** were generated in a Suzuki-type coupling of tribromotriphenylamine and TPE derivatives **1** or **3**. Polymers **P1** and **P2** were synthesized from monomers **4** and **5**, respectively, in Yamamoto-type couplings using $Ni(COD)_2$ as coupling reagent in a mixture of THF, COD and Bpy under microwave (MW) heating. Applying the MW method we could obtain the targeted conjugated polymers in short reaction times (12 min). The structure elucidation of the monomer was performed by NMR spectroscopy, mass spectrometry and elemental analysis. The chemical structure of the obtained polymers was finally confirmed by NMR spectroscopy, GPC and optical spectroscopy.

3.2.2 Photophysical Properties

Table 3.1. Optical data and HOMO/LUMO energy levels of **P1** and **P2**.

	λ_{UV}/nm in $CHCl_3$	λ_{PL}/nm in $CHCl_3$	λ_{UV}/nm in film	λ_{PL}/nm in film	η_{PL} (%) in $CHCl_3$	η_{PL} (%) in film	HOMO (eV)	LUMO (eV)
P1	384	511	386	511	0.8	16.9	-5.27	-2.37
P2	382	493	380	495	2.5	34.3	-5.31	-2.41

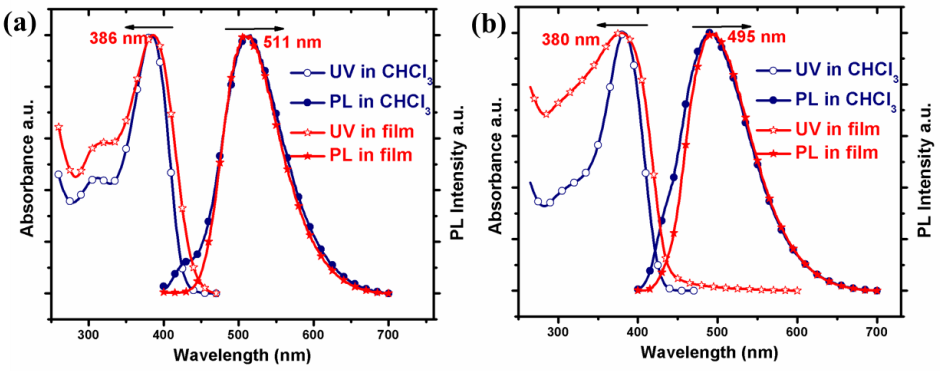

Figure 3.1. Absorption and PL spectra of (a) **P1** and (b) **P2** in dilute chloroform solution (10^{-5} M) and as spin-coated films (measured at room temperature).

Figure 3.1 shows absorption and PL spectra of **P1** and **P2** in dilute chloroform solution and as solid state films. The absorption spectra of both polymers are quite similar because of their identical backbone structures. The absorption maxima of the thin films are observed at 386 and 380 nm for **P1** and **P2**, respectively. In the PL spectra, the emission maxima peak at 511 nm for **P1**, and 495 nm for **P2**. The hypsochromic shift from a bluish green emission (511 nm) for **P1** to a sky-blue emission (495 nm) for **P2** is attributed to the presence of biphenyl linkers in **P2** that decrease the conjugative interaction between PTPA backbone and TPE side groups. It is worthy to note that, for both absorption and PL spectra, there is nearly no shift for the maxima peak between dilute solution and film. This should be caused by the incorporation of the bulky TPE side groups: they effectively suppress any π-π stacking in the condensed phase due to their propeller-shaped structure. The PLQYs of **P1** and **P2** in dilute chloroform solution, using quinine sulfate as standard, have been determined as 0.8% and 2.5%, respectively. The PLQYs distinctly increase to 16.9% and 34.3%, respectively, for solid powders, a 21 and 14 fold increase if compared to the chloroform solutions (see Table 3.1). Evidently, the transition into the condensed state dramatically enhances the PL intensity of **P1** and **P2**.

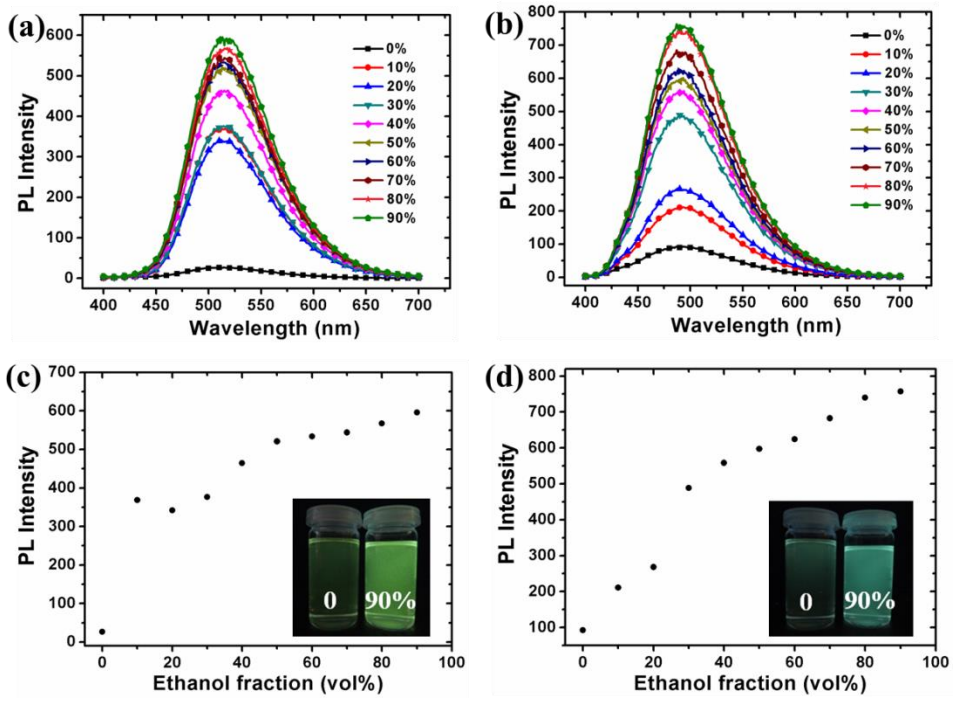

Figure 3.2. PL spectra of (a) **P1** and (b) **P2** in chloroform/ethanol mixtures with different ethanol content; PL intensity with increasing ethanol fraction for (c) **P1** and (d) **P2**, respectively (polymer concentration: 10^{-5} M). The insets of Figs. 3.2c/d show fluorescent images of **P1** and **P2** in pure chloroform and in chloroform/ethanol 1/9, respectively.

To further investigate the AIE properties of the polymers, their PL behavior in solvent/non-solvent mixtures was investigated, as shown in Figure 3.2. Chloroform and ethanol were chosen as solvent couple due to their full miscibility. Both **P1** and **P2** are weakly emissive in dilute chloroform solution, but their PL progressively increases during increasing the ethanol content. The insets of Figure 3.2c/d show PL images (UV excitation) of the polymers in chloroform and chloroform/ethanol 1/9. In the chloroform/ethanol mixture with 90% ethanol, the PL intensity is ca. 22 times increased if compared to pure chloroform for **P1**, and ca. 8 times for **P2**. As ethanol is non-solvent for **P1** and **P2**, both polymers are assumed to form solid state nano-aggregates at high ethanol contents. We could investigate the aggregation process by dynamic light scattering only for the initial step of ethanol addition (10%) for polymer **P1**. In chloroform/ethanol (9:1) the hydrodynamic radius of the aggregates was estimated to be ca. 317 nm. Apparently, the emission of both polymers is induced by aggregation; in other words, they are AIE-active. This is connected to the presence of the AIE-active TPE side groups: in dilute chloroform solution, a high internal conversion rate results in weak emission mainly caused by rotations of phenyl rings of the olefinic TPE units; in aggregates, however, these rotations are strongly suppressed, thus increasing the PL intensity due to the basic principles of the AIE effect[4].

3.2.3 Explosive Detection

The highly electron-rich nature of polytriphenylamine (PTPA) backbones is a promising sensing target for the interaction with electron-deficient nitroaromatic compounds. However, there are only a few reports on the use of PTPAs for explosive detection. Our TPA-based polymers **P1** and **P2** with their high solid state PLQYs caused by the AIE effect represent promising lead structures for the PL-based detection of nitroaromatic compounds.

3.2.3.1 TNB Detection based on P1 and P2 Films

To explore the potential for an application of **P1** and **P2** as solid state sensory materials for the detection of nitroaromatic compounds, thin films of both polymers were fabricated by spin-coating on glass substrates at a rate of 1500 rpm with a concentration of the stock solutions in chloroform of 0.5 mg/mL (thickness ca. 3-5 nm). The films were subsequently annealed at 50 °C for 2 h to remove remaining solvents. TNB was chosen as a prototypical nitroaromatic analyte. Figure 3.3a/b show time-dependent fluorescence quenching plots of **P1** and **P2** thin films during exposure to saturated TNB vapor. The fluorescence intensity gradually decreases as a function of exposure time with 40% PL quenching after 30 s and

50% PL quenching after 60 s for **P1**, or 53% after 30 s and 63% after 60 s for **P2**, respectively. For 600 s exposure to saturated TNB vapor, the fluorescence intensity is decreased by 85% and 89% for **P1** and **P2**, respectively. Figure 3.3c plots the relative PL quenching with respect to the exposure time for both polymers. With further increase in the exposure time above 600 s, the PL quenching saturates and the PL intensity does not change further. For comparison, some literature data for the detection of nitroaromatic explosives are summarized in Table 3.2. Our fluorescence quenching data demonstrate that polytriphenylamines with TPE side chains are among the best performing materials for this purpose. Figure 3.3d shows the reversibility of the PL response of a **P2** film towards TNB vapor. First, the film was exposed to saturated TNB vapor for 60 s at room temperature, followed by the PL measurement. Then the film was rinsed with methanol for 5 min, followed by a next PL measurement. Afterwards, the whole process was repeated. The results show that the initial PL characteristic was mainly conserved after 6 exposure/washing cycles, thus indicating good reversibility of the sensing scheme. As shown in Figure 3.3d, even after 6 cycles, the **P2** film still shows 62% PL quenching after exposure to TNB vapor for 60 s, please compare to the value of 63% for the first cycle.

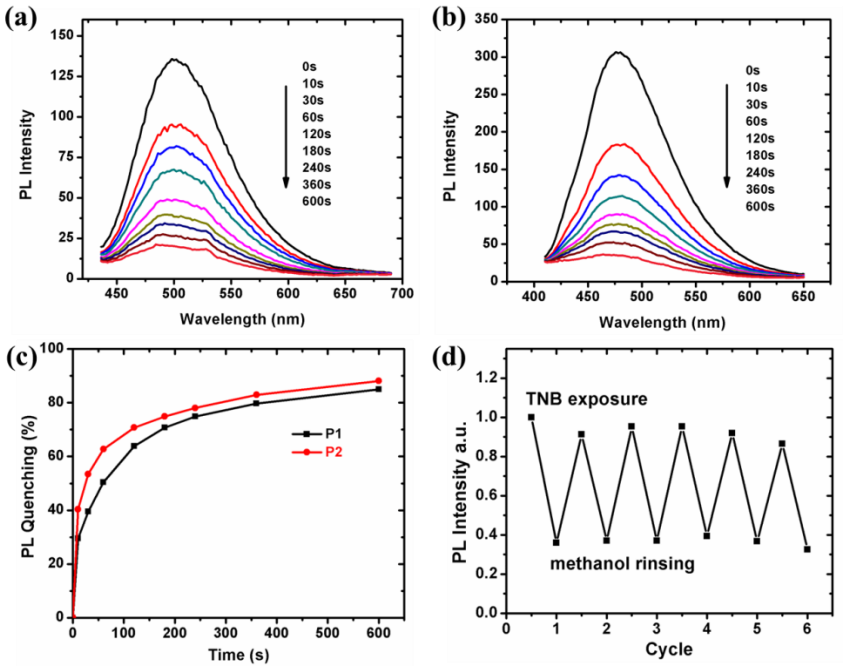

Figure 3.3. Time-dependent fluorescence intensity of (a) **P1** and (b) **P2** films when exposed to saturated TNB vapor. (c) The fluorescence response towards TNB vapor for **P1** and **P2** thin films as a function of the exposure time. (d) PL recovery cycles of a **P2** film. During each cycle, the films were first exposed to saturated TNB vapor for 60 s and, for PL recovery, subsequently rinsed with methanol (6 cycles are depicted).

Table 3.2. Fluorescence quenching data for nitroaromatic compounds from the literature. (PA: picric acid; TNT: 2,4,6-trinitrotoluene; DNT: 2,4-dinitrotoluene; TNB: 1,3,5-trinitrobenzene.)

Solid state sensing material (type of nitroaromatic explosive)	Fluorescence quenching effect		Reference
	after 60 s	In the equilibrium	
P1 (TNB)	50%	85% (10 min)	this work
P2 (TNB)	63%	89% (10 min)	this work
S_1 (PA)	21% (120 s)	80% (10 min)	[5]
S_3 (PA)	33%	92% (7 min)	[6]
PCZ (TNT)	73%	--	[7]
DMF-L (TNT)	--	~60% (60 min)	[8]
TAPB (TNT)	--	60% (20 min)	[9]
3 (DNT)	--	67% (10 min)	[10]
P1-porous film (TNT)	64%	82% (5 min)	[11]
P1-dense film (TNT)	10%	24% (5 min)	[11]
FTPA-HBCPN (TNT)	16%	60% (10 min)	[12]
H2-BCz-xerogel film (TNT)	--	77% (30 min)	[13]
H2-BCz-amorphous film (TNT)	--	51% (30 min)	[13]
P2 (TNT)	75%	--	[14]
TCAC-EP film (TNT)	39%	66% (10 min)	[15]
ACTC (TNT)	83%	--	[16]
9-xerogel film (TNT)	--	62% (5 min)	[17]

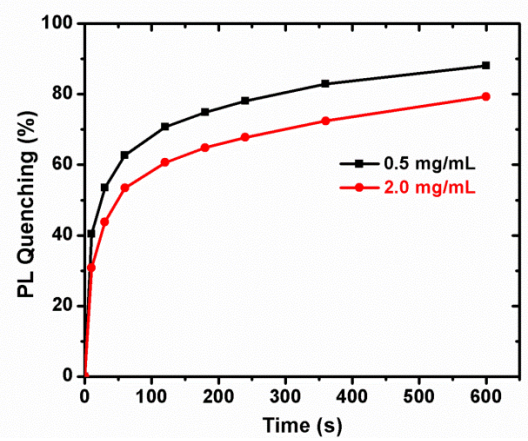

Figure 3.4. The fluorescence response towards TNB vapor for **P2** thin films as a function of the exposure time.

Also a thicker film of **P2** (thickness ca. 8-10 nm) has also been prepared by spin-coating from a 2 mg/mL polymer solution in chloroform for comparison. The thicker film exhibits only slightly decreased fluorescence quenching (see Figure 3.4 and Table 3.3) with 53% PL quenching after 60 s and 79% after 600 s.

Table 3.3. PL quenching behaviour of **P1** and **P2** films against TNB vapor.

Quenching efficiency / Polymer	30 s	60 s	600 s	Reversibility (60 s) after 6 cycles
P1 (3-5 nm)	40%	50%	85%	--
P2 (3-5 nm)	53%	63%	89%	62%
P2 (8-10 nm)	44%	53%	79%	--

3.2.3.2 Detection of Other Nitroaromatic Compounds based on P1 and P2 Films

The response of **P1** and **P2** thin films to two other nitroaromatic compounds DNB (1,3-dinitrobenzene) and NB (nitrobenzene) is depicted in Figure 3.5. Both DNB and NB also cause the PL quenching of **P1** and **P2**. Hereby, the response to DNB vapor is increased if compared to TNB, most probably due to its higher vapor pressure.

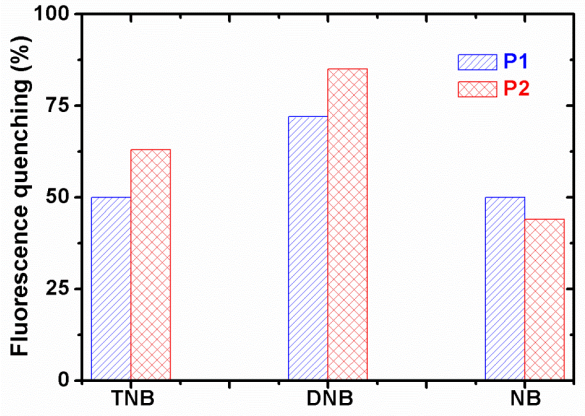

Figure 3.5. Fluorescence quenching (%) of **P1** and **P2** films exposed to TNB, DNB and NB (exposure time: 60 s).

3.2.3.3 Fluorescence Quenching Mechanism during Interaction with Nitroaromatic Compounds

Figure 3.6 illustrates that there is no overlap between the absorption spectrum of TNB and the PL spectra of **P1** and **P2**, respectively, as prerequisite for Förster-type excitation energy transfer, thus indicating that the main quenching mechanism for TNB exposure should be

electron transfer between the excited state of the host (**P1** or **P2**) and TNB. This process is driven by the LUMO-LUMO offset between TNB and **P1**/**P2**. The HOMO levels of **P1** and **P2** (shown in Table 3.1) were estimated to be ca. -5.27 and -5.31 eV, respectively (AC-2 method). Considering an optical bandgap (E_g) of ca. 2.90 eV both for **P1** and **P2** from the onsets of the UV/vis absorption bands, the LUMO levels of **P1** and **P2** are calculated to be ca. -2.37 eV and -2.41 eV, respectively. The LUMO level of TNB is located at ca. -3.1 eV, as estimated by cyclic voltammetry. So, these LUMO levels of **P1** and **P2** (-2.37 eV and -2.41 eV, respectively) allow for an excited state electron transfer to the energetically lower-lying LUMO level of TNB with a LUMO-LUMO offset of ca. 0.7 eV.

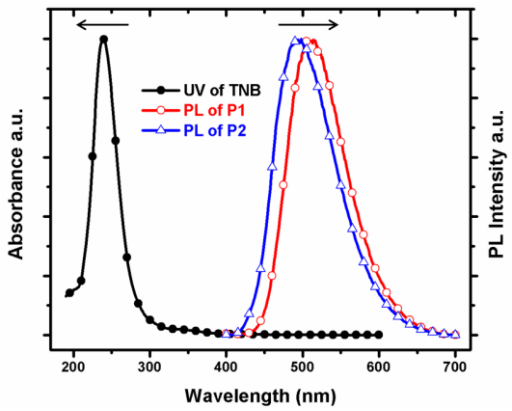

Figure 3.6. Normalized absorption spectrum of TNB and PL spectra of **P1** and **P2** in thin films.

3.2.4 Theoretical Calculations

For better understanding the optical and sensory properties of **P1** and **P2**, theoretical calculations were performed by density functional theory (DFT) level using the B3LYP functional and the 6-31g* basic set, as implemented in the Gaussian 09 program. The optimized structures and orbital distributions of the HOMOs and LUMOs of **P1** and **P2** are depicted in Figure 3.7, in both cases two repeat units are shown. The TPE side groups both in **P1** and **P2** adopt twisted conformations with a torsional angle ca. 133.0º between the planes of phenyl rings and olefinic bond. This assembly does not allow strong intermolecular interactions, thus preventing solid state PL quenching that is caused by π-π stacking. Moreover, the twisted TPE side chains of **P1** and **P2** may create three-dimensional exciton diffusion channels, which, during local interaction with TNB analytes, cause improved exciton diffusion to these quenching sites. The torsional angles between adjacent TPA units of the PTPA backbones of both polymers are very similar with 145.9º for **P1** and 145.6º for

P2, respectively. That indicates the bulky TPE side chains do not strongly affect the conjugative interaction within the PTPA backbones. This maintained on-chain π-conjugation ensures an efficient exciton transfer along the polymer backbone of sensory material. The HOMOs of both polymers are mainly located at the PTPA backbone, thus confirming the electron-donor character of the PTPA backbone, a property that will be beneficial for the interaction with electron-poor TNB analyte. Therefore, high solid state quantum yields caused by the AIE effect, the electron-donor character of the PTPA backbone, and the bulky, twisted structure of the TPE side groups together guarantee excellent sensing properties towards electron-deficient analytes, as nitroaromatic explosives.

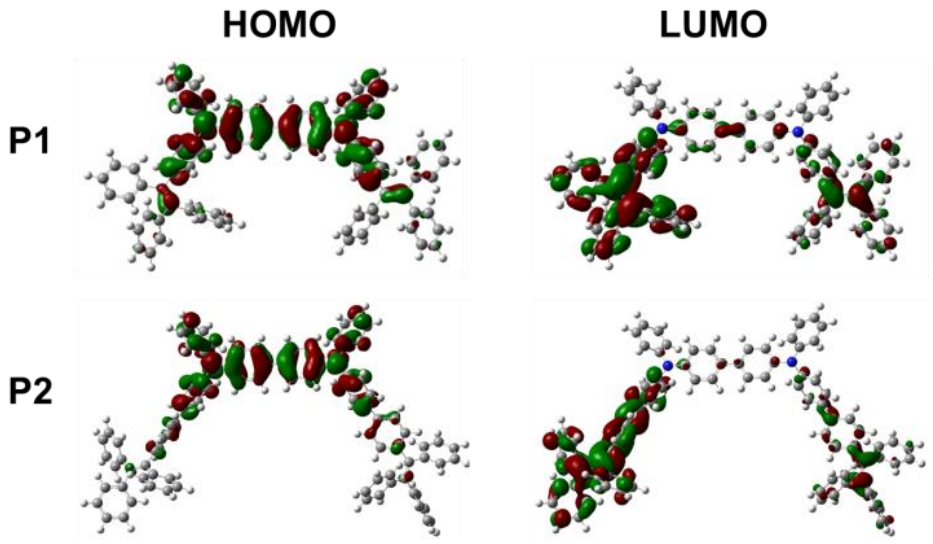

Figure 3.7. Calculated molecular orbital amplitude plots of the HOMO and LUMO energy levels of **P1** and **P2**.

3.3 Structural Modification of the Polytriphenylamines and Polycarbazoles

According to the above presented results, our polytriphenylamines **P1** and **P2** with their distinct AIE effects are promising materials for a sensitive detection of nitroaromatic analytes as TNB also in the solid state (as thin films). However, both polymers are characterized by an unpleasant solubility behaviour: They are only slightly soluble in THF or toluene, a bit better in chloroform or chlorobenzene. In order to overcome these solubility limitations, we incorporated additional bis(*tert*-butyl)-substituted TPE units into the polymer backbones thus obtaining polytriphenylamine-based copolymers PTPA1-TPE, PTPA2-TPE as well as the corresponding polycarbazole-based copolymer PCz-TPE. There are two advantages of introducing bis(*tert*-butyl)-TPE main chain units: (1) the presence of the *tert*-butyl

substituents will improve the solubility of the polymers; and (2) the bis(*tert*-butyl)-TPE unit should be more effective in suppressing unwanted π-π stacking in the aggregated state due to its bulky structure. Please note, that PTPA1-TPE, PTPA2-TPE and PCz-TPE are random copolymers that contain bis(*tert*-butyl)-TPE units as main-chain and additional TPE units as side chains.

3.3.1 Synthesis

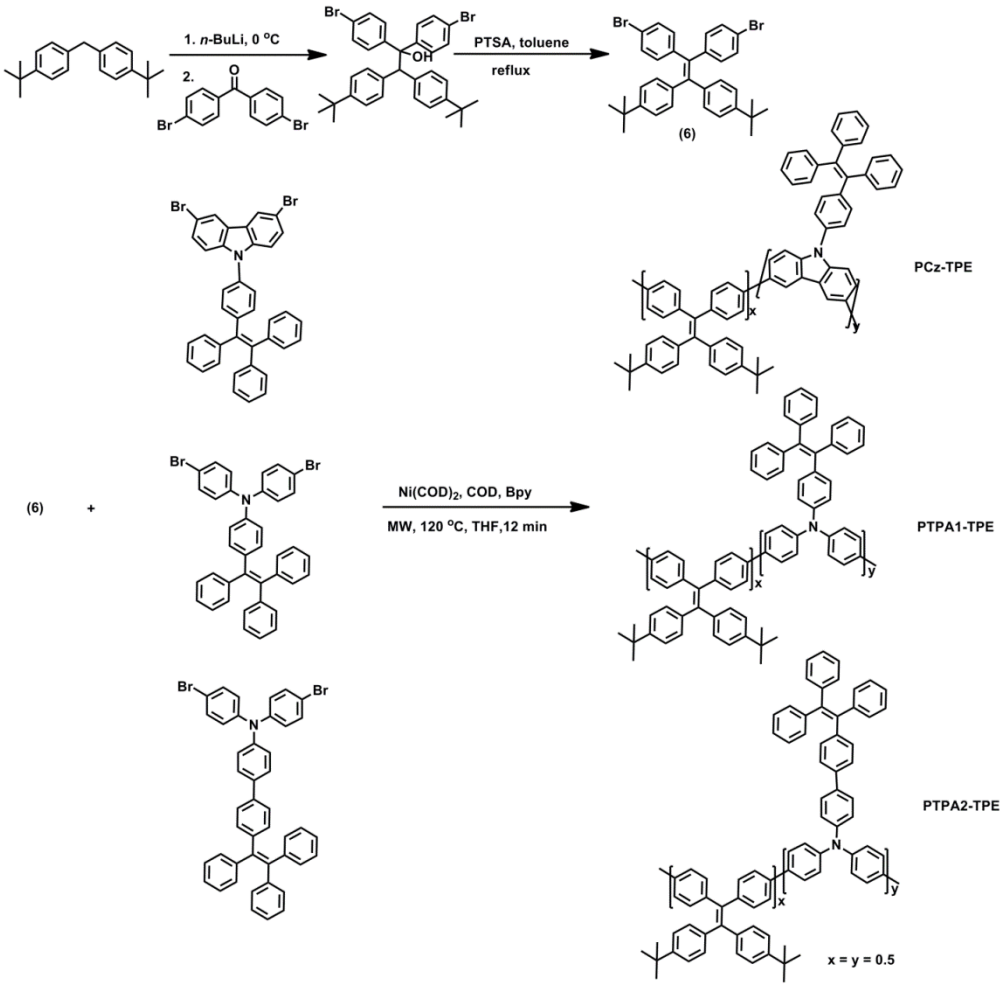

Scheme 3.2. Synthesis scheme towards monomer **6** and copolymers PCz-TPE, PTPA1-TPE and PTPA2-TPE.

The synthetic routes for monomer **6** and the polymers PCz-TPE, PTPA1-TPE and PTPA2-TPE are depicted in Scheme 3.2. The dibromo-TPE monomer **6** was obtained by treating 4-bromobenzophenone with bis(4-(*tert*-butyl)phenyl)methyl lithium followed by an acid-catalyzed dehydration. The random copolymers PCz-TPE, PTPA1-TPE and PTPA2-TPE were synthesized *via* Yamamoto-type couplings of 1:1 mixtures of monomer **6** and TPE-substituted dibromocarbazole (see Chapter 2.2), **4** or **5** (Scheme 3.1), respectively,

with $Ni(COD)_2$ as coupling reagent in a mixture of THF, COD and Bpy under microwave (MW) heating for 12 min. The obtained copolymers all showed good solubility in common solvents, such as chloroform, THF or toluene. The structure of the monomer was confirmed by NMR spectroscopy, mass spectrometry and elemental analysis. The chemical structure of the obtained polymers was finally confirmed by NMR spectroscopy, GPC, and optical spectroscopy.

3.3.2 Photophysical Properties

Table 3.4. Optical data of PCz-TPE, PTPA1-TPE and PTPA2-TPE.

	λ_{UV}/nm in THF	λ_{PL}/nm in THF	λ_{UV}/nm in film	λ_{PL}/nm in film	η_{PL} (%) in THF	η_{PL} (%) in powder
PCz-TPE	326	504	321	515	1.2	28
PTPA1-TPE	372	507	372	516	0.4	20
PTPA2-TPE	373	502	372	512	1.4	37

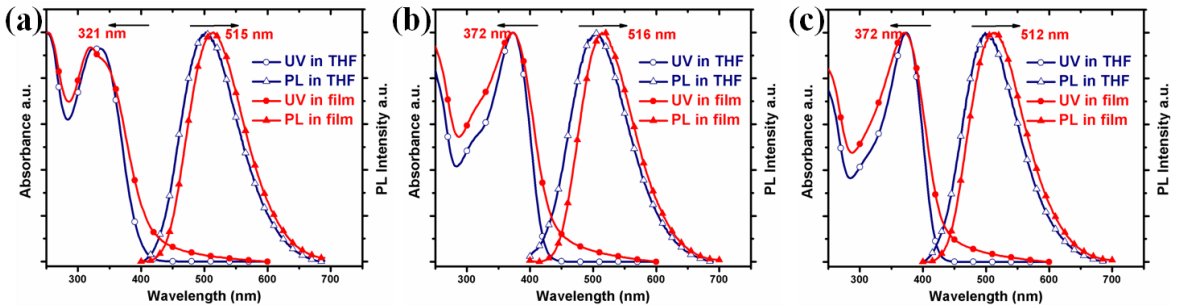

Figure 3.8. Normalized absorption and PL spectra of (a) PCz-TPE, (b) PTPA1-TPE and (c) PTPA2-TPE in dilute THF solution (10^{-5} M) and as spin-coated films (measured at room temperature).

Figure 3.8 shows the absorption and PL spectra of the three copolymers in dilute THF solution and as thin films. For polymer PCz-TPE, the absorption maximum appears at 321 nm and the PL maximum is observed at 515 nm, corresponding to a bathochromical shift of 20 nm if compared to PCzTPE (Figure 2.3, Chapter 2). This is attributed to the introduction of bis(*tert*-butyl)-TPE units into the copolymer backbone, thus increasing the effective conjugation length. The optical data are summarized in Table 3.4. The shapes of absorption and PL spectra of PTPA1-TPE and PTPA2-TPE are quite similar to the corresponding homopolytriphenylamines **P1** and **P2** (Figure 3.1), with absorption maxima at 372 nm and PL maxima at 516 nm and 512 nm, respectively. Both PTPA1-TPE and

PTPA2-TPE show green emissions. The PLQYs of PCz-TPE, PTPA1-TPE and PTPA2-TPE in dilute THF solution have been determined to be 1.2%, 0.4% and 1.4%, respectively, using quinine sulfate as reference. All of them emit faintly in dilute solution, however, they show a much stronger emission in the solid state. The PLQYs of solid powders are 28%, 20% and 37% for PCz-TPE, PTPA1-TPE and PTPA2-TPE, respectively, corresponding to 23, 50 and 26 times PL increase, respectively, if compared to the PLQYs in solution. These results again demonstrate the occurrence of distinct AIE effects. The increased AIE effects are attributed to the introduction of TPE units both in the backbone and side chain of the copolymers.

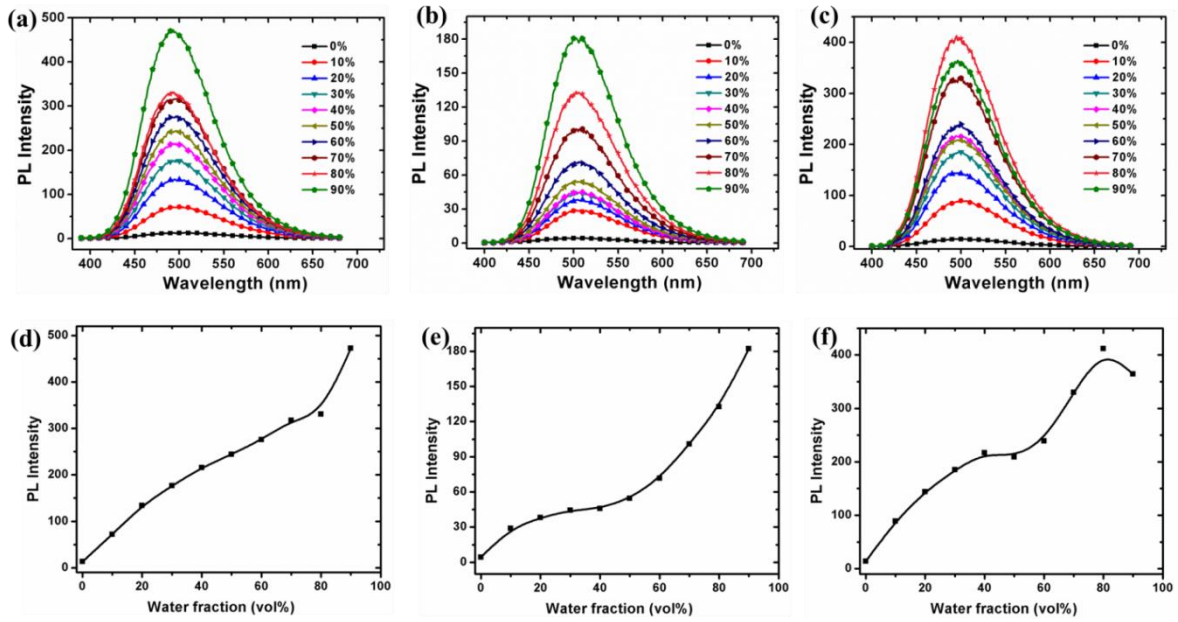

Figure 3.9. PL spectra of (a) PCz-TPE, (b) PTPA1-TPE and (c) PTPA2-TPE in THF/water mixtures with different water content; PL intensity with increasing water fraction for (d) PCz-TPE, (e) PTPA1-TPE and (f) PTPA2-TPE, respectively (polymer concentration: 10^{-5} M).

To further investigate the AIE phemomenons of the copolymers, a series of PL spectra was recorded in the solvent mixture THF/water (Figure 3.9). Since water is non-solvent for the copolymers, they are supposed to aggregate starting from a certain water content. The PL intensity of all copolymers increases with increasing water fraction, again confirming the occurrence of AIE effects. The maximum increase of PL intensity is 36, 42 and 30 times; in 90% water/THF for PCz-TPE and PTPA1-TPE or 80% water/THF for PTPA2-TPE, respectively, if compared to non-aggregated THF solutions. The introduction of bis(*tert*-butyl)-TPE units into the backbone of the copolymers leads to an enhancement of the

AIE effects coupled to an improved solubility of the copolymers, thus simplifying their solution processing.

3.4 Conclusions

Firstly, two homopolytriphenylamines (PTPAs) **P1** and **P2** with AIE-active tetraphenylethylene (TPE) side groups have been successfully synthesized. Both polymers show distinct AIE behavior in solvent/non-solvent mixtures and in the solid state, accompanied by high solid state quantum yields. Both **P1** and **P2** possess electron-rich PTPA backbones that are substituted by bulky and twisted TPE side groups, a structure that is beneficial for the interaction with electron-poor nitroaromatic analytes. **P1** and **P2** have been used as solid state sensing materials for electron-deficient nitroaromatic molecules. Hereby, the polymers exhibited high sensitivity and excellent reversibility in their interaction with 1,3,5-trinitrobenzene (TNB). Our results provide a promising molecular design strategy for sensitive, multi-use sensing materials for nitroaromatic analytes.

Moreover, the limited solubility of **P1** and **P2** is overcome by the introduction of bis(*tert*-butyl)-TPE groups into the backbone of the resulting copolymers. This strategy leads to a simultaneous improvement of AIE effects and copolymer solubility.

3.5 Experimental

3.5.1 Materials

All reagents were obtained from commercial suppliers and were used without further purification. All reactions were carried out under argon atmosphere by standard and Schlenk techniques. The solvents were used as commercial p.a. quality.

4,4,5,5-tetramethyl-2-(1,2,2-triphenylvinyl)-1,3,2-dioxaborolane (**1**)

To a solution of 1-bromo-1,2,2-triphenylethylene (10.0 g, 29.8 mmol) in dry THF (120 mL) a 2.8 M solution of *n*-BuLi in hexane (44.7 mmol) was added at -78 °C under argon atmosphere. The resulting solution was stirred for 2 h at -78 °C. To this solution 2-*iso*propoxy-4,4,5,5-tetramethyl-1,3,2-dioxaborolane (12.2 mL, 59.7 mmol) was added, and the reaction mixture was warmed up slowly to room temperature. After 48 h, the reaction was stopped by adding aqueous NH_4Cl solution. The organic layer was extracted with chloroform, and the combined organic layers were washed with a saturated brine solution and dried over $MgSO_4$. The solvent was evaporated, and the product was purified by silica gel

chromatography (eluent: hexane/ethylacetate = 9/1) to give the desired compound as white solid in 36% yield (4.1 g). ^{1}H NMR (600 MHz, $C_2D_2Cl_4$) δ (ppm) 7.28 (s, 5H), 7.16 - 7.03 (m, 6H), 7.00 (d, J = 3.4 Hz, 2H), 6.93 (d, J = 1.9 Hz, 2H), 1.09 (s, 12H). ^{13}C NMR (150 MHz, $C_2D_2Cl_4$) δ (ppm) 151.59, 144.84, 142.11, 141.89, 131.20, 129.96, 129.94, 128.27, 128.22, 127.99, 127.92, 127.10, 126.13, 83.98, 24.83.

1-(4-bromophenyl)-1,2,2-triphenylethylene (**2**)

To a solution of diphenylmethane (11.1 g, 65.7 mmol) in dry THF (100 mL) a 2.8 M solution of *n*-BuLi in hexane (65.7 mmol) was added at 0 °C under argon atmosphere. The resulting orange-red solution was stirred for 1 h at 0 °C. To this solution 4-bromobenzophenone (14.3 g, 54.8 mmol) was added, and the reaction mixture was allowed to warm up to room temperature overnight. The reaction was stopped by adding aqueous NH_4Cl solution. The organic layer was extracted with chloroform, and the combined organic layers were washed with a saturated brine solution and dried over anhydrous $MgSO_4$. The solvent was evaporated, and the resulting crude alcohol (containing excess diphenylmethane) was subjected to acid-catalyzed dehydration as follows. The crude alcohol was dissolved in toluene (200 mL) containing *p*-toluenesulphonic acid (2.7 g, 14.2 mmol) using a 500 mL flask, and the mixture was refluxed overnight. The toluene layer was washed with 10% aqueous $NaHCO_3$ solution, dried over $MgSO_4$ and evaporated to afford the crude tetraphenylethylene derivative. The crude product was purified by silica gel chromatography (eluent: hexane/dichloromethane = 3/1) to give the target compound as white solid in 64% yield (14.5 g). ^{1}H NMR (600 MHz, $CDCl_3$) δ (ppm) 7.25 (d, *J* = 8.6 Hz, 2H), 7.18 - 7.10 (m, 9H), 7.07 - 7.01 (m, 6H), 6.92 (d, *J* = 8.6 Hz, 2H).

4,4,5,5-tetramethyl-2-(4-(1,2,2-triphenylvinyl)phenyl)-1,3,2-dioxaborolane (**3**)

A mixture of **2** (10.0 g, 24.3 mmol), 4,4,4',4',5,5,5',5'-octamethyl-2,2'-bis(1,3,2-dioxaborolane) (8.64 g, 34.0 mmol), [1,1'-bis(diphenylphosphino)ferrocene]palladium(II) chloride as complex with dichloromethane ($Pd(dppf)Cl_2$) (596 mg, 0.73 mmol), and KOAc (7.2 g, 73.4 mmol) in degassed 1,4-dioxane (40 mL) was stirred at 90 °C for 24 h. The reaction was stopped by adding water, and the mixture was extracted with dichloromethane. The organic phase was collected, dried over $MgSO_4$, and concentrated in vacuum. The crude product was then purified by silica gel chromatography (eluent: hexane/dichloromethane = 2/1) to give the target compound as white solid in 75% yield (8.4 g). ^{1}H NMR (600 MHz, $C_2D_2Cl_4$) δ (ppm) 7.48 (d, *J* = 7.9 Hz, 2H), 7.13 - 7.05 (m, 9H), 7.05 - 6.95 (m, 8H), 1.29 (d,

J = 11.3 Hz, 12H). ^{13}C NMR (150 MHz, $C_2D_2Cl_4$) δ (ppm) 147.00, 143.75, 143.73, 143.71, 141.65, 141.00, 134.23, 131.54, 130.90, 128.00, 127.96, 127.92, 126.81, 126.69, 84.06, 25.25.

4-bromo-*N*-(4-bromophenyl)-*N*-(4-(1,2,2-triphenylvinyl)phenyl)aniline (**4**)

A mixture of tris(4-bromophenyl)amine (4.1 g, 8.5 mmol), **1** (3.0 g, 7.8 mmol), K_2CO_3 (1.1 g, 7.9 mmol), TBABr (0.3 g, 0.9 mmol) and $Pd(PPh_3)_4$ (272 mg, 0.24 mmol) was carefully degassed. Then, water (4 mL) and toluene (60 mL) were added. The resulting mixture was stirred at 95 °C for 24 h under argon atmosphere. After cooling down to room temperature, the reaction was stopped by adding water and the mixture was extracted with chloroform. The organic phases were collected, dried over $MgSO_4$ and concentrated in vacuum. The product was purified by silica gel chromatography (eluent: hexane/dichloromethane = 5/1) to give the desired compound as light green solid in 28% yield (1.45 g). ^{1}H NMR (600 MHz, $C_2D_2Cl_4$) δ (ppm) 7.30 (d, J = 8.9 Hz, 4H), 7.14 - 7.04 (m, 11H), 7.04 - 6.98 (m, 4H), 6.91-6.83 (m, 6H), 6.74 (d, J = 8.6 Hz, 2H). ^{13}C NMR (150 MHz, $C_2D_2Cl_4$) δ (ppm) 146.55, 145.01, 144.09, 143.69, 143.45, 141.24, 140.67, 139.53, 132.73, 132.55, 131.59, 131.56, 131.54, 127.97, 127.92, 127.84, 126.73, 126.69, 126.63, 125.53, 123.84, 115.46. MS (APLI): m/z calcd 657.05; found 657.04. Elemental anal. calcd: C, 69.42%; H, 4.14%; N, 2.13%. Found: C, 69.06%; H, 4.14%; N, 2.14%.

N,*N*-bis(4-bromophenyl)-4'-(1,2,2-triphenylvinyl)-[1,1'-biphenyl]-4-amine (**5**)

A mixture of tris(4-bromophenyl)amine (3.4 g, 7.0 mmol), **3** (2.9 g, 6.4 mmol), K_2CO_3 (0.9 g, 6.5 mmol), TBABr (0.2 g, 0.62 mmol) and $Pd(PPh_3)_4$ (222 mg, 0.19 mmol) was carefully degassed. Then, water (3 mL) and toluene (35 mL) were added. The resulting mixture was stirred at 95 °C for 24 h under an argon atmosphere. After cooling down to room temperature, the reaction was stopped by adding water and the mixture was extracted with chloroform. The organic phases were collected, dried over $MgSO_4$ and concentrated in vacuum. The product was purified by silica gel chromatography (eluent: hexane/dichloromethane = 5/1) to give the desired compound as light green solid in 33% yield (1.55 g). ^{1}H NMR (600 MHz, $C_2D_2Cl_4$) δ (ppm) 7.46 (d, *J* = 8.7 Hz, 2H), 7.36 - 7.30 (m, 6H), 7.13 - 6.99 (m, 19H), 6.95 (d, *J* = 8.9 Hz, 4H). ^{13}C NMR (150 MHz, $C_2D_2Cl_4$) δ (ppm) 146.55, 146.27, 143.93, 143.91, 143.87, 142.94, 141.33, 140.72, 137.69, 135.67, 132.69, 132.16, 131.66, 131.59, 128.05, 127.95, 127.92, 126.72, 126.69, 126.64, 125.82, 125.79, 124.88, 115.79. MS (APLI): m/z

calcd 733.08; found 733.07. Elemental anal. calcd: C, 72.04%; H, 4.26%; N, 1.91%. Found: C, 71.92%; H, 4.27%; N, 1.91%.

P1:

A solution of monomer **4** (600 mg, 0.91 mmol), $Ni(COD)_2$ (653 mg, 2.37 mmol), BPy (371 mg, 2.37 mmol) and COD (257 mg, 2.37 mmol) in THF (7 mL) was reacted under microwave (MW) heating at 120 °C for 12 min. The reaction was stopped by adding water and the mixture was extracted with chloroform. The collected organic phases were washed with aqueous 2 M HCl, aqueous $NaHCO_3$ solution, saturated, aqueous EDTA solution and brine, and finally dried over $MgSO_4$. Afterwards, the solvents were removed in vacuum. The resulting solid was dissolved in a small amount of chloroform and precipitated into methanol (500 mL) to afford the target polymer as light-green solid. Subsequent Soxhlet extractions were carried out with methanol, acetone, ethyl acetate and chloroform, respectively. After re-precipitation of the chloroform-soluble fraction into methanol, the light green polymer was obtained in 61% yield (275 mg). ^{1}H NMR (400 MHz, $C_2D_2Cl_4$, 60 °C) δ (ppm) 7.61 - 7.46 (m, 5H), 7.41 - 7.31 (m, 2H), 7.25 - 7.00 (m, 20H). M_n 11500, M_w 26800, and M_w/M_n 2.32 (GPC, PS calibration).

P2:

A solution of monomer **5** (600 mg, 0.82 mmol), $Ni(COD)_2$ (585 mg, 2.13 mmol), BPy (332 mg, 2.13 mmol) and COD (230 mg, 2.13 mmol) in THF (6 mL) was reacted under MW heating at 120 °C for 12 min. The workup procedure was similar to that described for the preparation of **P1**. The light-green polymer was obtained in 88% yield (413 mg). ^{1}H NMR (400 MHz, $C_2D_2Cl_4$, 60 °C) δ (ppm) 7.63 - 7.42 (m, 5H), 7.38 - 7.00 (m, 22H), 6.99 - 6.52 (m, 4H). M_n 25100, M_w 83700, and M_w/M_n 3.33 (GPC, PS calibration).

4,4'-(2,2-bis(4-(*tert*-butyl)phenyl)ethene-1,1-diyl)bis(bromobenzene) (**6**)

To a solution of bis[4-(*tert*-butyl)phenyl]methane (3.03 g, 10.82 mmol) in dry THF (20 mL) a 2.8 M solution of *n*-BuLi in hexane (3.86 mL, 10.82 mmol) was added at 0 °C under an argon atmosphere. The resulting orange-red solution was stirred for 1 h at that temperature. To this solution, 4,4'-dibromobenzophenone (3.07 g, 9.02 mmol) in THF (25 mL) was added. Next, the reaction mixture was allowed to warm up to room temperature overnight. The reaction was stopped by addition of saturated aqueous NH_4Cl solution. The aqueous layer was extracted with chloroform, and the combined organic layers were washed with a saturated

brine solution and dried over anhydrous $MgSO_4$. The solvents were removed by evaperation and the resulting crude alcohol (containing excess diphenylmethane) was subjected to acid-catalyzed dehydration as follows: The crude product was dissolved in toluene (50 mL) containing *p*-toluenesulphonic acid (0.45 g, 2.34 mmol) in a 100 mL flask, and the mixture was refluxed at 110°C overnight. The toluene layer was washed with aqueous $NaHCO_3$ solution and dried over $MgSO_4$ and evaporated to afford the crude tetraphenylethylene derivative. The product was purified by silica gel chromatography (eluent: dichloromethane/hexane = 1/9) to give desired compound as a white solid in 30% yield (1.63 g). ^{1}H NMR (600 MHz, $CDCl_3$) δ (ppm) 7.23 (d, *J* = 8.6 Hz, 4H), 7.15 (d, *J* = 8.5 Hz, 4H), 6.93 (d, *J* = 8.5 Hz, 4H), 6.88 (d, *J* = 8.6 Hz, 4H), 1.29 (s, 18H). ^{13}C NMR (150 MHz, $CDCl_3$) δ (ppm) 149.80, 142.70, 142.24, 140.03, 137.35, 133.01, 130.83, 130.80, 124.63, 120.35, 34.47, 31.28. MS (APLI): m/z calcd 602.10; found 602.08. Elemental anal. calcd: C, 67.78%; H, 5.69%. Found: C, 68.14%; H, 5.66%.

PCz-TPE

A solution of monomer **6** (200 mg, 0.33 mmol), TPE-substituted dibromocarbazole (see Chapter 2, 218 mg, 0.33 mmol), $Ni(COD)_2$ (457 mg, 1.66 mmol), BPy (259 mg, 1.66 mmol) and COD (180 mg, 1.66 mmol) in THF (5 mL) was reacted under MW heating at 120 °C for 12 min. The workup procedure was similar to that described for the preparation of **P1**. The light-green polymer was obtained in 76% yield (236 mg). ^{1}H NMR (400 MHz, $C_2D_2Cl_4$, 60 °C) δ (ppm) 8.43 (dd, *J* = 53.4, 26.6 Hz, 2H), 7.74 (d, *J* = 67.3 Hz, 2H), 7.58 - 7.26 (m, 10H), 7.26 - 6.90 (m, 27H), 1.28 (s, 18H). M_n 19000, M_w 40300, and M_w/M_n 2.12 (GPC, PS calibration).

PTPA1-TPE

A solution of monomer **6** (200 mg, 0.33 mmol), monomer **4** (218 mg, 0.33 mmol), $Ni(COD)_2$ (457 mg, 1.66 mmol), BPy (259 mg, 1.66 mmol) and COD (180 mg, 1.66 mmol) in THF (5 mL) was reacted under MW heating at 120 °C for 12 min. The workup procedure was similar to that described for the preparation of **P1**. The light-green polymer was obtained in 80% yield (248 mg). ^{1}H NMR (400 MHz, $C_2D_2Cl_4$, 60 °C) δ (ppm) 7.58 - 7.30 (m, 8H), 7.27 - 6.99 (m, 31H), 6.99 - 6.82 (m, 4H), 1.42 - 1.19 (m, 18H). M_n 56700, M_w 189000, and M_w/M_n 3.34 (GPC, PS calibration).

PTPA1-TPE

A solution of monomer **6** (200 mg, 0.33 mmol), monomer **5** (244 mg, 0.33 mmol), $Ni(COD)_2$ (457 mg, 1.66 mmol), BPy (259 mg, 1.66 mmol) and COD (180 mg, 1.66 mmol) in THF (5 mL) was reacted under MW heating at 120 °C for 12 min. The workup procedure was similar to that described for the preparation of **P1**. The light-green polymer was obtained in 87% yield (293 mg). ^{1}H NMR (400 MHz, $C_2D_2Cl_4$, 60 °C) δ (ppm) 7.62 - 7.44 (m, 6H), 7.44 - 7.28 (m, 6H), 7.28 - 6.89 (m, 35H), 1.28 (s, 18H). M_n 32700, M_w 165000, and M_w/M_n 5.03 (GPC, PS calibration).

3.5.2 Instrumentation

NMR spectra were recorded on a Bruker AVANCE 400 or AVANCE III 600. ^{1}H and ^{13}C NMR spectra were measured with tetramethylsilane (TMS) as internal standard. Gel permeation chromatography (GPC) measurements were carried out on a PSS/Agilent SECurity GPC System equipped with polystyrene gel columns using chloroform as eluent. APLI (Atmospheric Pressure Laser Ionization) measurements were carried out on Bruker Daltronik Bremen with micrOTOF. UV-visible absorption spectra were recorded on a Jasco V-670 spectrometer, and PL spectra on a Varian CARY Eclipse F2500. Elemental analyses were performed on a Vario EL II (CHNS) instrument. The PL quantum efficiencies of polymer solid powder were measured with an integrating sphere.The HOMO (highest occupied molecular orbital) levels were estimated on a Surface Analyzer MODEL AC-2 on RIKEN, given as the threshold where photoelectron emission first occurs.

3.6 References

1. W. Dong, Y. Pan, M. Fritsch and U. Scherf, *J. Polym. Sci., Part A: Polym. chem.*, 2015, **53**, 1753-1761.
2. X. Wu, H. Li, B. Xu, H. Tong and L. Wang, *Polym. Chem.*, 2014, **5**, 4521-4525.
3. W. Z. Yuan, R. Hu, J. W. Y. Lam, N. Xie, C. K.W. Jim and B. Z. Tang, *Chem. Eur. J.*, 2012, **18**, 2847-2856.
4. R. Hu, N. L. C. Leung and B. Z. Tang, *Chem. Soc. Rev.*, 2014, **43**, 4494-4562.
5. N. Venkatramaiah, S. Kumar and S. Patil, *Chem. Commun.*, 2012, **48**, 5007-5009.
6. N. Venkatramaiah, S. Kumar and S. Patil, *Chem. Eur. J.*, 2012, **18**, 14745-14751.
7. H. Nie, Y. Zhao, M. Zhang, Y. Ma, M. Baumgarten and K. Müllen, *Chem. Commun.*, 2011, **47**, 1234-1236.
8. J. L. Novotney and W. R. Dichtel, *ACS Macro Lett.*, 2013, **2**, 423-426.
9. P. Vishnoi, M. G. Walawalkar, S. Sen, A. Datta, G. N. Patwari and R. Murugavel, *Phys. Chem. Chem. Phys.*, 2014, **16**, 10651-10658.
10. S. Shanmugaraju, H. Jadhav, R. Karthik and P. S. Mukherjee, *RSC Adv.*, 2013, **3**, 4940-4950.
11. B. Xu, Y. Xu, X. Wang, H. Li, X. Wu, H. Tong and L. Wang, *Polym. Chem.*, 2013, **4**, 5056-5059.
12. X. Wu, H. Li, Y. Xu, B. Xu, H. Tong and L. Wang, *Nanoscale*, 2014, **6**, 2375-2380.
13. Z. Ding, Q. Zhao, R. Xing, X. Wang, J. Ding, L. Wang and Y. Han, *J. Mater. Chem. C*, 2013, **1**, 786-792.
14. J. Yang and T. M. Swager, *J. Am. Chem. Soc.*, 1998, **120**, 5321-5322.
15. H. Ma, L. Yao, P. Li, O. Ablikim, Y. Cheng and M. Zhang, *Chem. Eur. J.*, 2014, **20**, 11655-11658.
16. T. Naddo, Y. Che, W. Zhang, K. Balakrishnan, X. Yang, M. Yen, J. Zhao, J. S. Moore and L. Zang, *J. Am. Chem. Soc.*, 2007, **129**, 6978-6979.
17. P. Gong, P. Xue, C. Qian, Z. Zhang and R. Lu, *Org. Biomol. Chem.*, 2014, **12**, 6134-6144.

Chapter 4

4. Polycarbazole and Polytriphenylamine with 2,3,3-Triphenylacrylonitrile Side Groups[1]

Acceptor-substituted polycarbazole (PCzTPAN) and polytriphenylamine (PTPATPAN) bearing electron-deficient 2,3,3-triphenylacrylonitrile (TPAN) side groups have been successfully synthesized. Both of them are aggregation-induced emission (AIE)-active and show intramolecular charge transfer (ICT) behavior. PCzTPAN and PTPATPAN aggregates in 90% water/THF were used for the detection of 1,3,5-trinitrobenzene (TNB) as prototypical nitroaromatic compound. They show amplified PL quenching upon addition of TNB with a maximum quenching constant of 5.5×10^5 M^{-1}. As additional application example, the detection of the glass transition temperature of polystyrene (PS) was accomplished for PTPATPAN blended into PS at doping concentrations of 0.1-1.0 wt%.

4.1 Introduction

In the last two chapters, tetraphenylethylene (TPE) side groups were successfully incorporated into polycarbazole or polytriphenylamine backbones. The resulting polymers and copolymers both showed pronounced AIE effects as well as a high sensitivity in PL quenching experiments towards nitroaromatic compounds. As known from literature, not only TPE itself but also triphenylethylene derivatives, for example, 2,3,3-triphenylacrylonitrile (TPAN) can be utilized for designing AIE luminogens. TPAN is related to TPE by replacing one phenyl ring by a cyano group. For TPAN, a so-called crystallization-induced emission (CIE) effect was reported[2]. TPAN is weakly emissive in solution (PLQY of 1.1% in THF) and as amorphous powdery solid, but highly emissive in its crystalline state (PLQY of 43.4%), with a CIE coefficient α_{CIE} of 40.2. Many luminogens containing TPAN units were synthesized, showing AIE-activity, high contrast mechanochromism[3-6] and application potential in efficient OLEDs[7].

TPAN is an electron-deficient building block caused by the cyano group. Thus, TPAN can serve as an electron-acceptor moiety in the construction of donor-acceptor (D-A) dyads in combination with suited electron-rich moieties. D-A molecules[8-11] have attracted much

interest because of their unique optical and electronical properties, including intramolecular charge transfer (ICT), with potential applications in OLEDs, OPV devices, microenvironmental detectors, mechano-, chemo- and biosensors, *etc.* In this chapter, AIE-active polycarbazole (PCzTPAN) and polytriphenylamine (PTPATPAN) with electron-acceptor TPAN substituents have been successfully synthesized (depicted in Chart 4.1). TPAN as electron-deficient moiety was now attached to the backbone of electron-rich polycarbazole and polytriphenylamine thus designing donor-acceptor-type polymers. Here, the aggregation-induced emission (AIE) and the intramolecular charge transfer (ICT) properties of PCzTPAN and PTPATPAN have been investigated. Furthermore, the novel polymers were used for the detection of 1,3,5-trinitrobenzene (TNB) as prototypical nitroaromatic explosive. In addition, one polymer (PTPATPAN) was used as fluorescent probe in the detection of the glass transition temperature of polystyrene (PS).

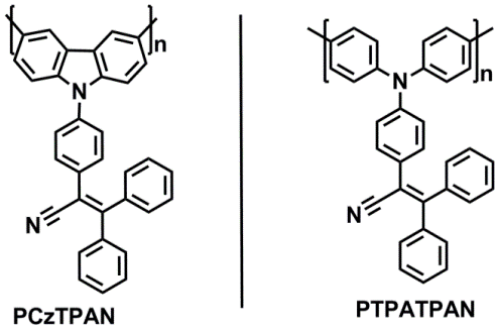

Chart 4.1. The chemical structures of polymer PCzTPAN and PTPATPAN.

4.2 Results and Discussion

4.2.1 Synthesis and Characterization

The synthetic route towards the monomers **1**/**2** and polymers PCzTPAN/PTPATPAN is depicted in Scheme 4.1. Monobromo-TPAN (2-(4-bromophenyl)-3,3-diphenylacrylonitrile) was obtained by treating a mixture of benzophenone and 2-(4-bromophenyl)acetonitrile with sodium hydride (NaH)[5]. Treatment of monobromo-TPAN with carbazole or diphenylamine under Buchwald-Hartwig coupling conditions afforded TPAN-substituted carbazole or triphenylamine in good yields. Dibromo-monomers **1** and **2** were obtained *via* bromination of TPAN-substituted carbazole or triphenylamine with NBS. Polymer PCzTPAN was synthesized by Yamamoto-type homocoupling with $Ni(COD)_2$, COD and Bpy in a solvent mixture of toluene and DMF under conventional heating at 80 °C. Polymer PTPATPAN was also synthesized by Yamamoto-type homocoupling, but in this case under microwave heating

to 120 °C. The structure elucidation of the monomers was performed by NMR spectroscopy, mass spectrometry and elemental analysis. The chemical structure of the obtained polymers was finally confirmed by GPC as well as NMR spectroscopy and optical spectroscopy.

For successful polymerization, increased catalyst and ligand (COD and Bpy) amounts as well as increased reaction times were applied, since the cyano groups of the TPAN units seem to cause a reduced activity of the catalytic Ni(0) complex.

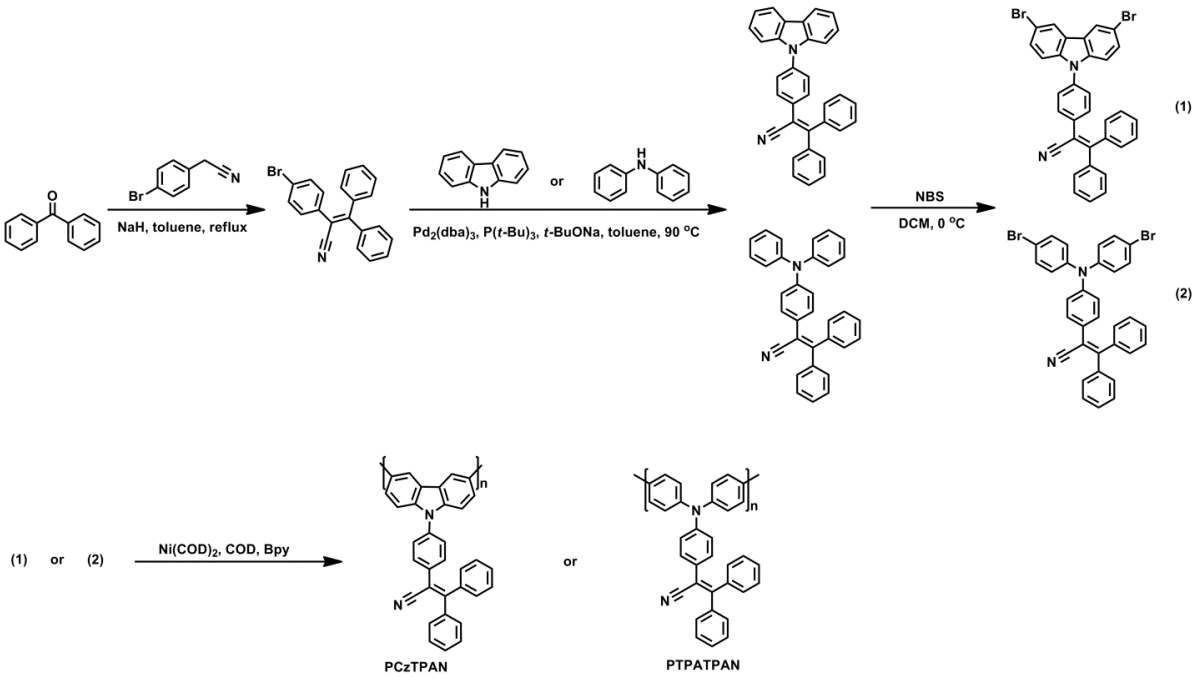

Scheme 4.1. The synthetic route to monomers **1**/**2** and polymer PCzTPAN and PTPATPAN, respectively.

4.2.2 Photophysical Properties

Table 4.1. Optical data and HOMO/LUMO energy levels of PCzTPAN and PTPATPAN.

	λ_{UV}/nm in THF	λ_{PL}/nm in THF	λ_{UV}/nm in film	λ_{PL}/nm in film	η_{PL} (%) in THF	η_{PL} (%) in film	HOMO eV	LUMO eV
PCzTPAN	307, 342(sh)	507	312, 348(sh)	546	4	10	-5.41	-2.53
PTPATPAN	381	637	378	595	4	19	-5.35	-2.58

Figure 4.1 shows the UV-vis and PL spectra of polymers PCzTPAN and PTPATPAN in dilute THF solution and as thin films. The absorption spectra in solution and solid state are quite similar since the twisted structure of the polymers does not allow significant intermolecular π-π stacking interactions in the solid state. As thin film, PCzTPAN shows an

absorption maximum at 312 nm with a shoulder at 348 nm; PTPATPAN an absorption maximum at 378 nm, attributed to the π-π transitions of the polymer backbones. In their PL spectra, the films of PCzTPAN and PTPATPAN show emission maxima at 546 nm and 595 nm, giving rise to a green or orange color of the emitted light, respectively. The corresponding solutions emitted at 507 nm and 637 nm, with a ~40 nm hypsochromic shift for PCzTPAN and bathochromic shift in the same order for PTPATPAN, respectively. The shifts are probably caused by different electronic properties of the electron-rich backbones thus resulting in different intramolecular charge-transfer (ICT) properties.

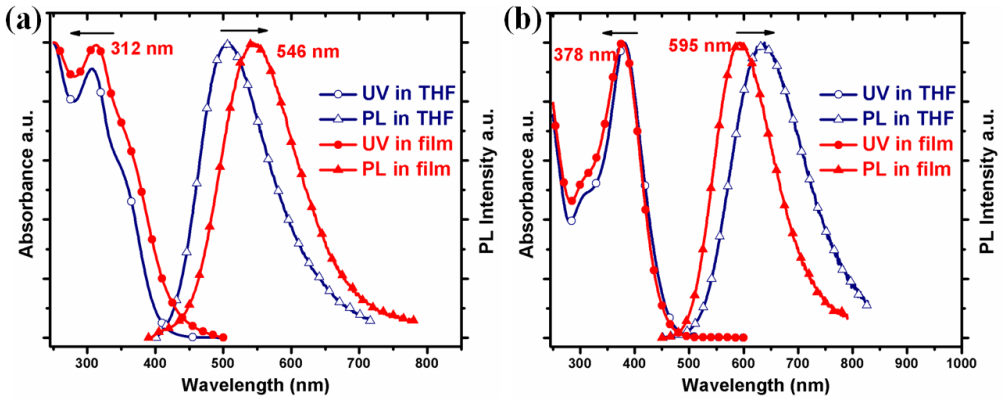

Figure 4.1. Normalized absorption and PL spectra of (a) PCzTPAN and (b) PTPATPAN in dilute THF solution (polymer concentration: 10^{-5} M) and as spin-coated films (measured at room temperature).

4.2.2.1 Intramolecular Charge Transfer Properties

The presence of electron-donating TPA or carbazole in combination with the electron-accepting cyano groups of the TPAN units should allow the occurrence of ICT processes. To investigate this topic, absorption and emission spectra of both polymers in varying solvents were recorded. Since the photophysical properties of such D-A conjugates are strongly dependent on the solvent polarity, solvatochromic effects of the PL spectra are expected for both polymers (Figure 4.2). The spectral profiles for both absorption spectra remain very similar (Figure 4.2a/c), suggesting a solvent polarity-independent electronic structure of the ground state. However, the emission maxima of both polymers are gradually bathochromically shifted with increasing solvent polarity, with a 68 or 64 nm red-shift for PCzTPAN and PTPATPAN (shown in Figure 4.2b/d), respectively, when going from toluene to DMF. Such a behavior may reflect an increased dipole moment of the excited state,

indicating that the lowest energy excited state S_1 of both polymers involves a strong CT component.

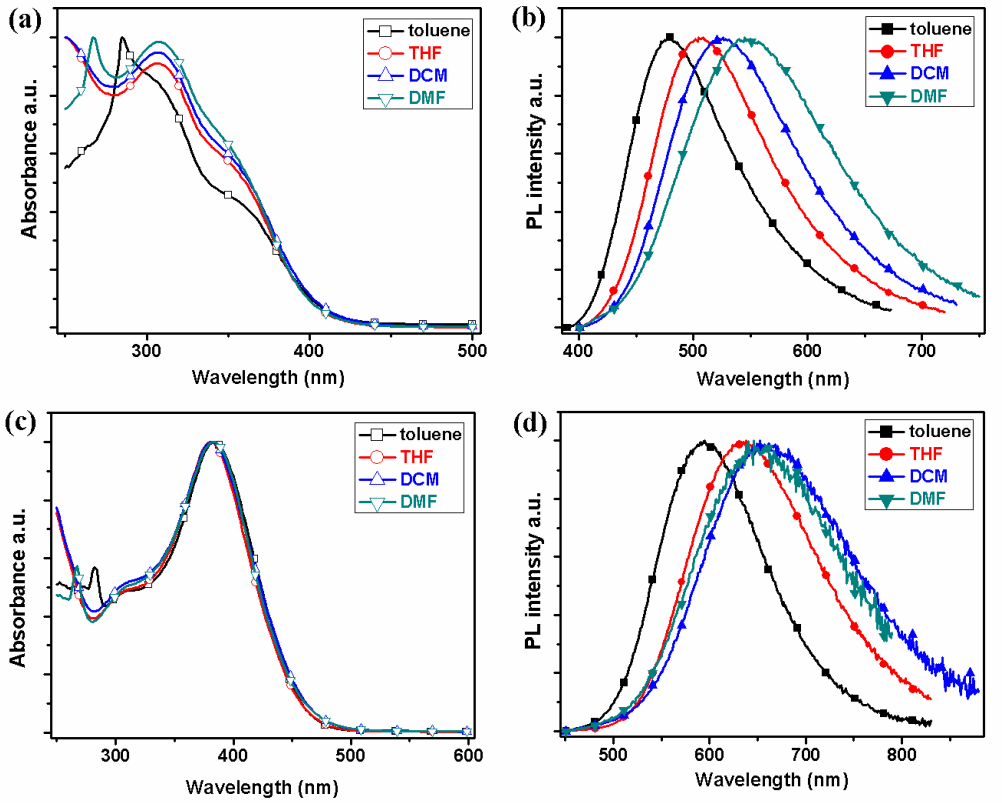

Figure 4.2. Normalized absorption and PL spectra of (a/b) PCzTPAN and (c/d) PTPATPAN, respectively, in toluene, THF, DCM and DMF solution (polymer concentration: 10^{-5} M).

The solvatochromic effect can be quantified through the slope of a plot of Stokes shift (Δv) *vs.* the orientation polarizability Δf of the solvents, according to the Lippert-Mataga equation [12,13]:

$$\Delta v = v_a - v_e = \frac{2\Delta f}{hca^3}(\mu_E - \mu_G)^2 + constant$$

where Δf is the orientational polarizability of the solvent, $v_a - v_e$ corresponds to the Stokes shifts, μ_E and μ_G are the excited state and ground-state dipole moment, respectively, h and c are the Planck constant and the speed of light, respectively, a is the Onsager solvent cavity radius.

Orientational polarizability Δf can be calculated as follow:

$$\Delta f(\varepsilon, n) = \frac{\varepsilon - 1}{2\varepsilon + 1} - \frac{n^2 - 1}{2n^2 + 1}$$

where ε and n are the static dielectric and optical refractive index of the solvent, respectively.

Table 4.2. Absorption and emission maxima of PCzTPAN and PTPATPAN, as well as Stokes shifts ($\Delta\nu$), dielectric constant of the solvents (ε), refractive index of the solvents (n) and orientation polarizability (Δf) of the solvents.

	solvent	λ_{UV} (nm)	λ_{PL} (nm)	$\Delta\nu$ (cm^{-1})	ε	n	Δf
PCzTPAN	toluene	302	479	12236	2.38	1.4969	0.013
	DCM	308	525	13420	8.93	1.4241	0.217
	THF	307	507	12849	7.58	1.4072	0.210
	DMF	308	547	14186	36.7	1.4305	0.274
	chlorobenzene	308	502	12547	5.62	1.5248	0.143
	chloroform	307	502	12653	4.81	1.4458	0.148
	o-dichlorobenzene	309	515	12945	9.93	1.5514	0.186
	1,4-dioxane	306	482	11933	2.25	1.4224	0.025
PTPATPAN	toluene	383	595	9303	2.38	1.4969	0.013
	DCM	382	659	11004	8.93	1.4241	0.217
	THF	381	637	10548	7.58	1.4072	0.210
	DMF	383	655	11842	36.7	1.4305	0.274
	chlorobenzene	387	637	10141	5.62	1.5248	0.143
	chloroform	384	640	10417	4.81	1.4458	0.148
	o-dichlorobenzene	387	644	10312	9.93	1.5514	0.186
	1,4-dioxane	383	604	9553	2.25	1.4224	0.025

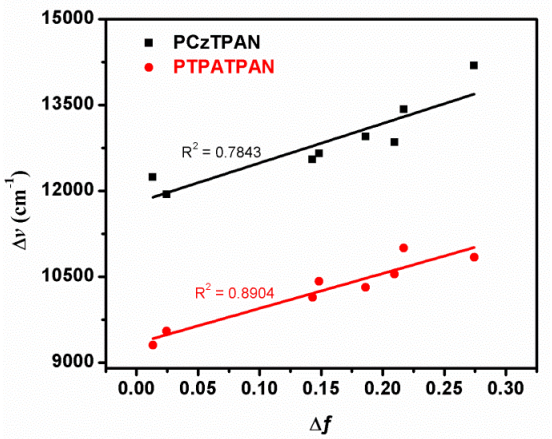

Figure 4.3. Stokes shift ($\Delta\nu$) vs. solvent polarity parameter (Δf) plots for PCzTPAN and PTPATPAN, for 8 solvents (toluene, 1,4-dioxane, chlorobenzene, chloroform, o-dichlorobenzene, THF, DCM, DMF).

In a linear fit of the experimental data ($\Delta\nu$ *vs.* Δf, Table 4.2), as shown in Figure 4.3, both polymers exhibit large slopes of 6904 cm^{-1} for PCzTPAN and 6095 cm^{-1} for PTPATPAN, respectively. The results confirm a substantial charge redistribution during excitation.

4.2.2.2 Aggregation-Induced Emission

The PL quantum yields of PCzTPAN and PTPATPAN in dilute THF solution, estimated by using quinine sulfate as standard, have been determined as ca. 4% for both of them. Thin films of the polymers exhibited much higher PLQYs of 10% and 19% for PCzTPAN and PTPATPAN, respectively (Table 4.1). Evidently, the transition into the condensed state enhances the PL of the polymers due to the presence of the TPAN side chains. The AIE phenomenon of PCzTPAN and PTPATPAN was further investigated in THF/water solvent mixtures. THF is a good solvent for both polymers; water serves as non-solvent. Figure 4.4 shows PL spectra as well as plots of relative PL intensities and the position of the PL maxima for different THF/water mixtures for both polymers. For PCzTPAN (Figure 4.4a/b), the relative PL intensity first decreases with increasing water content till 50%, accompanied by a bathochromic shift of the PL maximum, from 505 nm for pure THF to 555 nm for 50% water. The PL quenching as well as the bathochromic shift may result from an increased solvent polarity as typical ICT-related behavior. From 50% to 90% water, the PL intensity of PCzTPAN gradually increases without significant PL shift, a behavior that is characteristic for AIE chromophores that form nanoaggregates at high non-solvent contents, thus activating the RIR process. For PTPATPAN (Figure 4c/d), up to a water fraction of 10%, the PL intensity decreases; from 10% to 90% water, ongoing aggregation causes a 7-fold increase of the PL intensity. PTPATPAN displays, in contrast to PCzTPAN, a slight blue-shift during water addition. The blue-shift maybe caused by an introduction of geometrical disorder (increasing distortion) during aggregation. In comparison, the PCz backbone of PCzTPAN is more rigid and should be more resilient against torsional disorder. PL decay experiments support the discussion of our steady state PL data (Table 4.3): The mean PL lifetime of PCzTPAN decreases from 563 ps in THF to 392 ps in 50% water/THF and increases to 644 ps in 90% water/THF. For PTPATPAN, it decreases from 487 ps in THF to 295 ps in 10% water/THF and increases to 1174 ps in 90% water/THF. Generally, PL quenching is accompanied by a decrease of PL lifetimes. Oppositely, increased PL lifetimes indicate an increase of radiative excited state deactivation processes, thus leading to enhanced PL intensity. The observed changes of PL maxima, PL intensity and PL lifetimes in different solvent mixtures illustrate the competition between ICT and AIE behavior, occurring in our

polymers.

Table 4.3. Photoluminescence lifetime data of PCzTPAN and PTPATPAN in different THF/water mixtures, including decay times (τ), their percentage values (**a**) as well as the mean PL lifetimes ($<\tau>$).

polymer	solvent	τ_1 (ps)	τ_2(ps)	τ_3 (ps)	a_1	a_2	a_3	$<\tau>$ (ps)
PCzTPAN	THF	70	430	1740	0.453	0.321	0.226	563
	50%water	50	350	2190	0.595	0.285	0.12	392
	90%water	50	400	2710	0.517	0.299	0.184	644
PTPATPAN	THF	40	420	940	0.308	0.339	0.353	487
	10%water	50	270	1520	0.408	0.499	0.092	295
	90%water	140	630	2520	0.287	0.351	0.362	1174

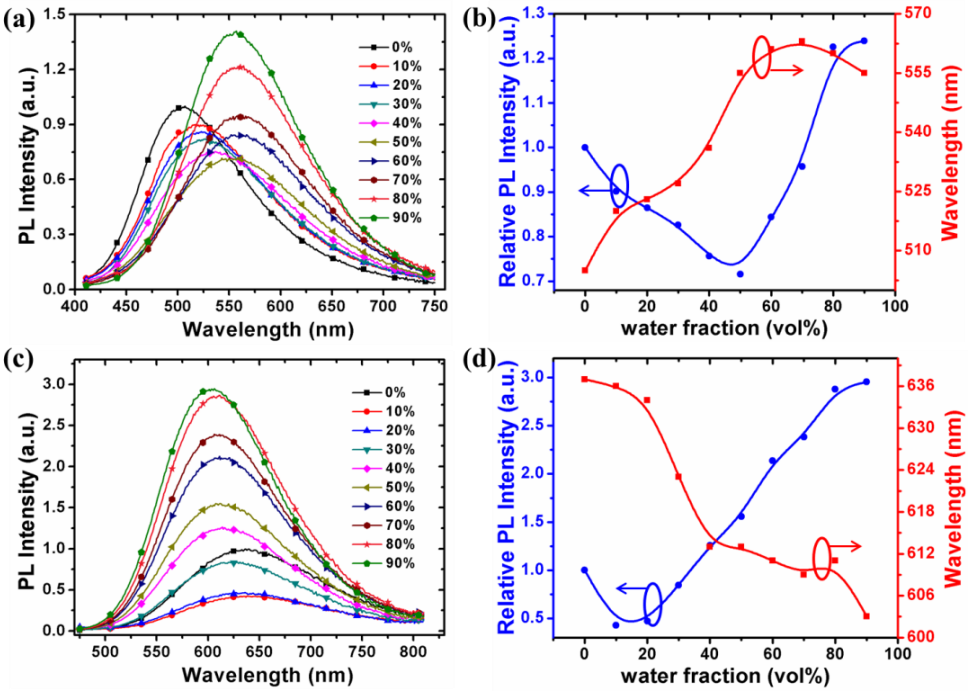

Figure 4.4. PL spectra of (a) PCzTPAN and (c) PTPATPAN in THF/water mixtures with different water content; PL intensity and PL maxima with increasing water content for (b) PCzTPAN and (d) PTPATPAN, respectively (polymer concentration: 10^{-6} M).

4.2.3 Theoretical Calculations

Theoretical calculations were carried out for further understanding of the electronic properties of both polymers by density functional theory (DFT) using B3LYP functional and 6-31g* basic sets, as implemented in the Gaussian 09 program. The optimized structures and

orbital distributions of the highest occupied molecular orbitals (HOMOs) and lowest unoccupied molecular orbitals (LUMOs) of PCzTPAN and PTPATPAN are depicted in Figure 4.5, in both cases two repeat units are shown. The TPAN side chains in both polymers adopt a highly twisted conformation, which is a prerequisite for the occurrence of AIE effects. In this way π-π stacking causing PL quenching in the aggregated state can be prevented. It is worthy to note that the HOMOs of both polymers are predominantly located at the electron-rich polycarbazole and polytriphenylamine backbones. In contrast, the LUMOs are mainly located at electron-poor TPAN side groups. Generally, this type of electron distribution allows for the occurrence of ICT effects what is consistent with our experimental results.

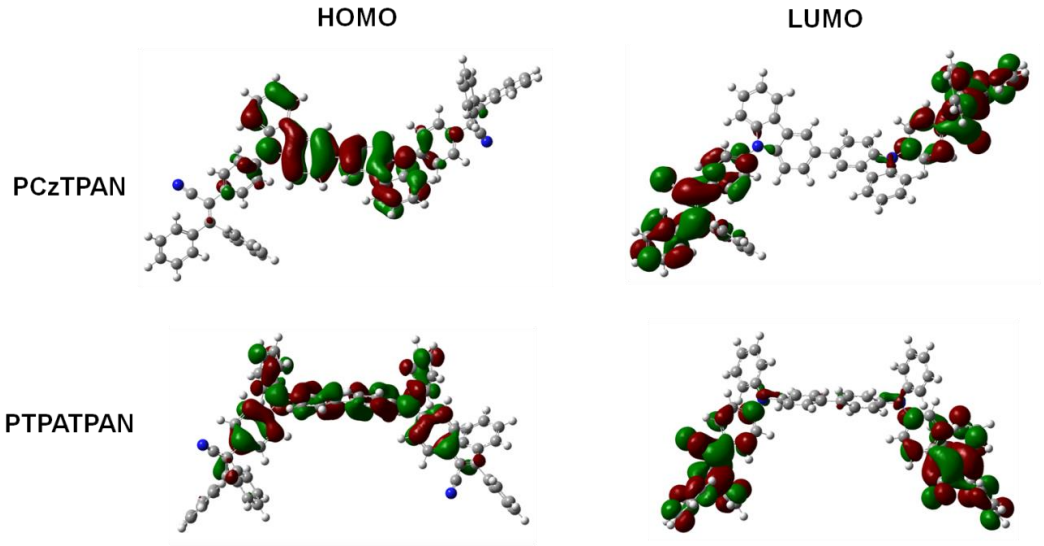

Figure 4.5. Calculated molecular orbital amplitude plots for HOMO and LUMO of PCzTPAN and PTPATPAN.

4.2.4 Explosive Detection

4.2.4.1 TNB Detection based on PCzTPAN and PTPATPAN Aggregates in 90% Water/THF

Presence of the electron-rich polycarbazole and polytriphenylamine backbones in combination with the AIE-based high solid state PL efficiencies, our polymers seem well-suited for the detection of electron-deficient nitroaromatic compounds. To explore the potential, we selected 1,3,5-trinitrobenzene (TNB) as prototypical nitroaromatic compound. The tests were carried out with dispersions of nanoaggregates of both polymers in 90% water/THF mixtures (polymer concentration: 1 μM). Figure 4.6a/c show the PL spectra of

those PCzTPAN and PTPATPAN dispersions treated with different amounts of TNB. Hereby, the PL intensity decreases progressively with increased concentration of TNB for both polymers, without any significant spectral change. For the PCzTPAN dispersion, 95% of the PL emission are quenched at a TNB concentration of 57 µM; for PTPATPAN 85% of the PL are quenched for a concentration of 143 µM. Stern-Volmer plots of relative PL intensity (I_0/I-1) *vs.* TNB concentration reflect the very promising sensing performance. The plots display upward-bent curves for both polymers (Figure 4.6b/d), indicating a more efficient quenching process, that means so-called amplified quenching, for higher quencher concentrations. Here, we split each curve into 3 subparts, each of them was linearly fitted. For PCzTPAN the obtained quenching constants are: 1.2×10^5 M^{-1} for a TNB concentration <19 µM, 3.4×10^5 M^{-1} for TNB concentrations between 19 µM and 40 µM, and 5.5×10^5 M^{-1} for TNB concentrations between 42 µM and 57 µM. For PTPATPAN somewhat lower quenching constants: 2.5×10^4 M^{-1} for a TNB concentration <46 µM, 4.0×10^4 M^{-1} for TNB concentrations between 48 µM and 83 µM, and 5.2×10^4 M^{-1} for TNB concentrations between 85 µM and 143 µM. These quenching constants belong to the top values within the published PL quenching schemes for the detection of nitroaromatic analytes[14].

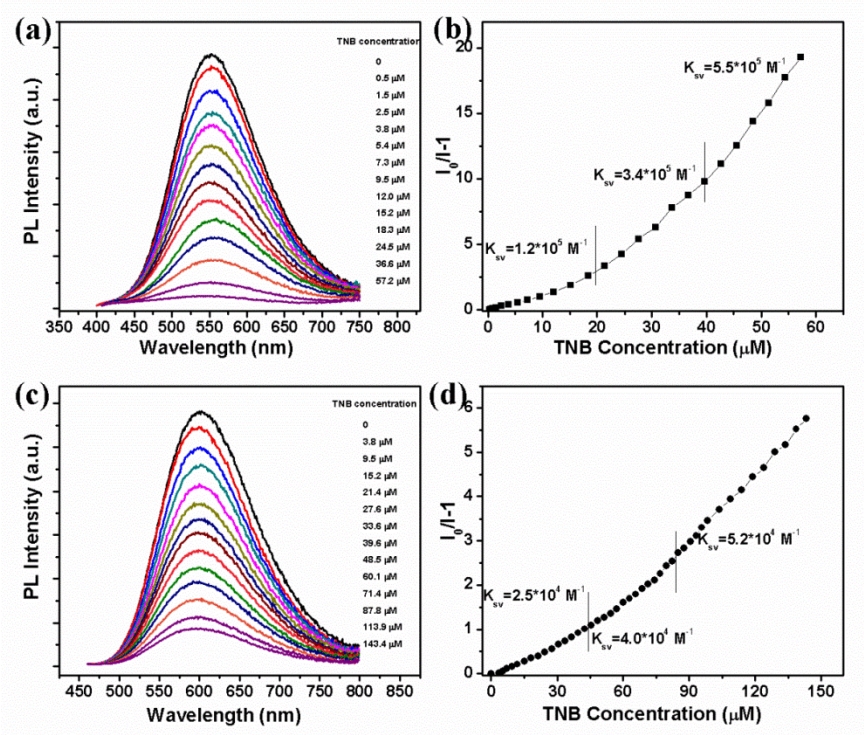

Figure 4.6. PL spectra of (a) PCzTPAN and (c) PTPATPAN, respectively, in THF/water 1/9 containing different amounts of TNB (polymer concentration: 10^{-6} M). (b) Stern-Volmer plots of relative PL intensity I_0/I-1 of (b) PCzTPAN and (d) PTPATPAN, respectively, *vs.* TNB concentration (I = PL intensity, I_0 = PL intensity at a TNB concentration of 0 M).

4.2.4.2 Fluorescence Quenching Mechanism during Interaction with Nitroaromatic Compounds

The quenching mechanism is based on an electron transfer between the excited state of the host (PCzTPAN or PTPATPAN) and TNB[15]. Please notice that there is no spectral overlap between absorption of TNB and PL of PCzTPAN and PTPATPAN (Figure 4.7), as prerequisite for Förster-type excitation energy transfer. This process is driven by the LUMO-LUMO offset between TNB and PCzTPAN/PTPATPAN. The HOMO levels of PCzTPAN and PTPATPAN (shown in Table 4.1) were estimated to be ca. -5.41 and -5.35 eV, respectively (AC-2 method). Considering an optical bandgap (E_g) of ca. 2.88 and 2.77 eV for PCzTPAN and PTPATPAN, respectively, from the onsets of the UV/vis absorption bands, the LUMO levels of PCzTPAN and PTPATPAN are calculated to be ca. 2.53 eV and -2.58 eV, respectively. So, these LUMO levels of PCzTPAN and PTPATPAN (-2.53 eV and -2.58 eV, respectively) allow for this excited state charge transfer to the energetically lower-lying LUMO level (-3.1 eV) of TNB with a LUMO-LUMO offset of ca. 0.57 and 0.52 eV, respectively.

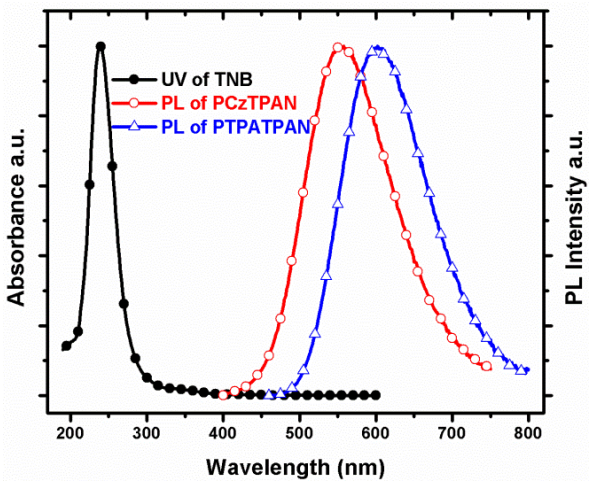

Figure 4.7. Normalized absorption spectrum of TNB and PL spectra of PCzTPAN and PTPATPAN dispersions in THF/water 1:9, respectively.

4.2.5 Detection of the Glass Transition Temperature of Polystyrene by Doping with an AIE-active Fluorescent Probe (PTPATPAN)

The glass transition is a characteristic and reversible thermal transition of amorphous materials (or the amorphous domains within semicrystalline materials). The correct detection of the glass transition temperature (T_g) is very important because pronounced changes of

thermal, electric and mechanical properties are observed when passing T_g. The fluorescence probe technique was introduced as a promising approach for detecting T_g, especially of thin films[16-19], as often used in optoelectronic devices. Several fluorescent probe molecules have been tested for this purpose, often with limited sensitivity, since the ACQ effect occurs. This problem was recently solved by Tang[20] *et al*. They utilized AIE-active TPE and TPE derivatives for the reliable detection of T_g. Hereby, the sensitivity could be improved by increasing the probe loading, without occurrence of ACQ effects.

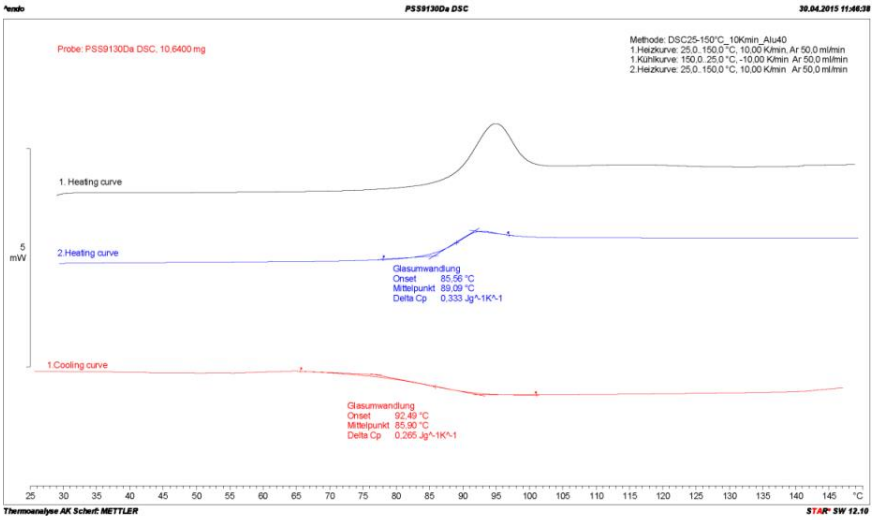

Figure 4.8. DSC measurement of the used PS sample (heating rate: 10 K/min).

Based on the initial report of the Tang group[20] on the use of AIE-active probes for the determination of the glass transition temperature (T_g) of polymers, we tested the use of our AIE polymer PTPATPAN as fluorescent probe. For T_g detection, an AIE-active probe is needed that does not electronically interact with the host polymer. For this purpose, a polystyrene (PS) sample with a narrow molecular weight distribution (M_n = 8010, M_w = 8210, PDI = 1.03) was selected as model polymer. First, the glass transition of the sample was independently measured by differential scanning calorimetry (DSC) to be ca. 89 ºC (Figure 4.8). Next, PTPATPAN was used as fluorescence probe in a concentration of 1 wt% PTPATPAN. Increasing the temperature decreases the PL intensity of the sample, a plot of PL intensity *vs.* temperature (Figure 4.9) shows a clear kink of the curve at T_g (88 ºC). Reason for this is a stronger restriction of intramolecular motions of the probe in the frozen, glassy state. After reaching T_g the free volume increases thus allowing segmental movements of the PS chains and increased intramolecular motions within the AIE-active probe.

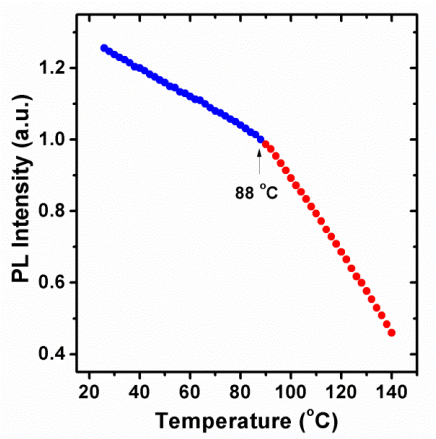

Figure 4.9. Integrated PL intensity of a PS sample doped with 1 wt% PTPATPAN as a function of temperature.

We also tested lower PTPATPAN doping (0.1 wt%). Also for the lowered dopant loading the T_g is detectable at 88 ºC, with a decreased contrast of the slopes above and below T_g (Figure 4.10a). The repeatability of the measurement was checked for a probe loading of 0.1 wt%, as shown in Figure 4.10b, for the PL intensity at 50 ºC (glassy state) and 110 ºC (softened state). The method seems especially suited for T_g measurements of thin polymer films, *e.g.* by following correlations between film thickness and T_g.

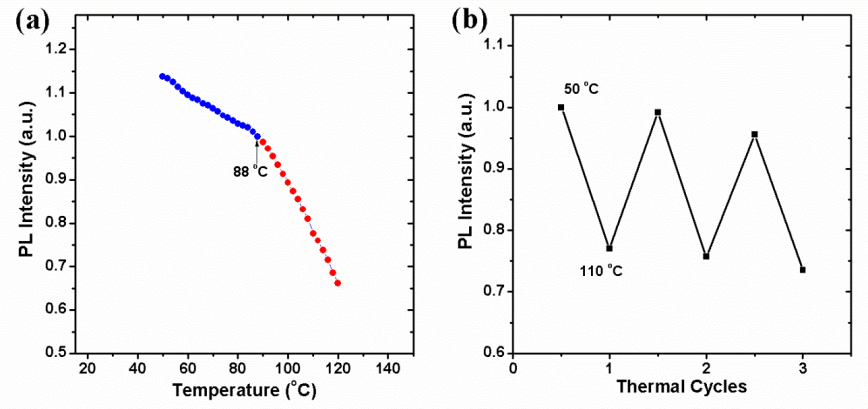

Figure 4.10. (a) PL intensity of PS doped with 0.1 wt% PTPATPAN as a function of temperature, and (b) repeatability of the measurements shown for the PL intensities at 50 °C and 110 °C.

4.3 Conclusions

Polycarbazole and polytriphenylamine derivatives with 2,3,3-triphenylacrylonitrile (TPAN) as side groups have been successfully synthesized *via* Yamamoto-type coupling procedures. The polymers exhibit both AIE as well as ICT properties, the latter caused by the interplay of

electron-poor TPAN substituents and electron-rich polycarbazole/polytriphenylamine backbones. The strategy of combining an electron-rich, conjugated backbone with AIE-active side groups is unique and introduces a couple of advantages, as mentioned in the introduction, related to *e.g.*: (1) the good processing properties of polymers, (2) the occurrence of strong interactions of the electron-rich backbone and electron-poor analytes, and (3) high exciton diffusion ability provided by the conjugated polymer backbone thus leading to an amplification in sensitivity towards suited analytes. The occurring ICT effects cause a distinct solvatochromism. PCzTPAN or PTPATPAN dispersions in 90% water/THF mixtures were used for the optical detection of nitroaromatic analytes (TNB). Both dispersions show high sensitivity, amplified PL quenching upon TNB addition. The maximum quenching constant was determined to be 5.5×10^5 M^{-1}. PTPATPAN was also used as PL probe for the optical detection of the glass transition temperature (T_g) of polystyrene (PS). Doping PS with our AIE probe allows for a reliable T_g measurement. The method is especially promising for T_g determination of thin films.

4.4 Experimental

4.4.1 Materials

All reagents were obtained from commercial suppliers and were used without further purification. All reactions were carried out under argon atmosphere by standard and Schlenk techniques. The solvents were used as commercial p.a. quality.

2-(4-Bromophenyl)-3,3-diphenylacrylonitrile

Into a 250 mL three-necked round bottom flask equipped with a condenser, benzophenone (4.65 g, 25.5 mmol), sodium hydride (60% NaH) (5 g, 128 mmol) and toluene (150 mL) were placed under argon. The mixture was stirred at 110 °C for 10 min. A solution of 4-bromobenzylnitrile (5 g, 25.5 mmol) in toluene (150 mL) was dropwise added into the above mentioned mixture over a period of ~60 min while maintaining reflux. After 20 h the mixture was cooled to room temperature, and water (100 mL) was added. The organic layer was collected and washed three times with brine solution. The organic phase was dried over anhydrous $MgSO_4$ and concentrated under vacuum. The residue was purified by silica gel chromatography (eluent: dichloromethane/hexane = 3/7) followed by recrystallization from ethanol to give the desired product as a light yellow solid in 37% yield (3.4 g). ^{1}H NMR (400 MHz, $CDCl_3$) δ (ppm) 7.61 - 7.42 (m, 5H), 7.42 - 7.36 (m, 2H), 7.36 - 7.30 (m, 1H),

7.28 - 7.23 (m, 2H), 7.23 - 7.15 (m, 2H), 7.06 (dd, J = 8.4, 1.0 Hz, 2H). ^{13}C NMR (100 MHz, $CDCl_3$) δ (ppm) 158.18, 139.96, 138.53, 133.66, 131.52, 131.10, 130.49, 129.92, 129.71, 129.11, 128.32, 128.28, 122.39, 119.50, 110.22. MS (GCMS): m/z calcd 360.2; found 361.0.

2-[4-(9*H*-Carbazol-9-yl)phenyl]-3,3-diphenylacrylonitrile

Tris(dibenzylideneacetone)dipalladium(0) ($Pd_2(dba)_3$) (48 mg, 0.052 mmol) and tri-*tert*-butylphosphane (P(*t*-Bu)$_3$) (11 mg, 0.052 mmol) were dissolved in dry toluene (12 mL) under argon and stirred for 10 min at room temperature (preformation of the catalyst). The catalyst solution was then added to a mixture of 9*H*-carbazole (700 mg, 4.19 mmol), 2-(4-bromophenyl)-3,3-diphenylacrylonitrile (1.81 g, 5.02 mmol) and sodium-*tert*-butylate (*t*-BuONa) (603 mg, 6.28 mmol) in dry toluene (26 mL). The reaction mixture was stirred at 90 °C overnight. The mixture was cooled down to room temperature, treated with water, and extracted three times with chloroform. The organic phase was collected, dried over $MgSO_4$ and concentrated under vacuum. The residue was purified by silica gel chromatography (eluent: dichloromethane/hexane = 1/1) to give the desired product as a light green solid in 86% yield (1.6 g). ^{1}H NMR (400 MHz, $C_2D_2Cl_4$) δ (ppm) 8.15 (d, *J* = 7.7 Hz, 2H), 7.57 - 7.39 (m, 13H), 7.39 - 7.24 (m, 5H), 7.16 - 7.08 (m, 2H). ^{13}C NMR (100 MHz, $C_2D_2Cl_4$) δ (ppm) 159.02, 140.60, 140.39, 138.88, 137.68, 133.89, 131.54, 131.06, 130.47, 130.26, 129.77, 128.89, 128.74, 126.89, 126.50, 123.65, 120.67, 120.51, 110.72, 110.08.

2-[4-(Diphenylamino)phenyl]-3,3-diphenylacrylonitrile

The synthetic procedure used was similar to that described for preparation of 2-[4-(9*H*-carbazol-9-yl)phenyl]-3,3-diphenylacrylonitrile: reactants are $Pd_2(dba)_3$ (53 mg, 0.058 mmol), P(*t*-Bu)$_3$ (12 mg, 0.058 mmol), diphenylamine (783 mg, 4.63 mmol), 2-(4-bromophenyl)-3,3-diphenyl-acrylonitrile (2 g, 5.55 mmol) and *t*-BuONa (667 mg, 6.94 mmol) in toluene (40 mL). The product was purified by silica gel chromatography (eluent: dichloromethane/hexane = 1/1) to give a yellow crystalline solid in 96% yield (2 g). ^{1}H NMR (600 MHz, $C_2D_2Cl_4$) δ (ppm) 7.47 - 7.37 (m, 5H), 7.29 - 7.18 (m, 7H), 7.10 - 7.00 (m, 10H), 6.84 (d, *J* = 8.8 Hz, 2H). ^{13}C NMR (150 MHz, $C_2D_2Cl_4$) δ (ppm) 156.47, 148.01, 147.19, 140.85, 139.47, 130.92, 130.75, 130.19, 129.99, 129.70, 129.24, 128.74, 128.56, 127.86, 125.25, 123.91, 122.11, 120.74, 111.44. ^{13}C NMR (DEPT, 150 MHz, $C_2D_2Cl_4$) δ (ppm) 130.93, 130.75, 130.20, 129.99, 129.70, 129.25, 128.75, 128.56, 125.25, 123.92, 122.11.

2-[4-(3,6-Dibromo-9*H*-carbazol-9-yl)phenyl]-3,3-diphenylacrylonitrile (**1**)

2-[4-(9*H*-Carbazol-9-yl)phenyl]-3,3-diphenylacrylonitrile (1.2 g, 2.69 mmol) was dissolved in dichloromethane (30 mL) under argon and cooled in an ice bath. The solution was stirred under protection of light. *N*-Bromosuccinimide (NBS) (1.0 g, 5.64 mmol) was slowly added in three portions. The reaction mixture was brought to room temperature and stirred overnight. Afterwards, the mixture was treated with water and extracted three times with chloroform. The organic phase was collected, washed with brine solution and dried over $MgSO_4$. The solution was concentrated under vacuum and the resulting product was purified by silica gel chromatography (eluent: dichloromethane/hexane = 1/1) to give the desired compound as a green solid in 87% yield (1.42 g). ^{1}H NMR (400 MHz, $C_2D_2Cl_4$) δ (ppm) 8.19 (d, *J* = 1.7 Hz, 2H), 7.60 - 7.45 (m, 9H), 7.37 (dd, *J* = 14.3, 7.9 Hz, 3H), 7.29 (t, *J* = 7.4 Hz, 2H), 7.24 (d, *J* = 8.7 Hz, 2H), 7.11 (d, *J* = 7.1 Hz, 2H). ^{13}C NMR (100 MHz, $C_2D_2Cl_4$) δ (ppm) 159.41, 140.24, 139.68, 138.78, 136.66, 134.70, 131.77, 131.06, 130.58, 130.24, 129.87, 128.90, 128.77, 126.84, 124.29, 123.57, 120.39, 113.64, 111.80, 110.43. ^{13}C NMR (DEPT, 100 MHz, $C_2D_2Cl_4$) δ (ppm) 131.77, 131.06, 130.58, 130.25, 129.87, 128.91, 128.77, 126.84, 123.57, 111.80. MS (Maldi-Tof): m/z calcd 604.33; found 604.22. Elemental anal. calcd: C, 65.59%; H, 3.34%; N, 4.64%. Found: C, 65.87%; H, 3.37%; N, 4.44%.

2-(4-[Bis(4-bromophenyl)amino]phenyl)-3,3-diphenylacrylonitrile (**2**)

The synthesis procedure used was similar to that described for preparation of 2-[4-(3,6-dibromo-9*H*-carbazol-9-yl)phenyl]-3,3-diphenylacrylonitrile (**1**): reactants are 2-[4-(diphenylamino)-phenyl]-3,3-diphenylacrylonitrile (1.22 g, 2.72 mmol) and NBS (1.02 g, 5.71 mmol) in dichloromethane (30 mL). The product was purified by silica gel chromatography (eluent: dichloromethane/hexane = 1/1) to give desired compound as a yellow solid in 76% yield (1.26 g). ^{1}H NMR (600 MHz, $C_2D_2Cl_4$) δ (ppm) 7.46 - 7.38 (m, 5H), 7.35 (d, *J* = 8.8 Hz, 4H), 7.26 (t, *J* = 7.4 Hz, 1H), 7.20 (t, *J* = 7.5 Hz, 2H), 7.08 (d, *J* = 8.7 Hz, 2H), 7.02 (d, *J* = 7.1 Hz, 2H), 6.90 (d, *J* = 8.8 Hz, 4H), 6.83 (d, *J* = 8.7 Hz, 2H). ^{13}C NMR (150 MHz, $C_2D_2Cl_4$) δ (ppm) 157.24, 146.98, 146.03, 140.64, 139.28, 132.84, 131.08, 130.90, 130.18, 130.14, 129.39, 129.27, 128.78, 128.58, 126.39, 122.95, 120.59, 116.58, 111.10. ^{13}C NMR (DEPT, 150 MHz, $C_2D_2Cl_4$) δ (ppm) 132.84, 131.08, 130.91, 130.18, 130.15, 129.40, 128.78, 128.58, 126.39, 122.95. MS (Maldi-Tof): m/z calcd 606.35; found 606.17. Elemental anal. calcd: C, 65.37%; H, 3.66%; N, 4.62%. Found: C, 65.02%; H, 3.54%; N, 4.64%.

Polymer PCzTPAN

Bis(1,5-cyclooctadiene)nickel(0) ($Ni(COD)_2$) (564 mg, 2.052 mmol) and 2,2'-bipyridine (BPy) (320 mg, 2.052 mmol) were added inside a glove box into a 25 mL Schlenk tube containing monomer **1** (310 mg, 0.513 mmol). 1,5-Cyclooctadiene (COD) (222 mg, 2.052 mmol), toluene (7 mL) and DMF (1.4 mL) were next added to the mixture with syringes under argon. Polymerization was allowed to proceed for 5 days at 80 °C. The reaction mixture was treated with an aqueous 2 M HCl solution and extracted with chloroform. The collected organic phase was washed with aqueous $NaHCO_3$ solution, saturated, aqueous EDTA solution, and brine, and finally dried over $MgSO_4$. Afterwards, the solvents were removed under vacuum. The resulting solid was dissolved in a small amount of chloroform and precipitated into methanol (500 mL) to afford the target polymer as a yellow powder. Subsequent Soxhlet extractions were carried out with methanol, acetone, ethyl acetate and chloroform, respectively. After re-precipitation of the chloroform-soluble fraction into methanol, the yellow polymer was obtained with 29% yield (65 mg). ^{1}H NMR (600 MHz, $C_2D_2Cl_4$, 60 °C) δ (ppm) 8.52 (bs, 2H), 7.82 (bs, 2H), 7.70 - 6.95 (m, 16H). M_n 4700, M_w 6170, M_w/M_n 1.31 (GPC, PS calibration).

Polymer PTPATPAN

A solution of monomer **2** (300 mg, 0.495 mmol), $Ni(COD)_2$ (544 mg, 1.979 mmol), BPy (309 mg, 1.979 mmol) and COD (214 mg, 1.979 mmol) in THF (8 mL) was reacted under microwave heating at 120 °C for 60 min. The workup procedure was similar to that described for the preparation of polymer PCzTPAN. The yellow polymer was obtained with 36% yield (80 mg). ^{1}H NMR (600 MHz, $C_2D_2Cl_4$, 60 °C) δ (ppm) 7.60 - 7.48 (m, 4H), 7.48 - 7.36 (m, 5H), 7.36 - 7.19 (m, 4H), 7.19 - 7.10 (m, 5H), 7.10 - 7.03 (m, 2H), 7.01 - 6.91 (m, 2H). M_n 8460, M_w 12800, M_w/M_n 1.51 (GPC, PS calibration).

4.4.2 Instrumentation

NMR spectra were recorded on a Bruker AVANCE 400 or AVANCE III 600. ^{1}H and ^{13}C NMR spectra were measured with tetramethylsilane (TMS) as internal standard. Gel permeation chromatography (GPC) measurements were carried out on a PSS/Agilent SECurity GPC System equipped with polystyrene gel columns using chloroform as eluent. GCMS measurements were obtained on a Shimadzu GC-17a with a Shimadzu GCMS-QP 5050 mass spectrometer (column: FS-OV1-CB-0.25) under helium. Maldi-TOF mass spectra

were recorded on a Bruker Reflex TOF. Elemental analyses were performed on a Vario EL (CHN) instrument. UV-visible absorption spectra were recorded on a Jasco V-670 spectrometer, and PL spectra on a HORIBA Scientific FluroMax-4. Fluorescence decays were measured using a picosecond time-correlated single-photon counting (TCSPC) apparatus. The PL quantum efficiencies of polymer films were measured with an integrating sphere. HOMO energy levels were estimated on a Surface Analyzer MODEL AC-2 from RIKEN, given as the threshold where photoelectron emission first occurs. DSC was performed on a DSC1 STAR System (Mettler Toledo) at a heating rate of 10 °C min^{-1} under argon.

4.5 References

1. W. Dong, J. Pina, Y. Pan, E. Preis, J. S. Seixas de Melo and U. Scherf, *Polymer*, online, DOI: 10.1016/j.polymer.2015.08.064.
2. W. Z. Yuan, Y. Gong, S. Chen, X. Y. Shen, J. W. Y. Lam, P. Lu, Y. Lu, Z. Wang, R. Hu, N. Xie, H. S. Kwok, Y. Zhang, J. Z. Sun and B. Z. Tang, *Chem. Mater.*, 2012, **24**, 1518-1528.
3. Y. Gong, Y. Tan, J. Liu, P. Lu, C. Feng, W. Z. Yuan, Y. Lu, J. Z. Sun, G. He and Y. Zhang, *Chem. Commun.*, 2013, **49**, 4009-4011.
4. P. Zhang, W. Dou, Z. Ju, X. Tang, W. Liu, C. Chen, B. Wang and W. Liu, *Adv. Mater.*, 2013, **25**, 6112-6116.
5. W. Z. Yuan, Y. Tan, Y. Gong, P. Lu, J. W. Y. Lam, X. Y. Shen, C. Feng, H. H-Y. Sung, Y. Lu, I. D. Williams, J. Z. Sun, Y. Zhang and B. Z. Tang, *Adv. Mater.*, 2013, **25**, 2837-2843.
6. Y. Gong, Y. Zhang, W. Z. Yuan, J. Z. Sun and Y. Zhang, *J. Phys. Chem. C*, 2014, **118**, 10998-11005.
7. Y. Gong, J. Liu, Y. Zhang, G. He, Y. Lu, W. B. Fan, W. Z. Yuan, J. Z.Sun and Y. Zhang, *J. Mater. Chem. C*, 2014, **2**, 7552-7560.
8. W. Li, L. Yao, H. Liu, Z. Wang, S. Zhang, R. Xiao, H. Zhang, P. Lu, B. Yang and Y. Ma, *J. Mater. Chem. C*, 2014, **2**, 4733-4736.
9. W. Qin, K. Li, G. Feng, M. Li, Z. Yang, B. Liu and B. Z. Tang, *Adv. Funct. Mater.*, 2014, **24**, 635-643.
10. B. Xu, X. Wu, H. Li, H. Tong and L. Wang, *Macromolecules*, 2011, **44**, 5089-5092.
11. X. Y. Shen, Y. J. Wang, E. Zhao, W. Z. Yuan, Y. Liu, P. Lu, A. Qin, Y. Ma, J. Z. Sun and B. Z. Tang, *J. Phys. Chem. C*, 2013, **117**, 7334-7347.
12. V. E. Z. Lippert, *Electrochemistry*, 1957, **61**, 962-975.
13. N. Mataga, Y. Kaifu, M. Koizumi, *Bull. Chem. Soc. Jpn.*, 1956, **29**, 465-470.
14. T. L. Duniho, B. J. Laughlin, A. A. Buelt, W. F. Baker, C. A. Conrad, R. C. Smith, *J. Polym. Sci., Part A: Polym. chem.*, 2014, **52**, 1487-1492.
15. Y. Salinas, R. Martínez-Máñez, M. D. Marcos, F. Sancenón, A. M. Costero, M. Parra, S. Gil, *Chem. Soc. Rev.*, 2012, **41**, 1261-1296.
16. M. M. Mok and T. P. Lodge, *J. Polym. Sci., Part B: Polym. Phys.*, 2012, **50**, 500-515.
17. J. Xu, L. Ding, J. Chen, S. Y. Gao, L. L. Li, D. S. Zhou, X. Li and G. Xue, *Macromolecules*, 2014, **47**, 6365-6372.

18. B. M. I. Flier, M. C. Baier, J. Huber, K. Müllen, S. Mecking, A. Zumbusch and D. Woll, *J. Am. Chem. Soc.*, 2012, **134**, 480-488.
19. C. J. Ellison and J. M. Torkelson, *Nat. Mater.*, 2003, **2**, 695-700.
20. S. Bao, Q. Wu, W. Qin, Q. Yu, J. Wang, G. Liang and B. Z. Tang, *Polym. Chem.*, 2015, **6**, 3537-3542.

Chapter 5

5. Polyphenothiazines and Polythiophenes with Tetraphenylethylene or 2,2,3-Triphenylacrylonitrile Side Chains

Four heteroaromatic polymers with tetraphenylethylene (TPE) or 2,2,3-triphenylacrylonitrile (TPAN) side chains have been synthesized, containing polyphenothiazine (PTzTPE and PTzTPAN) or polythiophene (homoPT and coPT) backbones. Notably, PTzTPE and PTzTPAN showed the occurrence of clear AIE phenomena with high photoluminescence quantum yields in the solid state if compared to corresponding solutions. However, homoPT and coPT both exhibit typical ACQ effects, what is unexpected in the presence of TPE side chains. The observed different behavior should result from a competition between interchain π-π stacking and restriction of intramolecular motion.

5.1 Introduction

Phenothiazine[1-5] and thiophene[6-10] are widely used building blocks for the construction of semiconducting oligomers and polymers for OLEDs, OPV devices, chemosensors and others. Recently, phenothiazine has been utilized as core unit of AIE-active luminogens, thus extending the family of AIE luminogens as siloles and TPE-based compounds. The AIE effect observed for phenothiazine-based luminogens might be attributed to the nonplanar conformation of the phenothiazine moiety, which hinders close molecular packing and diminishes intermolecular quenching effects[11]. AIE-active, phenothiazine-based oligo-/polymers have been designed for use in red/NIR-emitting OLEDs[12], and because of their delayed fluorescence[13], solvatochromic[11,14] and mechanoluminescence[15] properties. Thiophene-based oligo-/polymers are frequently used in OPV devices, because of their high hole mobility, good environmental stability, *etc*.

In this chapter, polyphenothiazine and polythiophene backbones were chosen for constructing electron-rich polymers that are decorated with AIE-active TPE or CIE-active TPAN side chains. The polymers were synthesized *via* Yamamoto- or Stille-type aryl-aryl couplings

under microwave heating. The structures of the four polymers are depicted in Chart 5.1. The occurrence of AIE phenomena is expected. The photophysics of the polymers will be also discussed in this chapter.

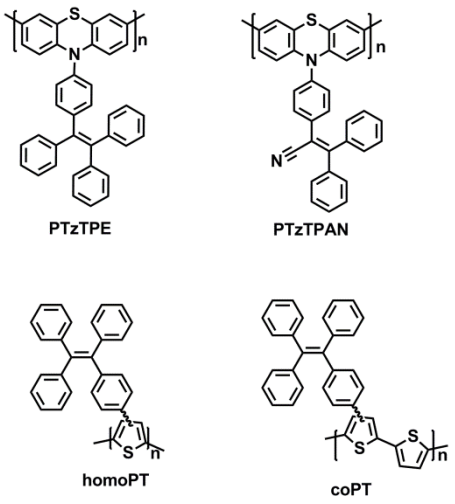

Chart 5.1. The chemical structures of polyphenothiazines and polythiophenes with TPE/TPAN substituents.

5.2 Polyphenothiazines

5.2.1 Synthesis and Characterization

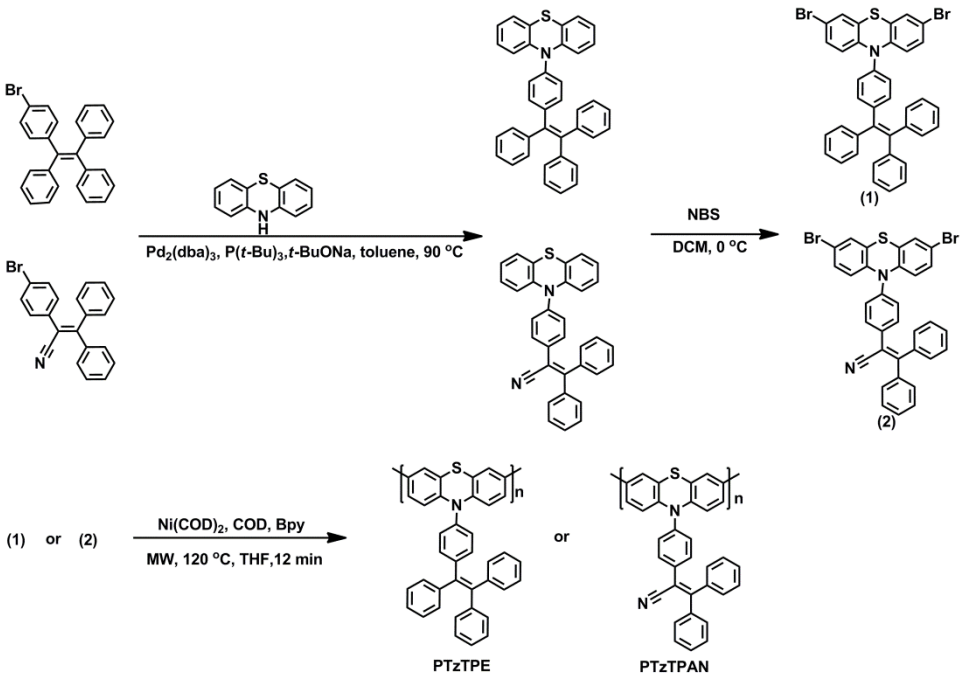

Scheme 5.1. Synthesis scheme for monomers **1** and **2** as well as the corresponding polymers PTzTPE and PTzTPAN, respectively.

The synthesis route to monomers and polymers is depicted in Scheme 5.1. Monobromo-TPE and monobromo-TPAN were synthesized as described in Chapters 3 and 4, respectively. The attachment of monobromo-TPE or monobromo-TPAN to phenothiazine was accomplished by Buchwald-Hartwig coupling and afforded TPE/TPAN-substituted phenothiazine monomers. Next, the corresponding dibromophenothiazine derivatives **1** and **2** were synthesized by bromination with *N*-bromosuccinimide (NBS) at 0 °C. The polymers PTzTPE and PCzTPAN were generated starting from the monomers **1** and **2**, respectively, in Yamamoto-type aryl-aryl couplings, using $Ni(COD)_2$ as coupling reagent in a mixture of THF, COD and Bpy under microwave (MW) heating for 12 min. The structure analysis of the monomers was performed by NMR spectroscopy, mass spectrometry and elemental analysis. The chemical structure of the obtained polymers was finally confirmed by NMR spectroscopy, GPC and optical spectroscopy.

5.2.2 Photophysical Properties

Table 5.1. Optical data for PTzTPE and PTzTPAN.

	λ_{UV}/nm in THF	λ_{PL}/nm in THF	λ_{UV}/nm in film	λ_{PL}/nm in film	η_{PL} (%) in THF	η_{PL} (%) in film
PTzTPE	294, 385(sh)	473, 498(sh)	294, 380(sh)	483, 508(sh)	2.3	15
PTzTPAN	293, 380(sh)	630	293, 382 (sh)	643	0	0.3

Figure 5.1 shows absorption and PL spectra of polymers PTzTPE and PTzTPAN in dilute THF solution and as thin films. In the absorption spectra, due to their similar chemical structure, both polymers show similar spectral profiles with peak maxima at 294 nm with a shoulder at 380 nm for PTzTPE, and 293 nm with a shoulder at 382 nm for PTzTPAN, respectively. For the skyblue emissive PTzTPE, the PL spectrum in solution peaks at 473 nm, with a shoulder at 498 nm and an additional, broad tail-off band peaking at 620 nm. As film, the PL spectrum of PTzTPE peaks at 483 nm with a shoulder at 508 nm, ca. 10 nm red-shifted if compared to the dilute solution. For PTzTPAN, the PL maximum in solution and in the solid state is ca. 160 nm bathochromically shifted if compared to PTzTPE. This significant red-shift is attributed to the introduction of the dipolar cyano groups, leading to an intramolecular charge transfer (ICT) effect between donor and acceptor units. PL spectra for solvatochromism studies in different polar solvents could not be recorded for PTzTPAN due to its weak emission especially in polar solvents. The solution PL quantum yields for

PTzTPE and PTzTPAN are 2.3% and ~0, respectively. In solid state, they increase to 15% and 0.3%, respectively (Table 5.1).

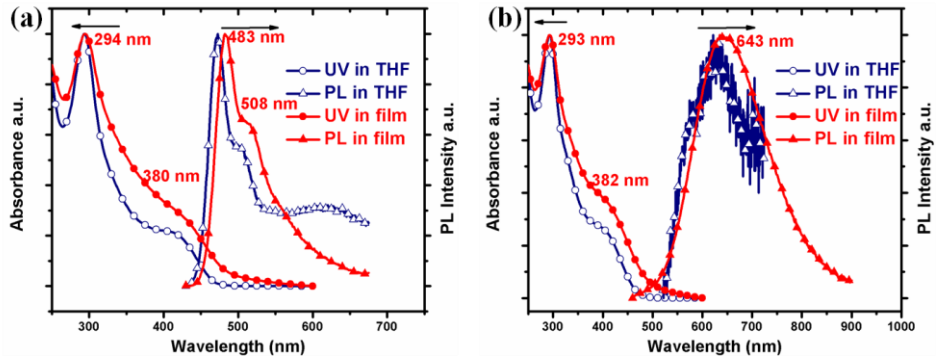

Figure 5.1. Absorption and PL spectra of (a) PTzTPE and (b) PTzTPAN in dilute THF solution (10^{-5} M) and as spin-coated films (measured at room temperature).

To further investigate possible AIE properties of PTzTPE, PL spectra in solvent mixtures (THF/water) were recorded (Figure 5.2). As shown, the PL intensity of PTzTPE increases gradually with increasing water content, indicating the occurrence of AIE properties for PTzTPE. For 90% water/THF, the PL intensity reaches its highest value, which is 3 times higher if compared to the value of a THF solution. For PTzTPAN the PL in the water/THF solvent mixtures is too weak for recording suitable PL spectra.

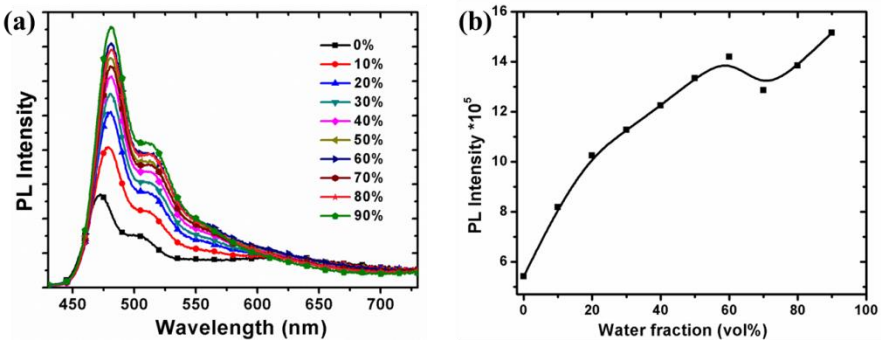

Figure 5.2. (a) PL spectra of PTzTPE in THF/water mixtures with different water content; (b) PL intensity with increasing water fraction for PTzTPE (polymer concentration: 10^{-5} M).

5.3 Polythiophenes

5.3.1 Synthesis and Characterization

The synthesis route to monomer **3** and the corresponding polymers homoPT and coPT is depicted in Scheme 5.2. The synthesis of TPE boronic ester was already described in

Scheme 3.1 (Chapter 3). TPE-substituted thiophene was obtained in a Suzuki-type aryl-aryl crosscoupling between 3-bromothiophene and TPE boronic ester. The TPE-substituted dibromothiophene monomer **3** was synthesized by bromination with NBS at 0 °C. 2,5-Bis(trimethylstannyl)thiophene was purchased from Sigma-Aldrich without further purification. Polymer homoPT was generated in a Yamamoto-type homocoupling with the mixture of $Ni(COD)_2$, COD, Bpy and THF under microwave (MW) heating at 120 °C for 12 min. Polymer coPT was made in a Stille-type crosscoupling with the mixture of $Pd(PPh_3)_4$ and DMF under MW heating at 140 °C for 20 min. The structure elucidation of monomer **3** was performed by NMR spectroscopy, mass spectrometry and elemental analysis. The chemical structure of the obtained polymers was finally confirmed by NMR spectroscopy, GPC and optical spectroscopy.

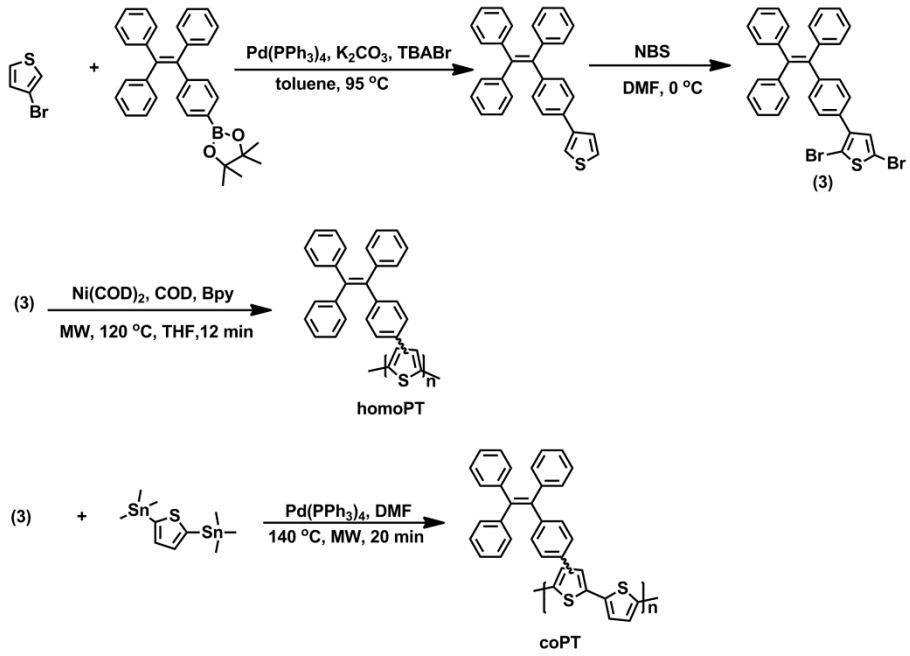

Scheme 5.2. The synthesis route to monomer **3** and the corresponding polymers homoPT and coPT.

5.3.2 Photophysical Properties

Table 5.2. Optical data and HOMO/LUMO energy levels of homoPT and coPT.

	λ_{UV}/nm in THF	λ_{PL}/nm in THF	λ_{UV}/nm in film	λ_{PL}/nm in film	η_{PL} (%) in toluene	η_{PL} (%) in film	HOMO eV	LUMO eV
homoPT	328, 450	585	333, 445	585	12	8	-5.40	-2.27
coPT	323, 495	591, 620 (sh)	330, 520	612, 645 (sh)	19	8	-5.26	-2.07

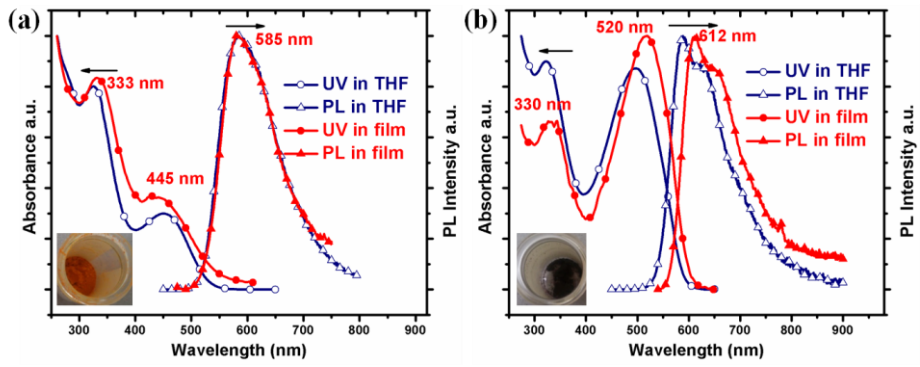

Figure 5.3. Normalized absorption and PL spectra of (a) homoPT and (b) coPT in dilute THF solution (polymer concentration: 10^{-5} M) and as spin-coated films; the insets in (a) and (b) are photographs of solid homoPT and coPT samples, respectively, under sunlight.

Figure 5.3 shows normalized absorption and PL spectra of homoPT and coPT in dilute THF solution and as thin films. HomoPT in dilute solution shows two absorption peaks, at 328 nm (TPE side chains) and 450 nm (polythiophene backbone). As thin film, the first absorption maxima shows a 5 nm red-shift if compared to the solution data. The second band is observed at 445 nm. In the PL spectra, an orange emission peaking at 585 nm is observed both for the solution and the film, which is indicative for weak intermolecular interaction between polymer strands due to the bulky TPE side groups. Also for coPT, two absorption peaks for backbone and side groups are observed. In dilute solution, the absorption peaks are at 323 nm and 495 nm, attributed to TPE side chains and polythiophene backbone, respectively. In the film state, the backbone-related absorption peak at 495 nm shifts to 520 nm corresponding to a red-shift of 25 nm. In the PL spectra, red emission is observed, peaking at 591 nm with a shoulder at 620 nm in dilute solution and at 612 nm with a shoulder at 645 nm in the film. The ~20 nm red-shift in absorption and PL spectra between film and solution might be caused by some intermolecular stacking of polymer chains. Moreover, the viaible colors of polymers homoPT and coPT are quite different (insets of Figure 5.3). For homoPT, the polythiophene backbone should adopt a more twisted conformation due to the high substitution density with TPE side groups at each thiophene unit. On the other hand, for coPT, only each second thiophene unit carries a TPE side chain, resulting in a more planar polythiophene backbone thus allowing intermolecular interactions and red-shifts of the optical spectra. The HOMO levels of homoPT and coPT were estimated to be ca. -5.40 and -5.26 eV, respectively (AC-2 method). The corresponding LUMO levels were calculated to be -2.27 and -2.07 eV, respectively, from the UV/vis absorption onsets (optical bandgap energies) of the polymers. The detailed optical data are summarized in Table 5.2. The PLQYs

in toluene solution for homoPT and coPT were measured to be 12% and 19%, respectively, with quinquethiophene (α5) as reference. Linear α5 shows a PLQY of 36% in 1,4-dioxane[16]. In the solid state film, the PLQY was estimated with an integrating sphere to be ca. 8% for both polymers. Therefore, both polymers show no AIE effect, only a weak ACQ effect.

To further investigate the PL behavior for both polythiophenes, a series of PL measurements in THF/water mixtures were carried out. PL spectra of homoPT and coPT in THF/water mixtures are shown in Figure 5.4a/c. With increasing water content, the PL intensity progressively decreases for both polymers, with a maximum decrease of 1.7 times for homoPT and a maximum decrease of 7.7 times for coPT, respectively (pure THF to 90% water/THF). It is worthy to note that the PL intensity drops along with red-shift of the emission maximum, the plots of emission maxima *vs.* water content are also shown in Figure 5.4b/d. For homoPT, the red shift is ca. 12 nm from pure THF solution to 90% water/THF, and ca. 26 nm for coPT, respectively. Increasing the water fraction should cause aggregation which may cause some intermolecular stacking or suppress the intramolecular rotation within the TPE units. While the former may weaken and red shift the emission the latter would increase the PL intensity (AIE effect). The observed PL properties result from a competition between both effects. For homoPT and coPT, the first effect wins and both of them did not show AIE behavior.

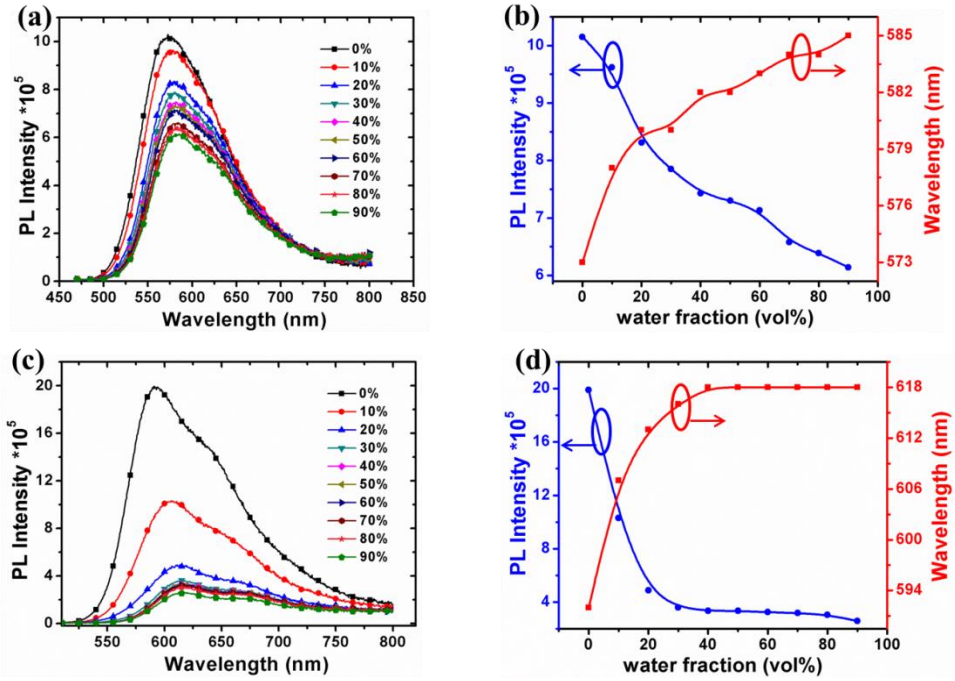

Figure 5.4. PL spectra of (a) homoPT and (c) coPT in THF/water mixtures with different water content; PL intensity and maximum emission wavelength with increasing water fraction for (b) homoPT and (d) coPT, respectively (polymer concentration: 10^{-5} M).

5.4 Conclusions

Polyphenothiazines PTzTPE and PTzTPAN with AIE-active TPE or CIE-active TPAN side groups were successfully synthesized in Yamamoto-type aryl-aryl homocouplings. Both polymers show AIE effects. PTzTPAN combines electron-rich polyphenothiazine backbones with electron-poor cyano-containing TPAN side chains allowing intramolecular charge transfer (ICT). However, a detailed photophysical characterization of the ICT properties was not possible because of the weak PL.

HomoPT and coPT with AIE-active TPE side group have been successfully synthesized in Yamamoto-type and Stille-type aryl-aryl couplings, respectively. Both polymers show different colors, orange for homoPT to dark red for coPT, which might be explained by the more planar polymer backbone of coPT with its lower substitution density. Unlike the polymers with polycarbazole, polytriphenylamine, and polyphenothiazine backbones, both homoPT and coPT show ACQ effects. Hereby, intermolecular stacking may dominate the emission properties.

5.5 Experimental

5.5.1 Materials

All reagents were obtained from commercial suppliers and were used without further purification. All reactions were carried out under argon atmosphere by standard and Schlenk techniques. The solvents were used as commercial p.a. quality.

10-[4-(1,2,2-triphenylvinyl)phenyl]-10*H*-phenothiazine

Tris(dibenzylideneacetone)dipalladium(0) ($Pd_2(dba)_3$) (87 mg, 0.095 mmol) and tri-*tert*-butylphosphane (P(*t*-Bu)$_3$) (0.02 mL, 0.095 mmol) were dissolved in dry toluene (20 mL) under argon and stirred for 10 min at room temperature (preformation of the catalyst). The catalyst was then added to a mixture of 10*H*-phenothiazine (1.526 g, 7.66 mmol), bromo-TPE (3 g, 7.29 mmol) and sodium-*tert*-butylate (*t*-BuONa) (1.051 g, 10.94 mmol) in dry toluene (90 mL). The reaction mixture was stirred at 90 °C overnight. The reaction was cooled down to room temperature and treated with water. The mixture was extracted with chloroform for three times. The organic phases were collected, dried over $MgSO_4$ and concentrated under vacuum. The residue was purified by silica gel chromatography (eluent: dichloromethane/hexane = 3/7) to give desired compound as a light

green solid in 91% yield (3.5 g). ^{1}H NMR (400 MHz, $CDCl_3$) δ (ppm) 7.28 (d, *J* = 8.4 Hz, 2H), 7.23 - 7.05 (m, 17H), 7.02 (dd, *J* = 7.4, 1.7 Hz, 2H), 6.89 (td, *J* = 7.8, 1.6 Hz, 2H), 6.83 (t, *J* = 7.0 Hz, 2H), 6.17 (dd, *J* = 8.1, 1.0 Hz, 2H). MS (APLI): m/z calcd 529.19; found 529.16.

3,7-dibromo-10-[4-(1,2,2-triphenylvinyl)phenyl]-10*H*-phenothiazine (**1**)

10-[4-(1,2,2-Triphenylvinyl)phenyl]-10*H*-phenothiazine (2.50 g, 4.72 mmol) was dissolved in dichloromethane (30 mL) under argon and cooled by an ice bath. The solution was stirred under protection of light and NBS (1.68 g, 9.44 mmol) was slowly added in three portions. The reaction mixture was slowly warmed to room temperature and stirred overnight. The reaction mixture was treated with water and extracted with chloroform three times. The organic layer was collected, washed with brine solution and dried over $MgSO_4$. The solution was concentrated under vacuum and the product was purified by silica gel chromatography (eluent: dichloromethane/hexane = 1/4) to give desired compound as a light green solid in 77% yield (2.5 g). ^{1}H NMR (400 MHz, $CDCl_3$) δ (ppm) 7.30 (d, *J* = 8.5 Hz, 2H), 7.25 - 7.14 (m, 11H), 7.14 - 7.02 (m, 8H), 6.96 (dd, *J* = 8.8, 2.3 Hz, 2H), 5.96 (d, *J* = 8.8 Hz, 2H). ^{13}C NMR (100 MHz, $CDCl_3$) δ (ppm) 144.68, 143.48, 142.96, 142.89, 142.68, 142.39, 139.94, 137.97, 133.89, 131.36, 131.18, 131.15, 129.78, 129.63, 128.72, 127.93, 127.76, 127.60, 126.83, 126.80, 121.17, 116.97, 114.64. MS (APLI): m/z calcd 687.01; found 687.00. Elemental anal. calcd: C, 66.39%; H, 3.67%; N, 2.04%; S, 4.66. Found: C, 66.64%; H, 3.63%; N, 1.94%; S, 4.84%.

2-[4-(10*H*-phenothiazin-10-yl)phenyl]-3,3-diphenylacrylonitrile

The synthesis procedure was similar to that described for the preparation of 10-[4-(1,2,2-triphenylvinyl)phenyl]-10*H*-phenothiazine, with $Pd_2(dba)_3$ (50 mg, 0.054 mmol), P(*t*-Bu)$_3$ (11 mg, 0.054 mmol), 10*H*-phenothiazine (871 mg, 4.37 mmol), 2-(4-bromophenyl)-3,3-diphenylacrylonitrile (1.5 g, 4.16 mmol), *t*-BuONa (0.6 g, 6.25 mmol) and toluene (55 mL) as components. The product was purified by silica gel chromatography (eluent: dichloromethane/hexane = 3/7) to give yellow powder in 85% yield (1.7 g). ^{1}H NMR (400 MHz, $CDCl_3$) δ (ppm) 7.57 - 7.41 (m, 7H), 7.35 - 7.29 (m, 1H), 7.28 - 7.18 (m, 4H), 7.14 - 7.06 (m, 4H), 6.96 (td, *J* = 7.8, 1.7 Hz, 2H), 6.90 (td, *J* = 7.4, 1.2 Hz, 2H), 6.35 (dd, *J* = 8.1, 1.2 Hz, 2H).

2-[4-(3,7-dibromo-10*H*-phenothiazin-10-yl)phenyl]-3,3-diphenylacrylonitrile (**2**)

The synthesis procedure was similar to that described for preparation of 3,7-dibromo-10-[4-(1,2,2-triphenylvinyl)phenyl]-10*H*-phenothiazine (1) with 2-(4-(10*H*-phenothiazin-10-yl)phenyl)-3,3-diphenylacrylonitrile (1.41 g, 2.95 mmol), NBS (1.05 g, 5.90 mmol) and dichloromethane (20 mL) as components. The product was purified by silica gel chromatography (eluent: dichloromethane/hexane = 2/3) to give desired compound as a yellow solid in 85% yield (1.6 g). ^{1}H NMR (400 MHz, $CDCl_3$) δ (ppm) 7.56 - 7.44 (m, 7H), 7.33 (t, *J* = 7.4 Hz, 1H), 7.25 (t, *J* = 7.5 Hz, 2H), 7.19 (d, *J* = 8.6 Hz, 2H), 7.15 (d, *J* = 2.3 Hz, 2H), 7.11 - 7.03 (m, 2H), 7.00 (dd, *J* = 8.8, 2.3 Hz, 2H), 6.05 (d, *J* = 8.8 Hz, 2H). ^{13}C NMR (100 MHz, $CDCl_3$) δ (ppm) 159.11, 142.57, 140.25, 139.79, 138.78, 135.24, 132.41, 130.79, 130.27, 129.92, 129.78, 129.41, 129.09, 128.56, 128.27, 122.51, 119.74, 117.70, 115.26, 110.28. MS (APLI): m/z calcd 635.97; found 636.98. Elemental anal. calcd: C, 62.28; H, 3.17; N, 4.40; S, 5.04. Found: C, 62.51%; H, 3.09%; N, 4.30%; S, 5.19%.

Polymer PTzTPE

A mixture of monomer **1** (600 mg, 0.873 mmol), $Ni(COD)_2$ (624 mg, 2.269 mmol), BPy (354 mg, 2.269 mmol) and COD (245 mg, 2.269 mmol) in THF (6 mL) was treated under microwave heating at 120 °C for 12 min. The reaction mixture was treated with water and extracted with chloroform. The collected organic phases were washed with aqueous 2 M HCl, aqueous $NaHCO_3$ solution, saturated, aqueous EDTA solution, and brine, and finally dried over $MgSO_4$. Afterwards, the solvents were removed under vacuum. The resulting solid was dissolved in a small amount of chloroform and precipitated into methanol (500 mL) to afford the target polymer as a green solid. Subsequent Soxhlet extractions were carried out with methanol, acetone, ethyl acetate and chloroform, respectively. After re-precipitation of the chloroform-soluble fraction into methanol, a green polymer was obtained with 52% yield (251 mg). ^{1}H NMR (600 MHz, $CDCl_3$, 40 °C) δ (ppm) 7.31 (bs, *J* = 40.9 Hz, 2H), 7.27 - 7.05 (m, 19H), 7.05 - 6.80 (m, 2H), 6.15 (bs, 2H). M_n 17800, M_w 110000, M_w/M_n 6.15 (GPC, PS calibration).

Polymer PTzTPAN

A mixture of monomer **2** (600 mg, 0.943 mmol), $Ni(COD)_2$ (674 mg, 2.451 mmol), BPy (383 mg, 2.451 mmol) and COD (265 mg, 2.451 mmol) in THF (6 mL) was reacted under microwave heating at 120 °C for 12 min. The workup procedure was similar to that described

for the preparation of PTzTPE. The dark yellow polymer was obtained with 12% yield (55 mg). ^{1}H NMR (600 MHz, $CDCl_3$, 40 °C) δ (ppm) 7.62 - 7.41 (m, 7H), 7.39 - 7.16 (m, 7H), 7.14 - 6.96 (m, 4H), 6.35 - 6.17 (m, 2H). M_n 5300, M_w 7100, M_w/M_n 1.34 (GPC, PS calibration).

3-[4-(1,2,2-triphenylvinyl)phenyl]thiophene

A mixture of 3-bromothiophene (1.17 g, 7.2 mmol), 4,4,5,5-tetramethyl-2-[4-(1,2,2-triphenylvinyl)phenyl]-1,3,2-dioxaborolane (3.0 g, 6.54 mmol), K_2CO_3 (0.905 g, 6.54 mmol), TBABr (0.211 g, 0.654 mmol) and $Pd(PPh_3)_4$ (227 mg, 0.196 mmol) was carefully degassed. Then, water (3.3 mL) and toluene (45 mL) were added. The resulting mixture was stirred at 95 °C for 24 h under argon atmosphere. After cooling to room temperature, the mixture was treated with water and extracted with chloroform. The organic phases were collected, dried over $MgSO_4$ and concentrated under vacuum. The product was purified by silica gel chromatography (eluent: hexane/dichloromethane = 7/3) to give the desired compound as white solid in 96% yield (2.6 g). ^{1}H NMR (400 MHz, $C_2D_2Cl_4$) δ (ppm) 6.13 (t, *J* = 2.1 Hz, 1H), 6.11 - 6.06 (m, 4H), 5.90 - 5.75 (m, 17H).

2,5-dibromo-3-[4-(1,2,2-triphenylvinyl)phenyl]thiophene (**3**)

Under exclusion of light, a solution of NBS (2.16 g, 12.16 mmol) in DMF (8 mL) was added dropwise to a solution of 3-[4-(1,2,2-triphenylvinyl)phenyl]thiophene (2.4 g, 5.79 mmol) in DMF (12 mL) at 0 °C. The resulting mixture was kept for 1 h at 0 °C and then allowed to warm up to room temperature. Afterwards the product was poured into water and the mixture extracted with dichloromethane. The organic phase was washed with saturated, aqueous $NaHCO_3$ solution and water and dried over $MgSO_4$. After evaporation of the solvent, the crude product was purified by silica gel chromatography (eluent: hexane/dichloromethane = 7/3) to give the desired compound as white solid in 45% yield (1.5 g). ^{1}H NMR (600 MHz, $C_2D_2Cl_4$) δ (ppm) 7.23 (d, *J* = 8.4 Hz, 2H), 7.13 - 7.06 (m, 9H), 7.06 - 7.00 (m, 8H), 6.99 (s, 1H). ^{13}C NMR (150 MHz, $C_2D_2Cl_4$) δ (ppm) 143.75, 143.72, 143.70, 143.60, 141.91, 141.79, 140.56, 132.04, 131.87, 131.64, 131.57, 131.56, 128.02, 128.00, 127.94, 127.85, 126.82, 126.75, 126.71, 111.43, 107.64. MS (APLI): m/z calcd 571.96; found 571.94. Elemental anal. calcd: C, 62.95%; H, 3.52%; S, 5.60%. Found: C, 62.96%; H, 3.08%; S, 6.13%.

Polymer homoPT

A mixture of monomer **3** (400 mg, 0.699 mmol), $Ni(COD)_2$ (500 mg, 1.817 mmol), BPy (284 mg, 1.817 mmol) and COD (197 mg, 1.817 mmol) in THF (6 mL) was reacted under microwave heating at 120 °C for 12 min. The workup procedure was similar to that described for the preparation of PTzTPE. The orange polymer was obtained with 52% yield (150 mg). ^{1}H NMR (600 MHz, $C_2D_2Cl_4$, 60 °C) δ (ppm) 7.26 - 6.60 (m, 20H). M_n 14600, M_w 57800, M_w/M_n 3.96 (GPC, PS calibration).

Polymer coPT

Monomer **3** (400 mg, 0.699 mmol), 2,5-bis(trimethylstannyl)thiophene (286 mg, 0.699 mmol) and $Pd(PPh_3)_4$ (40.4 mg, 0.035 mmol) were added into a 20 mL microwave-tube. The mixture was carefully degassed under vacuum for 15 min. Next, dry DMF (10 mL) was added into the tube under argon and the resulting mixture was heated to 140 °C under microwave conditions for 20 min. After that, 2-(tributylstannyl)thiophene (5.2 mg, 0.014 mmol) was added as end-capping agent and the mixture reacted for another 5 min. The mixture was cooled down to room temperature, treated with aqueous 2M HCl solution and extracted with chloroform three times. The organic phases were collected and dried over $MgSO_4$. Afterwards, the solvents were removed under vacuum. The resulting solid was dissolved in a small amount of chloroform and precipitated into methanol (500 mL) to afford the target polymer as a dark red solid. Subsequent Soxhlet extractions were carried out with methanol, acetone, ethyl acetate and chloroform, respectively. After re-precipitation of the chloroform-soluble fraction into methanol, the dark red polymer was obtained with 69% yield (240 mg). ^{1}H NMR (600 MHz, $C_2D_2Cl_4$, 60 °C) δ (ppm) 7.49 - 6.59 (m, 22H). M_n 14500, M_w 76600, M_w/M_n 5.28 (GPC, PS calibration).

5.5.2 Instrumentation

NMR spectra were recorded on a Bruker AVANCE 400 or AVANCE III 600. ^{1}H and ^{13}C NMR spectra were measured with tetramethylsilane (TMS) as internal standard. Gel permeation chromatography (GPC) measurements at high temperature (135 °C) were carried out on Waters Alliance 2000 System equipped with PLgel-Guard, PLgel-MIXED-B-column (both from Agilent Technologies) using 1,3,5-trichlorobenzene as eluent, with RI-detector and measured against polystyrene. APLI (Atmospheric Pressure Laser Ionization) measurements were carried out on Bruker Daltronik Bremen with micrOTOF. UV-visible

absorption spectra were recorded on a Jasco V-670 spectrometer, and PL spectra on a HORIBA Scientific FluroMax-4. Elemental analyses were performed on a Vario EL II (CHNS) instrument. The PL quantum efficiencies of polymer films were measured with an integrating sphere.

5.6 References

1. B. Garg and Y.-C. Ling, *Chem. Commun.*, 2015, **51**, 8809-8812.
2. Y. Park, B. Kim, C. Lee, A. Hyun, S. Jang, J.-H. Lee, Y.-S. Gal, T. H. Kim, K.-S. Kim and J. Park, *J. Phys. Chem. C*, 2011, **115**, 4843-4850.
3. Q. Zou, X. Li, Q. Xu, H. Agren, W. Zhao and Y. Qu, *RSC Adv.*, 2014, **4**, 59809-59816.
4. A. Baheti, K. R. J. Thomas, C.-T. Li, C.-P. Lee and K.-C. Ho, *ACS Appl. Mater. Interfaces*, 2015, **7**, 2249-2262.
5. Z. Zhang, Z. Wu, J. Sun, B. Yao, G. Zhang, P. Xue and R. Lu, *J. Mater. Chem. C*, 2015, **3**, 4921-4932.
6. B. J. Worfolk, D. A. Rider, A. L. Elias, M. Thomas, K. D. Harris and J. M. Buriak, *Adv. Funct. Mater.*, 2011, **21**, 1816-1826.
7. N. Liu, C.-G. Qi, Y. Wang, D.-F. Liu, J. Yin, Y.-Y. Zhu and Z.-Q. Wu, *Macromolecules*, 2013, **46**, 7753-7758.
8. G. M. Su, E. Lim, A. R. Jacobs, E. J. Kramer and M. L. Chabinyc, *ACS Macro Lett.*, 2014, **3**, 1244-1248.
9. L. Zhang, F. Liu, Y. Diao, H. S. Marsh, N. S. Colella, A. Jayaraman, T. P. Russell, S. C. B. Mannsfeld and A. L. Briseno, *J. Am. Chem. Soc.*, 2014, **136**, 18120-18130.
10. Q. Tao, Y. Xia, X. Xu, S. Hedström, O. Backe, D. I. James, P. Persson, E. Olsson, O. Inganas, L. Hou, W. Zhu and E. Wang, *Macromolecules*, 2015, **48**, 1009-1016.
11. S. J. Ananthakrishnan, E. Varathan, V. Subramanian, N. Somanathan and A. B. Mandal, *J. Phys. Chem. C*, 2014, **118**, 28084-28094.
12. L, Yao, S, Zhang, R, Wang, W, Li, F, Shen, B, Yang and Y. Ma, *Angew. Chem., Int. Ed.*, 2014, **53**, 2119-2123.
13. S. Xu, T. Liu, Y. Mu, Y.-F. Wang, Z. Chi, C.-C. Lo, S. Liu, Y. Zhang, A. Lien and J. Xu, *Angew. Chem., Int. Ed.*, 2015, **54**, 874-878.
14. J. Zhang, B. Xu, J. Chen, L. Wang and W. Tian, *J. Phys. Chem. C*, 2013, **117**, 23117-23125.
15. M. Zheng, M. Sun, Y. Li, J. Wang, L. Bu, S. Xue and W. Yang, *Dyes Pigm.*, 2014, **102**, 29-34.
16. R. S. Becker, J. Seixas de Melo, A. L. Maçanita and F. Elisei, *J. Phys. Chem.*, 1996, **100**, 18683-18695.

Chapter 6

6. Outlook

6.1 Summary of Chapters 2-5

A series of linear polymers, with polycarbazole, polytriphenylamine, polyphenothiazine and polythiophene backbones, many of them with AIE activity have been successfully synthesized. Electron-rich carbazole, triphenylamine, phenothiazine and thiophene units were chosen as repeat units of the polymer backbone and AIE(CIE)-active TPE or TPAN moieties as side chains in order to induce AIE activity without strongly affecting the electronic properties of the backbones. Many of the obtained polymers showed high fluorescence quantum yields in the solid state, thanks to the occurrence of distinct AIE effects.

The photophysical properties of the polymers in solution, and in the aggregated (solid) state have been studied, as well as potential applications in the detection of nitroaromatic explosives (in dispersion and in the film). Moreover, one AIE-active polymer was used as photoluminescent dopant in the detection of the glass transition temperature of polystyrene films. Notably, a highly sensitive detection of TNB as prototypical nitroaromatic compound was possible, with a maximum quenching constant of up to 1.26×10^{6} M^{-1} in dispersion and 89% fluorescence quenching for 600 s contact time for a thin film. In the detection of the glass transition of polymer (in our case for polystyrene), the use of AIE-active dopants is a new sensitive, reliable and straightforward approach, especially for T_g-detection of films.

6.2 Outlook

Click chemistry[1] first described by Sharpless *et al*. in 2001, is a useful synthetic tool for connecting building blocks[2,3], with high yield and stereospecificity, under simple and mild reaction conditions in a fast reaction that is non-sensitive to oxygen or water. Several AIE oligomers and polymers have been synthesized *via* click reactions and used for the applications in chemosensors[4-9], mechanochromic sensors[10], in cell imaging[11,12] and other applications[13-17].

Thiol-ene click reactions[18,19] can be performed without solvent under thermal or photochemical initiation. Solvent-free thiol-ene click reactions allow for the fabrication of

thin films of polymer networks despite the common insolubility of polymer networks. Such network often possesses a high chemical and thermal stability. They can adopt a microporous structure if the synthesis uses rigid building blocks (tectors), what makes them promising for applications in optoelectronic devices and chemosensors, *etc*.

Therefore, further experiments could be carried out to generate thin-film of polymer networks that contain AIE-active TPE units, *e.g. via* thiol-ene click chemistry with *e.g.* 1,1,2,2-tetrakis(4-vinylphenyl)ethene and multifunctional thiol monomers in a photochemical crosslinking procedure (Scheme 6.1). The obtained films could be tested in sensors or optoelectronic devices.

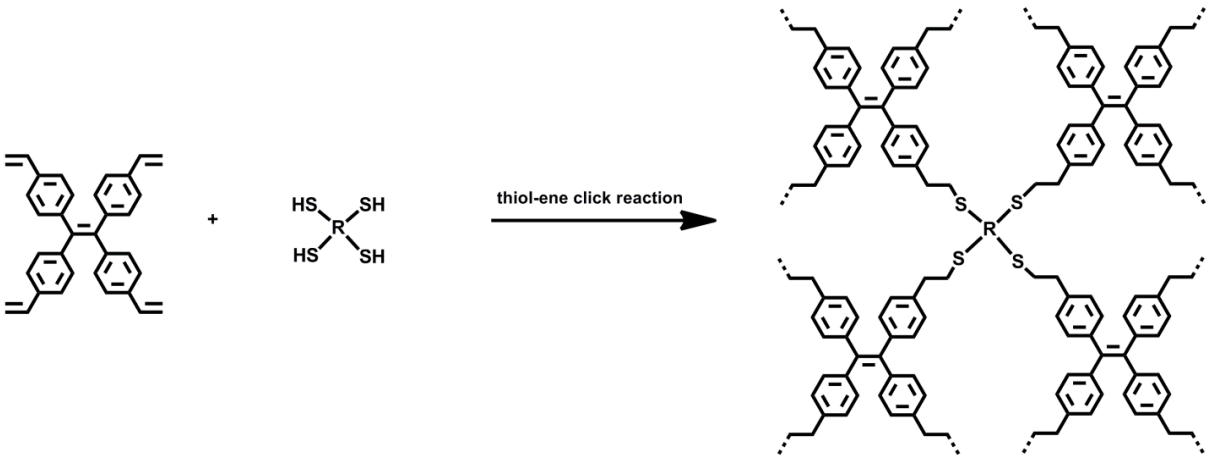

Scheme 6.1. The synthetic route to polymer network containg TPE units.

6.3 References

1. H. C. Kolb, M. G. Finn, and K. B. Sharpless, *Angew. Chem., Int. Ed.*, 2001, **40**, 2004-2021.
2. A. B. Lowe, *Polym. Chem.*, 2010, **1**, 17-36.
3. W. Xi, T. F. Scott, C. J. Kloxin and C. N. Bowman, *Adv. Funct. Mater.*, 2014, **24**, 2572-2590.
4. A. Qin, J. W. Y. Lam, L. Tang, C. K. W. Jim, H. Zhao, J. Sun and B. Z. Tang, *Macromolecules*, 2009, **42**, 1421-1424.
5. H. Li, J. Wang, J. Z. Sun, R. Hu, A. Qin and B. Z. Tang, *Polym. Chem.*, 2012, **3**, 1075-1083.
6. X. Wang, J. Hu, T. Liu, G. Zhang and S. Liu, *J. Mater. Chem.*, 2012, **22**, 8622-8628.
7. W.-H. Yu, C. Chen, P. Hu, B.-Q. Wang, C. Redshaw and K.-Q. Zhao, *RSC Adv.*, 2013, **3**, 14099-14105.
8. L. Zhang, W. Hu, L. Yu and Y. Wang, *Chem. Commun.*, 2015, **51**, 4298-4301.
9. Y. Zhang, G. Chen, Y. Lin, L. Zhao, W. Z. Yuan, P. Lu, C. K. W. Jim, Y. Zhang and B. Z. Tang, *Polym. Chem.*, 2015, **6**, 97-105.
10. J. Wang, J. Mei, R. Hu, J. Z. Sun, A. Qin and B. Z. T., *J. Am. Chem. Soc.*, 2012, **134**, 9956-9966.
11. F. Mahtab, J. W. Y. Lam, Y. Yu, J. Liu, W. Yuan, P. Lu and B. Z. Tang, *Small*, 2011, **7**, 1448-1455.
12. Y. Liu, Y. Yu, J. W. Y. Lam, Y. Hong, M. Faisal, W. Z. Yuan and B. Z. Tang, *Chem. Eur. J.*, 2010, **16**, 8433-8438.
13. W. Z. Yuan, Z.-Q. Yu, Y. Tang, J. W. Y. Lam, N. Xie, P. Lu, E.-Q. Chen and B. Z. Tang, *Macromolecules*, 2011, **44**, 9618-9628.
14. C. Li and S. Liu, *Chem. Commun.*, 2012, **48**, 3262-3278.
15. W. Z. Yuan, F. Mahtab, Y. Gong, Z.-Q. Yu, P. Lu, Y. Tang, J. W. Y. Lam, C. Zhu and B. Z. Tang, *J. Mater. Chem.*, 2012, **22**, 10472-10479.
16. B. Yao, J. Mei, J. Li, J. Wang, H. Wu, J. Z. Sun, A. Qin and B. Z. Tang, *Macromolecules*, 2014, **47**, 1325-1333.
17. S. Li and C. Gao, *Polym. Chem.*, 2013, **4**, 4450-4460.
18. K. L. Killops, L. M. Campos and C. J. Hawker, *J. Am. Chem. Soc.*, 2008, **130**, 5062-5064.
19. C. E. Hoyle and C. N. Bowman, *Angew. Chem., Int. Ed.*, 2010, **49**, 1540-1573.

Der Lebenslauf ist in der Online-Version aus Gründen des Datenschutzes nicht enthalten.

To protect the personality rights of the author the curriculum vitae has been deleted.

Publications:

1. "Polycarbazoles and Polytriphenylamines Showing Aggregation-Induced Emission (AIE) and Intramolecular Charge Transfer (ICT) Behavior for the Optical Detection of Nitroaromatic Compounds"
   W. Dong, J. Pina, Y. Pan, E. Preis, J. S. Seixas de Melo and U. Scherf*, *Polymer*, online, DOI: 10.1016/j.polymer.2015.08.064. (Chapter 4)
2. "High Sensitivity Sensing of Nitroaromatic Explosive Vapors based on Polytriphenylamines with AIE-active Tetraphenylethylene Side Groups"
   W. Dong, Y. Pan, M. Fritsch and U. Scherf*, *J. Polym. Sci. Pol. Chem.*, 2015, 53, 1753. (Chapter 3)
3. "Aggregation Induced Emission and Amplified Explosive Detection of Tetraphenylethylene Substituted Polycarbazoles"
   W. Dong, T. Fei, A. Palma-Cando, U. Scherf*, *Polym. Chem.*, 2014, 5, 4048. (Chapter 2)
4. "Functionality of Peripheral Side Chain for Enhanced Performance of Conjugated Polymer-F8BT as an Example"
   W. Dong, S. Xue, P. Lu, J. Deng, D. Zhao, C. Gu and Y. Ma*, *J. Polym. Sci. Pol. Chem.*, 2011, 49, 4549.
5. "Microporous, Tetraarylethylene-based Polymer Networks Generated in a Reductive Polyolefination Process"
   E. Preis, **W. Dong**, G. Brunklaus and U. Scherf*, *J. Mater. Chem. C*, 2015, 3, 1582.
6. "Cross-Linked Multifunctional Conjugated Polymers Prepared by In Situ Electrochemical Deposition for a Highly-Efficient Blue-Emitting and Electron-Transport Layer"
   C. Gu, **W. Dong**, L. Yao, Y. Lv, Z. Zhang, D. Lu, Y. Ma*, *Adv. Mater.*, 2012, 24, 2413.
7. "Time-Resolved Spectroscopy Study of Donor–Acceptor-Type Copolymers in a Monodisperse System: The Effect of Ratio between the Acceptor and the Donor"
   Y. Wang, L. Gong, **W. Dong**, P. Lu, Z. Kang, T. Huang, Y. Ma, H. Zhang*, *J. Polym. Sci. Pol. Phys.*, 2013, 51, 992.
8. "Highly-efficient Solution-processed OLEDs based on New Bipolar Emitters"
   M. Zhang, S. Xue, **W. Dong**, Q. Wang, T. Fei, C. Gu and Y. Ma*, *Chem. Commun.*, 2010, 46, 3923.
9. "RGB Small Molecules Based on a Bipolar Molecular Design for Highly Efficient Solution-Processed Single-layer OLEDs"

L.Yao, S. Xue, Q. Wang, **W. Dong**, W. Yang, H. Wu, M. Zhang, B. Yang and Y. Ma*, *Chem. Eur. J.*, 2012, 18, 2707.

10. "Iridium Complex Grafted to 3,6-Carbazole-alt-tetraphenylsilane Copolymers for Blue Electro-phosphorescence"
    T. Fei, G. Cheng*, D. Hu, **W. Dong**, P. Lu and Y. Ma*, *J. Polym. Sci. Pol. Chem.*, 2010, 48, 1859.
11. "Peripheral Cyanohexyl Substituent in Wide Bandgap Polymer: Increase the Electron Injection Property for Blue Phosphorescence Light Emitting Device"
    D. Hu, G. Cheng, P. Lu*, H. Liu, F. Shen, F. Li, Y. Lv, **W. Dong** and Y. Ma*, *Macromol. Rapid Commun.*, 2011, 32, 1467.

Conference publication:

1. "Aggregation-induced Emission and Amplified Explosive Detection of Tetraphenylethylene-substituted Polycarbazoles", Macromolecular Colloquium Freiburg 2015, Feb. 25-27, Freiburg, Germany.

W. Dong and U. Scherf, *Macromol. Rapid Commun*., 2015, 36, F64. (Presented as poster)

2. "High Sensitivity Sensing of Nitroaromatic Explosive based on Polymers with AIE-active Tetraphenylethylene Side Groups", GDCh-Wissenschaftsforum Chemie 2015, Dresden, Germany.

W. Dong and U. Scherf, 2015 Aug. 30 – Sept. 2, poster.

Acknowledgement

When I am writing this part, I just realize that my life as a student will end very soon. Time flies so fast, and I have been a student for 22 years, from my hometown Harbin to Changchun in China, and then to Wuppertal in Germany. I am so happy to have three years PhD study funded by CSC. It makes me grow up, not only in research but also in everyday life. It helps me to discovery a different part of me.

First, I'd like to give my great gratitude to my advisor, Prof. Dr. Ullrich Scherf. Thanks for offering me the opportunity to work in his macromolecular chemistry research group, as well as his continuous support and encouragement. His broad scientific knowledge and thoughtful ideas help me so much along my study and I will always remember them.

Many thanks to Kerstin Müller, she gave me so much help in my life in Germany. Every time when I had a problem and went to her, and she always solved it quickly and perfectly. Thank you!

Many thanks to Suman K. Samanta, Alex Palma and Eduard Preis for the good advices and correction of my thesis.

I would like to thank all my colleagues from Scherf's group, for the helps they have given me in lab work as well as everyday life. Everyone of them has helped me when I need German translation for visa extension, going to a doctor, looking for an apartment…They will recognize themselves even though I do not name them.

My thanks also go to Jõao Pina, Prof. Sergio Seixas de Melo and Carlos Serpa for their kind help during my work in the University of Coimbra in Portugal. I really enjoyed the time there.

My special thanks to my dear husband, Teng, for his support of my PhD study and his one year companion in Germany. He always brings me comfort and help in my life. Thanks for his steadfast love, even to my defect and my bad temper sometimes, which makes my life full of happiness.

At last, I'd like to give my great thanks to my dear parents and my little sister. They are supportive and concerned about me in my whole life. I wish them all the best in their lives.

To all the families and friends, this thesis cannot be accomplished without you. Thank you very much, all of you!

July, 2015 @Wuppertal

Wenyue Dong